INVESTIGATION OF PERFORMANCE EVALUATION AND DESIGN TECHNIQUES FOR LARGE INDUSTRIAL MUFFLERS

by

Scott Mang

B. S. in Mechanical Engineering, University of Pittsburgh, 2012

Submitted to the Graduate Faculty of

Swanson School of Engineering in partial fulfillment

of the requirements for the degree of

M. S. in Mechanical Engineering

University of Pittsburgh

2013

UNIVERSITY OF PITTSBURGH

SWANSON SCHOOL OF ENGINEERING

This thesis was presented

by

Scott Mang

It was defended on

June 25, 2013

and approved by

William W. Clark, PhD, Professor, Department of Mechanical Engineering and Materials Science

Daniel G. Cole, PhD, Associate Professor, Department of Mechanical Engineering and Materials Science

Jeffrey S. Vipperman, PhD, Associate Professor, Department of Mechanical Engineering and Materials Science, Department of Bioengineering

Thesis Advisor: Jeffrey S. Vipperman, PhD, Associate Professor, Department of Mechanical Engineering and Materials Science, Department of Bioengineering

INVESTIGATION OF PERFORMANCE EVALUATION AND DESIGN TECHNIQUES FOR LARGE INDUSTRIAL MUFFLERS

Scott Mang, M. S.

University of Pittsburgh, 2013

This document is the culmination of an investigation into the techniques used to design and evaluate the acoustic performance of large industrial mufflers using three-dimensional acoustic theory. Three performance criteria were considered. These criteria were noise reduction (NR), insertion loss (IL), and transmission loss (TL). Three different large sized mufflers were considered in this study. Each muffler was experimentally evaluated through field measurements. These field measurements were then used to validate finite element analysis (FEA) software that is designed to predict muffler performance. A method to corroborate *in situ* measurements with idealistic FEA simulations was developed. Once the software was validated, it was used to perform parametric studies that investigated the effects of certain muffler design elements on the TL performance of the muffler. The parametric studies yielded a significantly better understanding of the effects of individual muffler features, and their role in a complex geometry.

TABLE OF CONTENTS

LIST OF TABLES

LIST OF FIGURES

PREFACE

I would like to thank Dr. Vipperman, the team at MIRATECH Corp., and the University Of Pittsburgh Swanson School Of Engineering for making this research possible.

1.0 INTRODUCTION

Recent U.S. Government legislation has placed stricter regulations on noise pollution. These regulations can be tough to meet, and certain industries will require higher performance noise control in order to satisfy all of the restrictions. Many companies that manufacture high performance mufflers are seeking to improve their test and design processes so that they can fulfill the specifications that result from the new regulations. The following research is an investigation of mufflers and the processes that are used to design and test the performance of these mufflers.

Most design and analysis work for mufflers has been done with one-dimensional plane wave theory. This type of analysis is fine for small sized mufflers. Such as the kind you would see on a car. However, as will be seen in a moment, when the size of the muffler is scale dup to the size typically seen on exhaust systems for power plants or diesel engine, the acoustic propagation becomes three-dimensional. This can render plane wave analysis and design very inaccurate. The main goal of this research is to lay groundwork to develop a more accurate and efficient design process that is based in the three-dimensional analysis and design of industrial mufflers.

In this research, the three-dimensional finite element analysis(FEA) program LMS Virtual.Lab Acoustics (http://www.lmsintl.com/virtuallab) was validated against field measurements to determine the relative agreement of the two processes. Measurements were conducted in a field due to cost and space restrictions. However, the field measurements were considered to be a more real approximation of the performance obtained in application (*in situ*) compared to measurements made in a lab. The conditions that arose because of the *in situ* nature of the measurements required the development of methods not found in literature so that the idealistic FEA simulations could be properly compared.

After the validation, the FEA program was used to conduct a parametric study in which the performance of different muffler features in a complex geometry with three-dimensional propagation is investigated. The parametric study was performed by slightly varying the dimensions of certain features and observing the impact on performance of these variations. The intention of the parametric study was to obtain insight on the effectiveness of current design techniques developed from plane wave theory on

large sized mufflers. The remainder of the current chapter is used to provide a general overview of muffler technology.

1.1 THREE DIMENSIONAL ACOUSTICS AND LIMITS OF ANALYTICAL SOLUTIONS

To start off a few basic terms and concepts that will be useful throughout the paper will be defined. There are five variables that are typically used to describe an acoustic wave. They are speed of propagation, wavelength, frequency, amplitude, and wavenumber. The speed of propagation is intuitively the speed at which an acoustic wave will travel through a medium. The speed of propagation is dependent only on the medium that it is traveling through and ambient conditions. It will not be affected by any other properties of the acoustic wave. As shown in Figure 1.1, acoustic waves are sinusoidal functions. The wavelength is the distance that is required for the completion of one full period of oscillation. The frequency is the number of oscillations that occur per second. As one may have already determined, the frequency, wavelength, and speed of propagation are all closely related. This relation is given in Equation 1-1. The amplitude is the magnitude of oscillation from the mean value to the peak value. The wavenumber is another way of expressing the wavelength. Instead of meters per oscillation the wavenumber is expressed in radians per meter. This tends to be more convenient in calculations. The wavenumber can be determined from Equation 1-2.

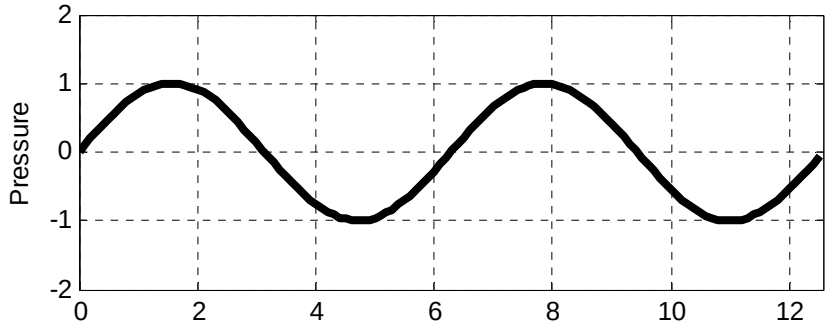

Figure 1.1: Sinusoidal representation of a single frequency acoustic wave with Amplitude 1 and wavelength 2π.

$$c = f\lambda \tag{1-1}$$

$$k = \frac{2\pi}{\lambda} \tag{1-2}$$

where c is the speed of sound, f is the frequency, λ is the wavelength, and k is the wavenumber. The speed of sound is well documented for many materials and mediums. However the speed of sound is temperature dependent. The equation for the speed of sound at a given temperature is given below.[1]

$$c = c_0\sqrt{\frac{T}{T_0}} \tag{1-3}$$

where c_0 is a known value for the speed of sound at temperature T_0, and c is the speed of sound at temperature T. Both T and T_0 are absolute temperatures.

Mufflers aim to decrease the amplitude of acoustic waves. The ability of a muffler to do this is measured in three ways: insertion loss, transmission loss, and noise reduction. Insertion loss is the comparison of sound pressure levels before and after a muffler is installed in an exhaust system. Transmission loss is the measure of how much acoustic power is lost by a wave as it travels through a muffler. Noise reduction is the comparison of the sound pressure levels of a point upstream of the muffler and a point downstream of the muffler. Each of these performance standards will be covered in more detail in the measurement section.

Two more terms that are useful to define are acoustic impedance and characteristic acoustic impedance. Acoustic systems may be analyzed as an equivalent impedance circuits. This process is the same as when electrical circuits are analyzed as equivalent impedance circuits. Acoustic impedance represents the pressure change created by a wave divided by the volume velocity that is imparted to the medium by the same wave.[2] Acoustic impedance is a property of the device that a wave is traveling in. The characteristic acoustic impedance is a material property and is represented by the density of a material multiplied by the speed of sound in that material. These two properties are generally used because of their convenience in certain calculations.

Up until the past couple of decades, most of the analysis of acoustic mufflers has been through one dimensional plane wave analysis. This one dimensional analysis assumes that the pressure is the same at every point in a cross section perpendicular to the direction of propagation. In other words, at any given instant, the pressure only varies in the direction of wave propagation. For the small mufflers that you would find on a car or other small engine, this assumption is actually very accurate. However, as the duct size grows with respect to the acoustic wave, the wave is allowed to propagate in more dimensions. The

following sub-sections will explain when this multidimensional propagation starts, the effects that it has, and the difficulties that arise when trying to analyze and predict these effects.

1.1.1 Mode cut on frequencies, and effects of multidimensional propagation

In a duct exposed to multiple frequencies waves may be travelling in one, two, and three dimensions all at the same time. The low frequency waves will be the most likely to travel in one dimension, while the high frequency waves will be the most likely to travel in three dimensions. This is because the higher the frequency of wave, the smaller the wavelength will be. As mentioned before, when the wavelength is small compared to the duct size the wave will have room to propagate in multiple directions instead of just axially. One dimensional waves and multidimensional waves are shown in the same finite cylinder at different frequencies in Figure 1.2. Modes 1 and 2 show a one dimensional wave in the cylinder. The pressure is uniform across the cross section of these modes. Modes 10 and 11 both have multidimensional waves present them. The pressure is not uniform across their cross sections. If these cylinders were longer, the patterns seen in the figure would repeat to form a wave pattern in the pipe.

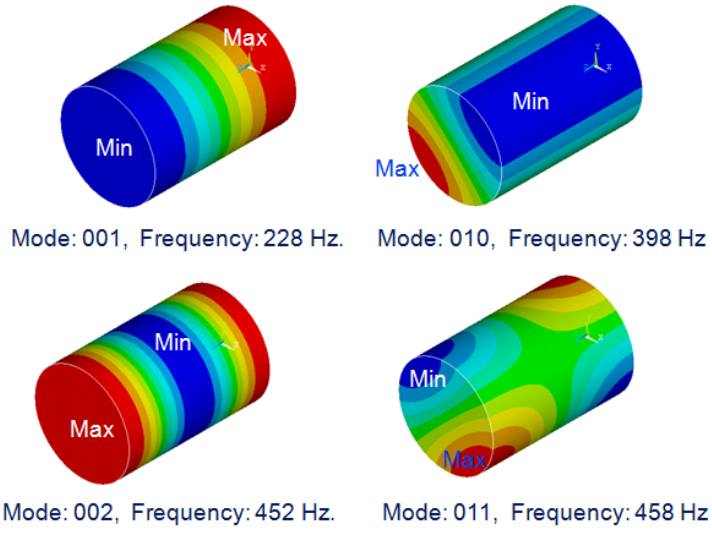

Figure 1.2: Illustration of plane waves and higher order modes.

A three dimensional wave can be described by the mode shape in which it is propagating. Each mode shape has a particular "cut on frequency" above which it is allowed to propagate. To better illustrate this idea, a rectangular duct is considered. For a rectangular duct the cut on frequency is given by:[3]

$$f_c = \frac{c}{2\pi}\left[\left(\frac{m\pi}{a}\right)^2 + \left(\frac{n\pi}{b}\right)^2\right]^{.5}\sqrt{1-M^2} \qquad (1\text{-}4)$$

where f_c is the cut on frequency, c is the speed of sound in the duct medium, M is the Mach number, a and b are the duct dimensions while m and n are the number of cross nodes along the duct dimensions a and b respectively. Figure 1.3 illustrates the mode shapes for a rectangular duct. In this figure the solid lines represent the walls of the duct while the dotted lines represent the nodal or zero acoustic pressure lines of the waves. The area in between the lines represents the alternating maximum and minimum pressure regions of the wave as denoted by the "+" and the "–" signs respectively.

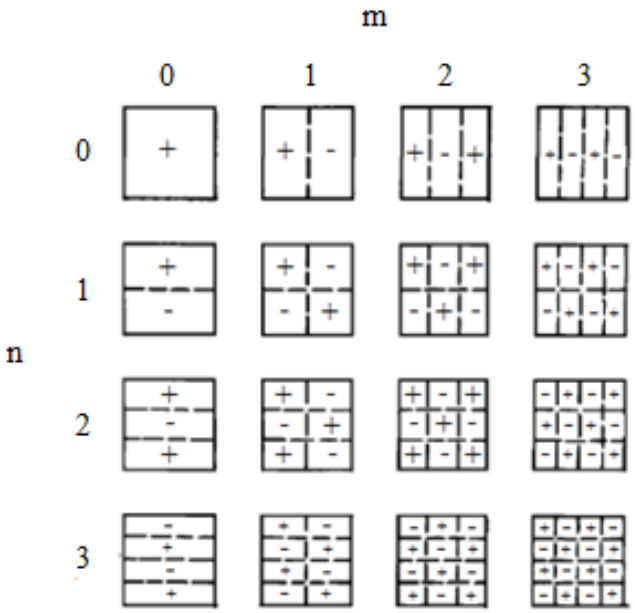

Figure 1.3: The mode shapes of the first three cut on frequencies for either duct dimension.[3]

The cut on frequencies for a circular duct also behave in a similar fashion. The difference being that the diameter is the measurement of interest and instead of cross modes in two directions there are cross modes and radial modes. The cut off frequencies for a circular duct are given by:[3]

$$f_c = J_{m,n} \times \frac{c}{\pi D}\sqrt{1 - M^2} \tag{1-5}$$

where D is the diameter of the duct, and $J_{m,n}$ is the zero of a Bessel function for the mode of interest, m is the order of the Bessel function and the number of cross nodes and n is the number of radial nodes. The Mach number is the ratio of the flow speed in the duct to the speed of sound ($M=v/c$). This labeling scheme is shown in Figure 1.4. The Bessel function zero associated with each mode is listed underneath the mode. Plus and minus signs are added to the antinodes in the first few modes where there was room to do so.

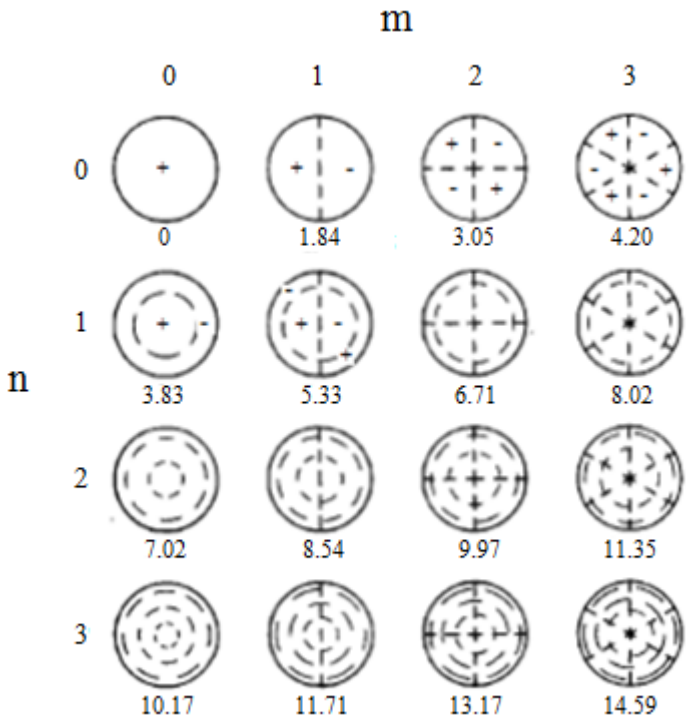

Figure 1.4: Mode labeling scheme for circular ducts.[3]

Each higher order mode traveling in the duct of a muffler can also reach a resonance point, causing the problem of attenuating the noise within the muffler to become even more complex.[3] If these modes are allowed to propagate through and escape the muffler, the performance of the muffler will be drastically compromised. There are two ways in which one of these higher order modes may escape the muffler.[3] The first way is through simple propagation. In this case the muffler and tailpipe are large enough to have one of these modes become excited and propagate through the duct until it escapes. The second way is when the tailpipe and/or the muffler are too small to allow the propagation of a higher order mode that has been excited. When the excited mode reaches a duct region that is too small for it to propagate in, it is attenuated over the course of a wavelength or two. This is the point that the mode becomes evanescent. If the region that does not allow the propagation of the mode is shorter than a couple of wavelengths for a given evanescent mode, then the evanescent mode will still escape the muffler without being fully attenuated.

1.1.2 Multidimensional analysis

In order to explain the difficulties of multidimensional analysis it is first necessary to go through a derivation of the linear wave equation. We will start by giving the relevant physical equations. The first equation is the mass continuity equation.[2,4]

$$\rho_0 \frac{\partial s}{\partial t} + \nabla \cdot (\rho_0 u) = 0 \tag{1-6}$$

$$s = \frac{\rho - \rho_0}{\rho_0} \tag{1-7}$$

$$\nabla = \frac{\partial}{\partial x} + \frac{\partial}{\partial y} + \frac{\partial}{\partial z} \tag{1-8}$$

where ρ_0 is the ambient density, ρ is the density at any given moment (this will fluctuate due to the acoustic pressure wave), u is the particle velocity, and s is the percent density change. s is also known as the condensation.∇ is a mathematical operator representing the partial derivative of a variable with respect

to three directions. The first term in this equation represents the mass change in a system with respect to time, and the second term represents the net flow of mass into the system. The next equation is the dynamic equilibrium or momentum equation.[4] Through Newton's second law the forces are balanced and the equation of motion is obtained. From here the other equations obtained (mass continuity, and state relations) will be used to turn the momentum equation into a single variable differential equation.

$$\rho_0 \frac{\partial u}{\partial t} + \nabla \cdot (p) = 0 \tag{1-9}$$

$$p = P - P_0 \tag{1-10}$$

where P is the instantaneous pressure, P_0 is the ambient pressure, and p is the acoustic pressure level. The first term in Equation 1-9 represents the acceleration field multiplied by the mass, and the second term represents the pressure field in the system.

By taking the divergence of the dynamic equilibrium equation, deriving the continuity equation with respect to time, and subtracting the two we arrive at the following equation:[4]

$$\rho_0 \frac{\partial^2 s}{\partial t^2} - \nabla^2 p = 0. \tag{1-11}$$

By taking the definition of the bulk modulus (Equation 1-12), substituting in s and p and solving for s (Equation 1-13), and then substituting in the isentropic energy equation (Equation 1-14) [2], we can insert the results to Equation 1-11 and arrive at the homogeneous linear wave equation (Equation 1-15).

$$E = \rho_0 \frac{P - P_0}{\rho - \rho_0} \tag{1-12}$$

$$s = \frac{p}{E} \tag{1-13}$$

$$\frac{P - P_0}{\rho - \rho_0} = c^2 \tag{1-14}$$

$$\nabla^2 p - \frac{1}{c^2}\frac{\partial^2 p}{\partial t^2} = 0 \tag{1-15}$$

where E is the bulk modulus of the duct medium. Equation 1-15 is a homogeneous second order partial differential equation; the plane wave and three dimensional solutions of which are given in Equations 1-16 and 1-17 respectively.[2]

$$p(x,t) = C_1 e^{j\omega(t-x/c)} + C_2 e^{j\omega(t+x/c)} \tag{1-16}$$

$$p(x,y,z,t) = \left(C_1 e^{-jk_x x} + C_2 e^{jk_x x}\right) \times \left(e^{-jk_y y} + C_3 e^{jk_y y}\right) \times \left(e^{-jk_z z} + C_4 e^{jk_z z}\right) \tag{1-17}$$

$$\sqrt{k_x^2 + k_y^2 + k_z^2} = \frac{\omega}{c} \tag{1-18}$$

where p is the acoustic pressure, $C_{1,2,3,4}$ are constants that are determined from the boundary conditions, a $k_{x,y,z}$ are the wave numbers in the x, y, and z directions, and ω is the frequency in radians/sec.

From the solutions in Equations 1-16 and 1-17, one can see how the complexity of the solution grows very quickly when considering multiple dimensions. These equations also grow more intricate when other factors affecting propagation are considered, such as a mean flow, viscosity of the fluid, non-ideal fluids effects, acoustic wave sources, complex geometries, complex boundary conditions, and nonlinearities in the acoustic wave. For this reason analytical solutions to these equations can be very difficult to arrive at. Parametric studies are even more difficult and time consuming because a new solution must be used for each model.

In order to quickly and efficiently model a muffler or any other elaborate physical system, numerical methods are used instead of analytical methods. Numerical methods use iterative approximations made over very small spaces and times to arrive at a solution for a larger system. One method that is highly proliferated today in the acoustic world is finite element analysis. This method will be briefly and conceptually covered in the next section.

1.2 FINITE ELEMENT ANALYSIS

As mentioned in the last section, finite element analysis (FEA) is one of the most well-known numerical methods in use today. In FEA, a complex continuous system governed by a few differential equations is turned into a discrete system governed by many linear equations. These linear equations represent the behavior of very small portions of an entire structure or domain. The smaller the area governed by a single equation, the more accurate the model will be.[5] An easy analogy to make is for that of a circle. Although it is known that a circle has a constant curvature, with no straight lines in it whatsoever, a circle may be accurately modeled by a large number of straight lines placed in the proper configuration. The more line segments that are used, the more the model will look like an actual circle. Keep in mind that this is only an analogy, and the finite element method (FEM) is much more advanced than just modeling a circle with lines.

The general form of the linear equations that is sought is usually presented as $[F]=[K]\times[U]$. The brackets represent matrices. This equation form can be thought of like a spring; force (F) is equal to stiffness (K) multiplied by displacement (U). To generalize that relation so that it will cover more than just structural analyses, we can think of it as a stimulus F, acting upon a system with property K, resulting in behavior U.[6]

1.2.1 Example: simple FEA analysis

It seems appropriate to provide an example of a simplified finite element analysis. The case that will be covered is that of a one dimensional simply supported beam. For a structural analysis the goal is usually to find out the deflection of the beam from an applied load. While the beam deflection equations are well known for simple load cases, we will see how this analysis will make it easier to predict the deflection of the beam for more complex loading cases. For this example the flexibility method will be used. This method treats the forces as unknown and the displacements caused as known.[7]

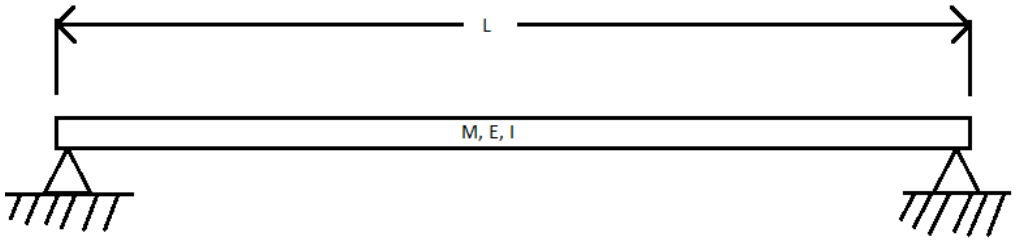

Figure 1.5: Simply supported beam of mass *M*, moment of inertia *I*, modulus *E*, and length *L*

The first step in any FEA analysis is to discretize the system. This is where the system is separated into blocks called elements. At all of the ends or corners of each element there is a node. A node is a discrete point at which the linear equations created for this system are going to be solved. The element is the area between these nodes where the solution will be interpolated.[7] The methods with which we create the linear equations and interpolate solutions across the elements will be shown later in the demonstration.

For the one dimensional beam, the nodes will be lumped masses that represent the entire beam. For simplicity's sake we will only consider three degrees of freedom (three nodes, multiplied by one dimension).

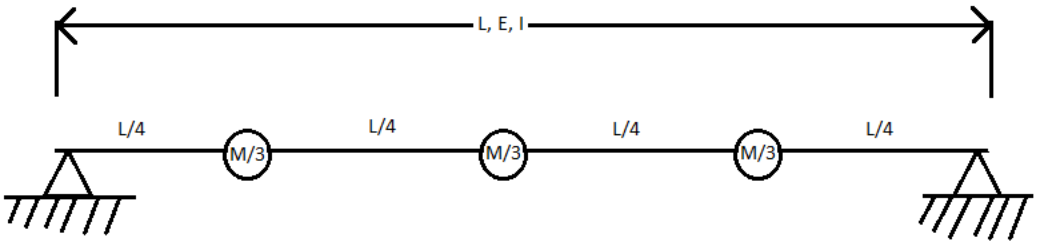

Figure 1.6: Simply supported beam discretized into lumped masses.

For the flexibility method a unit force is applied to each mass. The displacement of each mass resulting from the unit force is then entered into the flexibility matrix. The first column is made up of the displacements of each mass from a unit force on the first mass; the second column is the displacements from a unit force on the second mass. This process is repeated for each mass until an n x n matrix is created, where n is the number of degrees of freedom in the system. To fill out the flexibility matrix for this case, the beam deflection equations are used.[8]

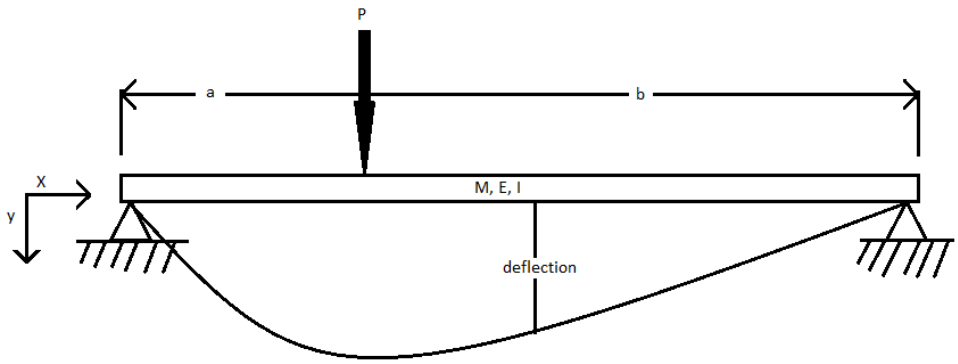

Figure 1.7: The deflection of a simply supported beam under a load along its length

$$y = \frac{Pbx}{6EIL}(L^2 - b^2 - x^2) \quad \text{for} \quad 0 \le x \le a \tag{1-19}$$

$$y = \frac{Pb}{6EIL}\left(\frac{L}{b}(x-a)^3 + (L^2 - b^2)x - x^3\right) \quad \text{for} \quad a \le x \le L \tag{1-20}$$

where y is the deflection of the beam, *P* is the load on the beam, *a* and *b* are as picture in Figure 1.7, *E* is the Young's modulus of the beam, *I* is the second moment of area of the beam, *L* is the length, and *x* is the position of interest along the beams length.

Applying these equations to our masses we receive the flexibility matrix:

$$\begin{bmatrix} a_{11} & a_{12} & a_{13} \\ a_{21} & a_{22} & a_{23} \\ a_{31} & a_{32} & a_{33} \end{bmatrix}$$

where each row represents the displacement of its respective mass and each column represents the displacements of each mass when its respective mass has been loaded.

The flexibility matrix represents the inverse of the stiffness matrix. Now that this matrix has been created, we may apply an arbitrary load to the nodes, and determine their displacements. If a force should act between two nodes, then it should just be proportionally split between them depending on the distance from each node. This method works for both static and dynamic loads.

In order to determine the displacements between the nodes, a shape function must be used. A shape function is an interpolation function used to model the system behavior of interest in locations

where node solutions have not been determined. The interpolation scheme combines the solutions from all nodes within the element. Each node solution is weighted by a shape function that is equal to one at its respective node, and zero at the next node. Each of these interpolated solutions are then superimposed upon each other creating the element solution. For this example, linear, one dimensional shape functions will be used.[5]

$$N_1 = 1 - \frac{x}{L} \tag{1-21}$$

$$N_2 = \frac{x}{L} \tag{1-22}$$

$$y(x) = N_1 y_1(x) + N_2 y_2(x) \tag{1-23}$$

where *y* is the displacement of a point between the nodes, *x* is the position in between the nodes where the displacement is being calculated, *N* is a shape function, and the subscripts *1* and *2* represent the nodes that are being interpolated between. When dealing with three dimensional models where more accuracy is needed, these shape functions can become much more involved. The linear interpolations used here will cause some error in the predictions of the beam displacement since we know that the beam does not undergo a linear displacement. Figure 1.8 illustrates how more degrees of freedom will generate a more accurate model. The prediction of beam deflection for one, three, and five masses is shown. The dotted line represents the actual deflection, and the solid line represents the predicted deflection.

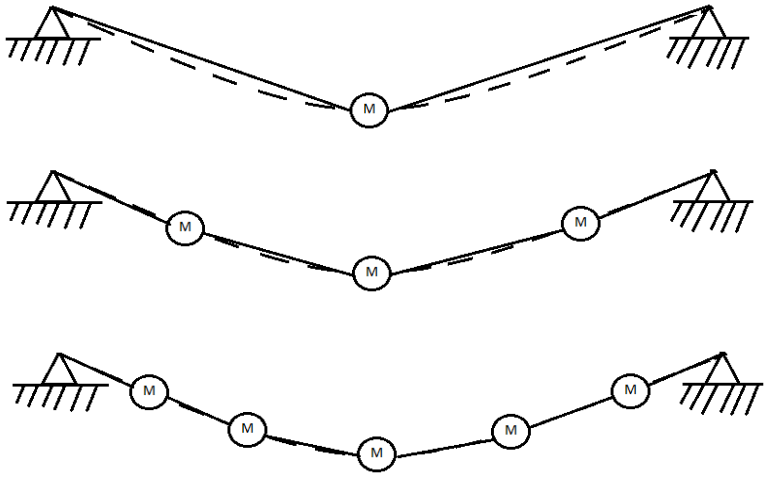

Figure 1.8: Predicted deflection of a beam for one five and three masses (two, four, and six elements respectively)

As previously mentioned, this model is only a linear model and the deflection can only be used to predict the stress and strain in one dimension. If a three dimensional model were to be constructed, a much more complex process would need to be followed in order to setup the system analysis. For a three dimensional problem, not only would three dimensional elements need to be selected to represent the system, but also a more complex method of determining the linear equations would be implemented. The equations of each element would need to be assembled, and then each set of element equations would be placed into a global equation matrix. The most common method of determining the linear equations is through Galerkin's method of weighted residuals. This process will be briefly described in the next section. The most common type of three dimensional elements used is the tetrahedral element, because it is very adaptable to many different complex geometries.[9]

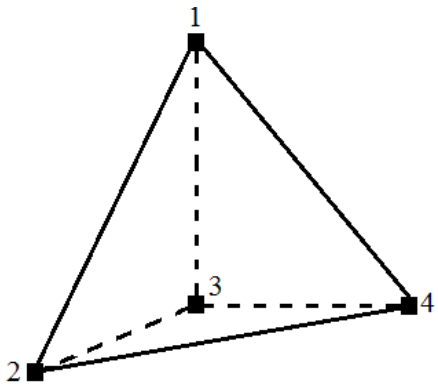

Figure 1.9: Three dimensional tetrahedral element with four nodes

1.2.2 Galerkin method

In the previous section the flexibility method was used to model the behavior of the system. There are many mathematical methods that produce much more accurate results than the flexibility method. The downside is that these methods tend to be much more involved mathematically and computationally. Variational models were among the first models used for finite element modeling of acoustic systems.[10] Today, the most widely used and studied model in finite element acoustics is the Galerkin weighted residual model.[11] The method of weighted residuals is a way in which the finite element method can be applied directly to the differential equation (DE) that governs a system. The first step is to plug a trial function into the DE that approximates the true solution. This will result in the addition of a residual term which represents the error between the result of using the trial function and the result if the true solution had been used. This residual then must be minimized using Equation 1-24.[12]

$$\int_D RW_i \, dD = 0 \qquad \text{i=1,2,…} \tag{1-24}$$

where R is the residual resulting from use of the trial function, D is the solution domain, and W_i is a weighting function which allows the residual to be minimized over the solution domain. In the Galerkin method, the shape functions mentioned above are used as the weighting functions. Using the fact that the residual is equal to the governing differential equation of the system with the trial function inserted as the solution, Equation 1-24 is used as the new governing equation. When all of the appropriate functions are plugged in Equation 1-24 will produce a linear equation for every shape function used in the system.

1.2.3 Advantages, disadvantages, and a recap of the FEM

The FEM is a very effective way to analyze a system numerically, and it has many advantages over other numerical methods. The first advantage that is possibly the most attractive feature of the finite element method is that there are a variety of software packages that implement the FEM, and thusly the method has been tested and verified in a massive range of applications. A number of different elements may be

chosen from so that any geometry can be modeled, which is another reason why this method is so popular. Also, the elements can each have their own properties so even materials with heterogeneous materials can be modeled with relative accuracy. Other advantages include that the FEM can handle an extremely large variety of engineering problems, loading conditions, and boundary conditions. The last advantage is that any degree of accuracy can be obtained through the use of less or more elements in the system model.[2]

There are, however, disadvantages to finite element analysis (FEA). The largest setback in using FEA is the computational cost of obtaining an accurate model. For complex systems, large numbers of elements are required for high accuracy. As the number of elements grows so does the number of linear equations that must be solved simultaneously. This can cause simulations to be very time consuming and costly in terms of a computer's available memory. Another disadvantage is that FEA programs are very prone to operator errors. Elements of the wrong type may be used in certain cases, or boundary conditions may be improperly applied. All of these can cause models to produce incorrect results. Also the FEM by nature only produces an approximate solution.[6]

The FEM has two major competing analysis types in the muffler world. The first are transfer matrix and acoustic impedance analysis tools. These types of programs focus on plane wave analysis, and as stated before, one dimensional analysis is no longer valid for the three-dimensional wave propagation that is typically present in large sized ducts. These types of programs are generally more useful for automotive mufflers. The other major competing analysis method is the boundary element method. The boundary element method (BEM) has the advantage of less data preparation. This is because nodal solutions are only found on the surfaces of bodies. The BEM also has the ability to predict infinite domains. However, the BEM has low accuracy on problems with a large surface area to volume ratio such as shell applications. This would make it poor at predicting muffler shell vibrations. The BEM also produces equation matrices that are fully populated as opposed to the FEM matrices which are symmetric. This means that when the number of degrees of freedom are the same, the time and memory needed for a solution is much longer and larger than that for the FEM. The BEM also does not compute solutions for any of the interior body of a volume. This does not allow for an accurate analysis of the interior volumes; especially in non-linear models. In light of these facts, it is decidedly better to use the FEM for most types of models.

Now that the FEM has been explained in some detail, a general process will be enumerated here. This process applies to all models regardless of the specific approaches taken.[7] Steps one and two are both taken care of during the meshing process in software programs.

Step 1: Discretize the system

Step 2: Select the shape functions

Step 3: Define the equations that govern the system

Step 4: Derive the element equations

Step5: Solve the system equations for the unknowns

Step6: Use solved unknown variables to obtain desired solutions

Step7: Analyze the results

1.3 MEASUREMENT OF ACOUSTIC PERFORMANCE

As mentioned earlier in the paper, there are three standard ways to quantify the acoustic performance of a muffler. They are insertion loss, transmission loss, and noise reduction. Each offers its own advantages and disadvantages. In this section, the focus will mainly be on transmission and insertion loss. These are the two measurement methods that are the most prominent in both industry and research. Each section will cover the advantages, disadvantages, and measurement methods for their respective performance metrics.

1.3.1 Insertion loss (IL)

Insertion loss is defined as the difference between sound pressure levels of a silenced system and some reference system. The reference system is usually just a straight pipe of the diameter that is typical to the system in place of the muffler. This pipe should also be the same length of the muffler being tested.[13] Insertion loss is calculated by Equation 1-25

$$IL = 20log\left(\frac{p_r}{p_m}\right) \tag{1-25}$$

where IL is the insertion loss, p_m is the measured sound pressure with the muffler installed, and p_r is the reference sound pressure.

There are two main advantages to using IL as the standard of performance. The first advantage is that, conceptually, IL is the true performance of a muffler for a given system. It is the comparison of the duct system before and after the muffler is introduced. This is why expected insertion loss is the measure of muffler performance used by many companies. The second advantage is that IL measurement is relatively easy, and only requires one microphone either inside the muffler in a pipe or outside the muffler in free space.[14]

There are also a few disadvantages. IL is difficult to predict analytically, because it is very system dependent. Both the source impedance and the load impedance must be taken into account when trying to predict IL.[15] This system dependence leads to another disadvantage which is that even if the same muffler is used, the insertion loss can vary for different systems, different sources, and different loads. This is why companies generally only offer expected IL as a performance measurement.

The experimental setup for IL is relatively simple. The muffler should be situated horizontally relative to the ground, and noise source in the same way that it will be in application, and the environment should simulate a free-field above a reflecting plane. In order to create this type of environment the muffler should be placed in an area where the noise outlet and microphone are at least thirty meters from any large reflecting surfaces including, but not limited to buildings, walls, vehicles, hills, and people.[16] Ideally there would be no reflecting surfaces near the noise source or microphone, but if that is not possible, the following guidelines will help to minimize their effect. If possible, the measurements should be made in an anechoic chamber to eliminate any effects from wind, background noise, or reflecting surfaces near the microphone. Should an anechoic chamber not be available, then measurements should be taken at a time when wind and background noise are at a minimum. The effects from these two sources should be at least 10 dB less than the noise source being measured.[17] If this is not possible, then time must be given to let the noise die down, or a new measurement environment must be selected. The reflecting plane in this case is the ground and should be either concrete or asphalt. The muffler should be replaced with a simple pipe of equal length for the reference system.[2] The microphone should be placed approximately one meter from the outlet of the exhaust system. This distance should help to reduce contamination from background noise in the measurement field. The measurements should also be taken at a number of positions around the outlet of the exhaust system in a circular pattern, in particular 0, 45, 90, and 100 degrees.[17,18] Once everything is set in place nothing in the setup should change when switching between the reference system and the silenced system. Figure 1.10 illustrates some of these guidelines.

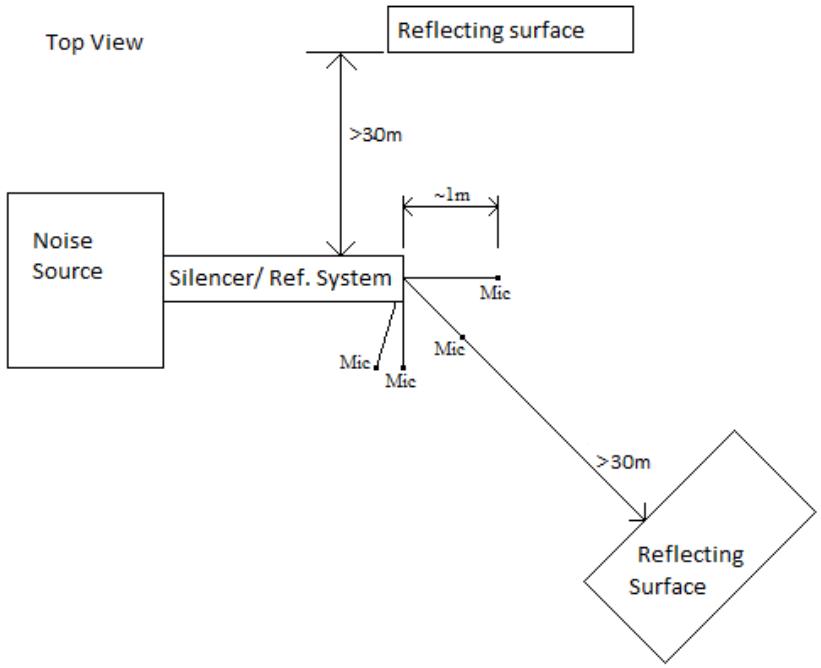

Figure 1.10: Top view of a typical IL setup. Drawing not to scale

1.3.2 Transmission loss (TL)

Transmission loss is defined as the ratio of incident sound power and transmitted sound power across the muffler being examined.[13]

$$TL = 10log\left(\frac{W_i}{W_t}\right) \tag{1-26}$$

where W_i is the incident sound power, W_t is the transmitted sound power, and TL is the transmission loss. Before we get started, it is worth mentioning that all methods of measuring TL are based in plane wave theory.

Transmission loss across a muffler is much easier to predict because it is independent of the source and load characteristics unlike the calculation of IL. This makes TL much more popular in the realm of research, because performance of mufflers and muffler elements is much easier to predict. The fact that TL is source-independent though makes its measurement much more difficult than that of IL. Incident and transmitted waves must be isolated so that proper calculation of the TL may be achieved.

This can be difficult because in the portions of piping immediately upstream and downstream of the muffler, there exists forward moving and reflected waves. These reflected waves are a result of the impedance mismatch discussed in section 3.

The incident wave is isolated through the method of wave decomposition. In the wave decomposition method, two microphones are placed upstream of the muffler. In a case where flow is present, a way to measure flow through the pipe will also need to be installed, because the wavenumber is affected by the flow rate, as seen in Equation 1-28. The information from these two microphones is then manipulated to separate the incident and reflected auto spectral densities.[19] A spectral density represents how the square of a signal is distributed across the frequency range of that signal. In this case, the signal will be the voltage from the microphone. That voltage will then be related to the pressure through the sensitivity provided by the manufacturer. Since auto and cross spectral densities can be calculated from measured pressures very readily by many mathematical programs and FFT analyzers, the calculation boils down to a simple formula for the auto spectral density of the incident wave:

$$S_{ii} = \frac{S_{11}+S_{22}-2C_{12}cos(k_r\Delta x)+2Q_{12}\sin(k_r\Delta x)}{4sin^2((k_i+k_r)\Delta x/2)} \quad (1\text{-}27),$$

$$k_i = \frac{k}{(1+M)} \ , \ k_r = \frac{k}{(1-M)} \quad (1\text{-}28),$$

$$k = \frac{2\pi f}{c} \quad (1\text{-}29).$$

where S_{ii} is the auto spectral density of the incident wave, S_{11} and S_{22} are the auto spectral densities of the acoustic pressures measured by microphones one and two respectively, C_{12} and Q_{12} are the real and imaginary parts of the cross spectral density, S_{12}, between the total acoustic pressures measured at microphones 1 and 2 respectively, k is the wavenumber, k_i and k_r are the incident and reflected wave numbers respectively, Δx is the distance between the microphones, M is the Mach number, f is the frequency of the acoustic wave, and c is the speed of propagation of the acoustic wave.[20] The subscript i stands for the incident wave, *1* and *2* are for measurements made at microphones 1 and 2 respectively, and r stands for the reflected wave.

On the downstream side of the muffler the auto spectral density of the transmitted wave must be obtained. Unfortunately, for this side of the muffler, the decomposition method is not applicable. Not only

does the transmitted wave reflect from the end of the duct, but that reflected wave again reflects when it reaches the muffler. This double reflection causes the decomposition method to render inaccurate results. One way to deal with this problem is to create an anechoic termination. This anechoic termination is designed to reduce the reflections from the termination to an insignificant level, and the spectral density of the transmitted wave may be calculated directly from the downstream measurement. The design of the anechoic termination will be covered in detail in the experimental setup section later in this paper. From both the incident and transmitted wave, the incident and transmitted acoustic power, W_i and W_t, can be calculated from Equations 1-30 and 1-31 followed by the TL via Equation 1-26.

$$p_i = \sqrt{S_{ii}} \quad , \quad p_t = \sqrt{S_{tt}} \tag{1-30}$$

$$W_i = \frac{{p_i}^2}{\rho_i c_i} A_i \ , \ W_t = \frac{{p_t}^2}{\rho_t c_t} A_t \tag{1-31}$$

where the subscripts *i* and *t* represent the incident and transmitted variables respectively, p is the pressure, ρ is the density of the medium, c is the speed of sound propagation in the medium, A is the cross sectional area of the duct, and S is the auto spectral density.[19]

The setup and placement of certain elements in the measurement of TL can greatly affect the accuracy of the results. A typical setup for TL measurement is shown in Figure 1.11.

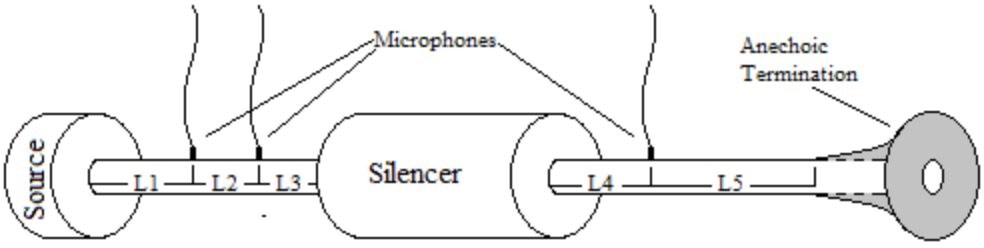

Figure 1.11: Typical setup for TL measurement.

To minimize the error from the measurement, the distances $L_{1,2,3,4,5}$ should be chosen according to the guidelines laid out by Seybert and Ross.[21] Lengths 3 and 4 should be made as small as possible.

Placing the microphones close to the muffler will reduce attenuation effects in the duct so that the measured transmitted and incident waves are as close as possible to the true transmitted and incident waves. Both length 5 and Length 1 should be as long as space will permit. This will minimize any measurement contamination due to reflections from the source or the anechoic termination. Since a perfectly anechoic termination is impossible to construct, this is a necessary guideline. Length 2 is the length that the most attention must be paid to. There are a number of constraints on it. Ideally, length 2 should be as small as possible. Length 2 needs to be small for two reasons. The first reason is to reduce the amount of wave attenuation between the two measurements, and the second being that when the microphone spacing is equal to a multiple of the half wavelength of the pressure wave, the decomposition theory equations produce sharp discontinuities in the data. To avoid this discontinuity the spacing of the microphones should be chosen according to Equation 1-32, which states that the spacing should be less than half the wavelength of the highest frequency being measured[22]

$$\Delta x \leq \frac{c}{2f_m} \tag{1-32}$$

where f_m is the maximum frequency, c is the speed of sound, and Δx is the microphone spacing. The limiting factor of the spacing between the microphones is that it should still be large enough that the position of the microphones may be approximated as the centerline of each microphone. This is why the spacing must be much larger than the microphone diameter. This may cause the discontinuity to be present in some of the measured frequencies. Fortunately this is only because of the equations used to model the effect and not because of a shortcoming of the decomposition method itself. If one of these discontinuities is encountered the data point may be simply ignored, and a curve fit may be used to estimate the data at the frequency.[21]

However, Equation 1-32 is an ideal spacing for the microphones. Many other factors in the measurement and calculation must be taken into account when deciding upon the spacing. An error analysis by Abom and Boden[23] resulted in a general formula that reduces error in the entire decomposition process by defining an acceptable frequency range for a given microphone spacing. Equation 1-33 should be used in tandem with the aforementioned constraint that the spacing of the microphones should be much larger than the diameter of the microphones.

$$\frac{.05c_0(1-M^2)}{\Delta x} < f < \frac{.4c_0(1-M^2)}{\Delta x} \tag{1-33}$$

where c_0 is the speed of sound, M is the Mach number(for cases with flow), Δx is the microphone spacing, and f is the frequency.

The two upstream measurements need to be taken simultaneously while the downstream measurement can be taken independently from the other two. The downstream measurement can be made independently as long as everything else in the system is held constant. This includes the system, the acoustic source, and the testing environment. The advantage of being able to take the downstream measurement separately is that only two microphones are needed for the measurement. One of the upstream microphones may be used to take the downstream measurement as well.

1.3.3 Noise reduction (NR)

Noise reduction is defined as the sound pressure level difference between two points in a system.[13] For a muffler, one point should be upstream and one point should be downstream of the muffler. Noise reduction is much like insertion loss in that it is very easy to measure, but is also source and load dependent making it hard to predict and calculate. The formula for noise reduction is

$$NR = 20 \log\left(\frac{p_u}{p_d}\right) \tag{1-34}$$

where NR is noise reduction, and p_u and p_d are the sound pressures at the upstream and downstream point respectively. Not much work has been done with NR, and thusly standards and research papers on it are hard to find. The reason for this is that NR itself does not tell us anything absolute about the performance of the muffler in the system or acoustic properties of the muffler, and the purpose of it is somewhat undecided. However, in many cases, NR is by far the simplest and easiest measurement to make in terms of the performance. Also, NR can be used as an approximation of the TL in many systems. For these two reasons NR is widely used in muffler performance studies. For the purposes of this study, the measurement of TL for very large mufflers can be impractical, so NR will kept track of and used as the defining metric for the acoustic properties of the larger mufflers. For the smaller muffler, NR may be measured simultaneously with the TL, and determined with much less analysis making it an easy quantity to keep track of even if only for comparison.

1.3.4 Microphone calibration

The two upstream microphones used to measure the incident wave for TL calculations must be phase and amplitude matched. This requirement can be circumvented by performing a relative calibration. The downstream microphone does not need to be calibrated so long as the microphone used as the standard is the one used to make the downstream measurement. A procedure for the relative calibration of two microphones is provided by Seybert and Ross.[21] An absolute calibration of the microphones is not needed because TL and NR are all based upon the ratio of two measurements relative to one another. First the microphones must be placed in a position relative to an acoustic wave so that the same amplitude with no phase shift is being measured by both microphones at the same time, preferably in an anechoic chamber, but a free field (outdoors or in a very large room) will work as well. Then the transfer function between the two microphones can be calculated with Equation 1-35. This transfer function is then used to calculate the phase shift (Equation 1-36), and correct for the differences in gain (1-37 thru 1-39) between the microphones. The subscript *1* will represent the microphone chosen as the reference.

$$H_{12} = \frac{S_{12}}{S_{11}} \tag{1-35}$$

$$\phi_{12} = tan^{-1}\left(\frac{Im[H_{12}]}{Re[H_{12}]}\right) \tag{1-36}$$

$$S_{11}^{c} = S_{11} \tag{1-37}$$

$$S_{22}^{c} = \frac{S_{22}}{|H_{12}|^2} \tag{1-38}$$

$$S_{12}^{c} = \frac{S_{12}}{H_{12}} \tag{1-39}$$

where the superscript *c* stands for the corrected measurements, the subscript represents the microphone to be calibrated, H_{12} is the transfer function between the two microphones, and ϕ_{12} is the phase shift between the two microphones. It should also be noted that H_{12} and S_{12} are complex quantities. These

corrected measurements may now be used to calculate *TL* and *NR*. This procedure is not needed for *IL* because only one microphone is used.

1.3.5 Measurement equipment

The equipment need for measurement is as follows:

- At least two pressure microphones.
  - Two will be needed for measurement of TL.

- One preamplifier for each microphone.
  - Increases the magnitude of the signal traveling from the microphone to the spectrum analyzer.

- One windscreen for each microphone.
  - So that measurements may be taken in the presence of wind or pipe flow.

- One signal conditioner for each microphone.
  - Often come with multiple channels so one can be used for multiple microphones.

- A microphone calibrator.
  - To ensure that the microphones are working properly.

- Accelerometers.
  - High temperature accelerometers should be bought if measurement is to be taken at operating temperature.
  - Accelerometers generally only measure one axis so at least three should be bought so that three different axes of vibration may be measured.

- Accelerometer calibrator.
  - To ensure that the accelerometers are working properly.

- In line charge converters.
  - If a device has a charge output, this will be needed to convert the output signal from a charge to a voltage.

- Probe microphones.
  - Probe microphones are used for pressure measurement in hot fluid flow.

- Speakers.
  - To create the acoustic wave.
  - Multiple may be needed to cover the frequency range interest and create the acoustic power needed to simulate operating conditions.

- A digital multimeter or a digital oscilloscope.

    - A multimeter or an oscilloscope would allow for real time monitoring of the signals coming from the measurement devices.

- The appropriate cables and connectors for all of the equipment.

- A spectrum analyzer.
    - A spectrum analyzer has the ability to record voltage signals and calculate different signal attributes such as spectral densities, and transfer functions.
    - Some also have the ability to generate noise signals to send to the speakers.

- An active crossover.
    - Will route signals to speakers so that all signals to a given loudspeaker are within the frequency range of that loudspeaker.

- An amplifier
    - Amplifies signal from spectrum analyzer and sends signal to speakers.

Regular microphones and accelerometers cannot handle high temperatures. If measurements are to be taken at high temperatures, then high temperature accelerometers and probe microphones must be used to monitor the vibrations and acoustic waves. A probe microphone uses vibrations from a long slender tube to sample a sound field at a small point. The difficulty with using a probe microphone is that the device is sensitive to the dynamics of the rod. If a standing wave is excited in the rod then the measurements may be distorted. For this reason, multiple measurements must be taken with multiple tubes of different properties. Each tube will be able to measure different frequency ranges without distortion.

1.4 REACTIVE MUFFLER DESIGN ELEMENTS

In the first section we stated that an acoustic system or element can be represented by its acoustic impedance in the same way that electrical circuit or component can be represented by its electrical impedance. In an electrical circuit, when an AC signal comes to a discontinuity or mismatch in the electrical impedance some of the signal energy will be reflected back in the opposite direction of propagation. This phenomenon is also present in acoustic systems. The primary function of design elements within a reactive muffler is to reflect propagating acoustic waves back towards their source. When an acoustic wave travels across the boundary of two different areas with different acoustic

impedances, a certain portion of the acoustic energy is reflected. As the disparity between these impedances grows, so will the portion of the wave that is reflected. When the wave is reflected it also experiences a phase change. This phase change creates destructive interference between the incident wave and the reflected wave. Through these physical mechanisms reactive mufflers lower the transmitted acoustic energy of a sound source. These types of muffler elements generally work best on low frequency noise. In order to create impedance mismatches and interference fields, the size of the muffler features generally needs to be on the same order as wavelength of the frequency being targeted. Thusly, it is not practical to fabricate features that target high frequencies. However, since the size of an element is usually related to the wavelength of the frequency it is meant to attenuate, the ability to attenuate high and low frequencies will be limited by the size of the muffler and manufacturing capabilities. This will be covered in more detail later. Components in a muffler may serve other purposes such as to dissipate acoustic energy into heat or to dampen shell vibration. Many components serve multiple purposes. These secondary functions will be addressed when necessary in the specific component sections.

1.4.1 Area discontinuities-expansions/contractions

Impedance of a given duct is closely tied in with the area of that duct. A sudden change in the area of a duct will create the impedance mismatch needed to reflect acoustic energy back towards a source. The greater the area discontinuity is, the greater the impedance mismatch will be. Quick estimates for the transmission loss of an area discontinuity and a simple expansion chamber are given by Munjal[2] and Sahasrabudhe[24] respectively.

For an area discontinuity: $$\mathrm{TL} = 10\log\left[\frac{(S_1+S_2)^2}{4S_1S_2}\right] \quad (1\text{-}40)$$

For a simple expansion chamber: $$\mathrm{TL} = 10\log[1 + .25(\mathrm{m} - \mathrm{m}^{-1})^2 \sin^2(\mathrm{kL})] \quad (1\text{-}41)$$

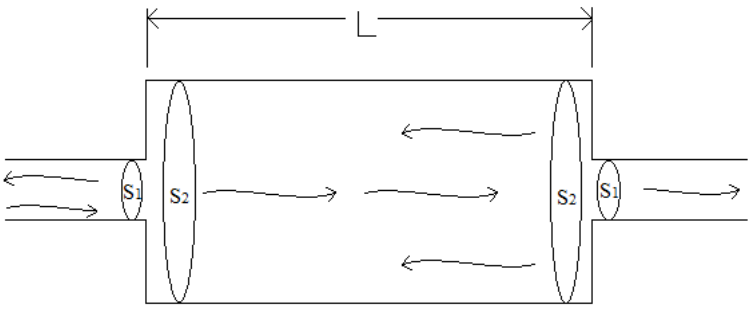

Figure 1.12: Expansion chamber with an acoustic source. Transmitted and reflected waves are shown.

where S_1 and S_2 are the respective areas of both sides of the discontinuity, m is the area expansion ratio, L is the length of the expansion chamber, and k is the wave number which was defined in section one. The dimensions for the expansion chamber are shown in Figure 1.12. By Equation 1-40 we can form the conceptual relation that the transmission loss will increase as the cross sectional area mismatch between the duct and the expansion chamber increases. It may be noticed that Equation 1-41 has a sinusoidal form. This means that an expansion chamber will have a cyclic transmission loss curve. The maximum peaks of this curve, or "resonance" points, will occur when the length of the expansion chamber is an odd multiple of a quarter wavelength. The minimum peaks occur when the length is an even multiple of the quarter wavelength.[24] This knowledge can be used to "tune" the muffler to be effective at desired frequencies.

$$L = \frac{n\lambda}{4} = \frac{nc}{4f} \qquad \text{TL Max. for } n=1,3,5,\ldots. \qquad \text{TL Min. for } n=0,2,4,\ldots. \tag{1-42}$$

where L is the length of the expansion chamber, λ is acoustic wavelength, c is the speed of sound, and f is the frequency. These equations should only be taken as liberal estimates since they are based on plane wave theory, and the concern of this review is mainly three dimensional wave propagation. Figure 1.11 shows the cyclic transmission loss, given by Equation 1-41, of a simple expansion chamber as well as the breakdown of the plane wave equations beyond the cut-on frequency (2839 Hz for this particular chamber). Figure 1.11 is a plot of the transmission loss obtained at a range of frequencies. The peaks of the transmission loss occur at the frequencies that supply solutions to Equation 1-42 for the length of the expansion chamber. If a broadband signal were to be applied to this particular expansion chamber, the dips represent the frequencies that would escape the chamber unattenuated while the peaks are the frequencies that would contribute the least the noise signal on the outlet side. Figure 1.13 shows a typical TL curve for an expansion chamber. Three dimensional propagation effects are not seen in the curve until

the first radial mode (0,1). This is due to the placement of the inlet and outlet (explained in next subsection).

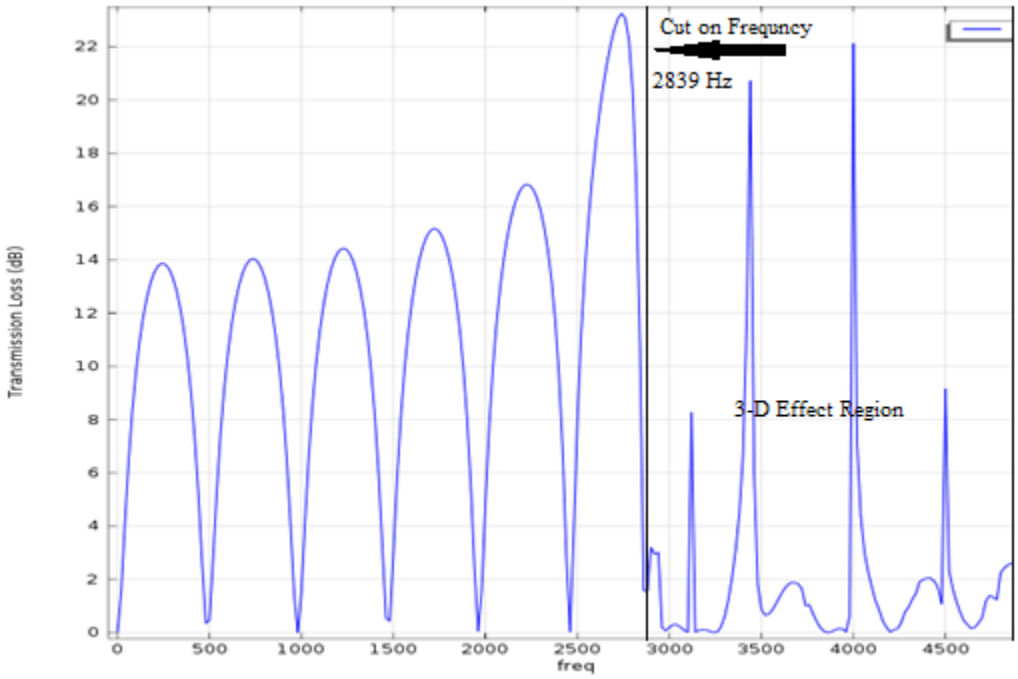

Figure 1.13: Transmission loss curve for a simple expansion chamber of diameter of 5.84", and length 13.87".

When using multiple chambers in a design, it is wise to keep chambers of similar resonance frequencies as far away from each other as possible to avoid interaction between resonances. This interaction can cause a "detuning" of the resonance chambers which will in turn lead to a reduction in the transmission loss.[25] In fact, different chambers (and baffle tube lengths as we will soon see) should be designed to attenuate different frequencies so that the nulls of one chamber are attenuated by another chamber. In this way the frequencies that are not attenuated by one chamber will be attenuated by the next and vice versa. No extra considerations are needed when modeling area discontinuities in a finite element analysis program.

1.4.2 Inlet, outlet, and baffle tubes

When creating multiple expansion chambers, it is common to separate the chambers with a thin wall known as a baffle. It is obvious that openings must be left in these baffles for gas to flow through the

muffler. Generally these openings are extended into the chamber a prescribed distance. This, in effect, creates more resonators within the chamber. The same can be done with the inlet and outlet tubes of the muffler. Each individual duct extension creates its own resonator. As with the expansion chamber the resonances of these extended tube sections are governed by Equation 1-42, where L is now the length that the duct specific to that resonator has been extended into the chamber. Two possible configurations are shown in Figure 1.14. These resonators may also be tuned in the same way as the expansion chamber. When extending these tubes one must be careful, because the effective length of the chamber is reduced to the length in between the extended tubes, thus changing the resonance frequencies of the expansion chamber.[24]

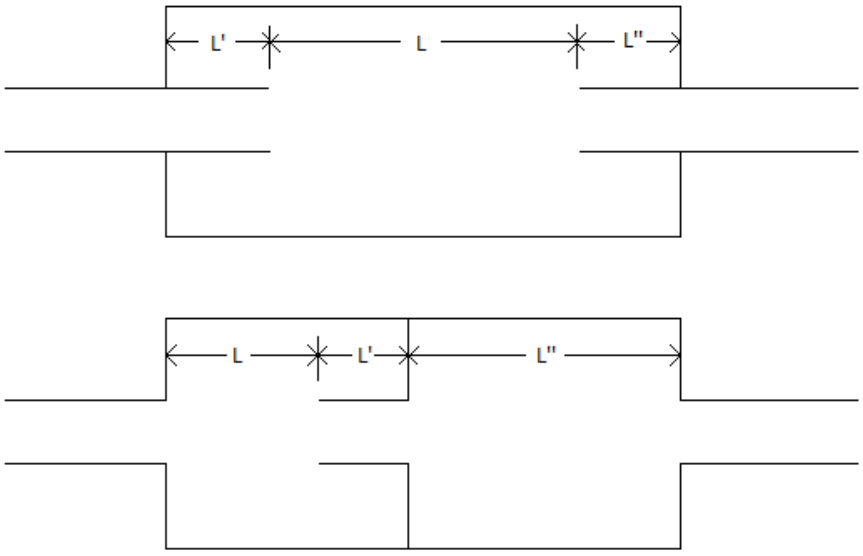

Figure 1.14: Two configurations showing different resonators that may be formed via extended ducts.

When three-dimensional acoustic propagation is present in the muffler, placement of the baffle, inlet, and outlet tubes relative to one another in the cross section of the chambers is an important factor to consider during design of a muffler as well. Three-dimensional propagation causes higher order modes to form in the muffler. When higher order modes are propagating through a muffler the placement of the inlet and outlet may cause the excitation and transmission of one of these modes. It may be useful to refer back to Figure 1.3 when trying to visualize this.

When the inlet is placed at the maximum pressure point of a mode, that mode becomes excited. If the outlet also happens to lie on one of the pressure maximums of these modes, then the wave will be transmitted though the muffler. The transmission of these modes, when excited, greatly reduces the performance of the muffler. Plane wave behavior of the muffler can be extended through strategic placement of the inlet, outlet, and baffle tubes of the chamber.[26] The configuration that tends to give the largest bandwidth of plane wave behavior is a centered inlet and an offset outlet. The centered inlet will make sure that none of the transverse modes are excited, because the axis is a nodal line of all of these types of modes. The offset outlet should be placed at the nodal point of the first circular mode. This configuration will allow plane wave behavior to continue until the second circular mode cuts on.[27] In a large sized muffler where plane wave behavior is not an option, the inlet and outlet should be placed so that problem frequencies do not have their modes excited or transmitted. A modal analysis of the muffler internal volume will provide the positions of the minimum pressure nodes. No extra considerations are need when modeling these extended tube resonators in an FEA program.

1.4.3 Acoustic packing materials

Acoustic packing materials are not a reactive muffler component. They are considered to be dissipative elements. This means that sound level reduction is achieved mainly through the transformation of sound energy into heat.[2] Dissipative elements perform best at higher frequencies, but offer attenuation of sound across a large bandwidth. This complements the low frequency performance of reactive elements very well. The materials used in dissipative elements are porous so that the acoustic wave may travel through them and be dissipated into heat. Typically the dissipative material is used as the lining of a muffler shell, but for larger ducts the parallel baffle approach is taken. This is where multiple parallel sections of dissipative material are placed through the cross section of the duct. These sections are generally concentric tubes of different diameters or parallel walls. The material is kept in place by plates or tubes that are perforated so that gas may flow through into the packing material. As the sections of packing material grow thicker, the attenuative performance at lower frequencies is improved, but the flow also becomes more restricted.[2] Figure 1.15 shows the normalized attenuation versus frequency curves for parallel baffle mufflers. The different graphs represent different open flow area ratios. The horizontal axis is the frequency of the wave normalized by the quantity $2h/c$. $2h$ is the distance between baffles and c is the speed of sound. L_h is the loss across the baffle element normalized by the propagation constant Γ_c.[28] Due to the porosity of these elements, there is a tendency to collect small particles that may be suspended in the gas flow of the duct. This will clog the material, and degrade the performance over time.[27]

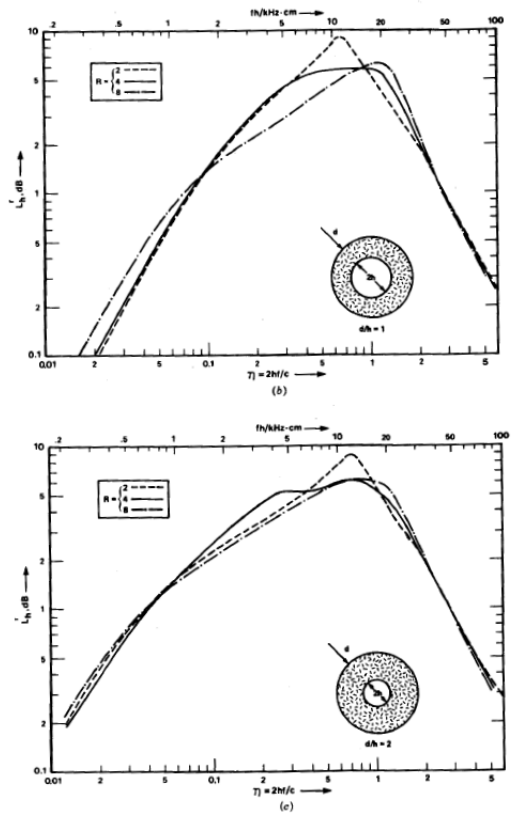

Figure 1.15: Normalized attenuation versus frequency curves for parallel baffle mufflers.[28]

When modeling these types of elements in an FEA program, certain acoustic material properties must be taken into special consideration. The acoustic packing material can be considered to be isotropic and homogeneous. In these types of materials wave propagation is governed by complex characteristic impedance and complex wave number.[29] The values for these two quantities are given by the Delany Bazley model of fibrous materials:

$$Z = \rho_0 C_0 \left[\left(1 + .0497\left(\frac{f}{R}\right)^{-.754}\right) + j\left(-.0758\left(\frac{f}{R}\right)^{-.732}\right)\right] \tag{1-43}$$

$$k = k_0 \left[\left(.169\left(\frac{f}{R}\right)^{-.595}\right) + j\left(1 + .0858\left(\frac{f}{R}\right)^{-..7}\right)\right] \tag{1-44}$$

Where

$$Z_0 = \rho_0 c_0 \tag{1-45}$$

And

$$k_0 = \frac{\omega}{c_0} \tag{1-46}$$

where f is the frequency, R is the airflow resistivity, c_0 is the speed of sound in air, and ρ_0 is the density of air, Z is the impedance, and Z_0 is the characteristic impedance. The airflow resistivity for many standard fibrous materials can be found in literature and from manufacturers.

1.4.4 Catalyst elements

Catalyst elements are used to chemically convert undesirable or dangerous pollutants into less toxic exhaust gases. Although catalytic converters are designed purely for control of chemical emissions from an engine, they also provide some acoustic attenuation in an exhaust system. The attenuation is generally small from these elements (just a few dB), but it is worth mentioning the effects.

Catalyst elements, like acoustic packing material, are also dissipative in nature.[30] They perform best at high frequencies, and must be modeled using complex properties.[31] These properties however are modeled as flow through cylindrical capillaries instead of as flow through an isotropic, homogeneous material. The formulations of these properties are given as: [30]

$$\rho_m = \rho_0 + \frac{\Re}{i*\omega} \tag{1-47}$$

$$c_m = \frac{c_0}{\sqrt{\left[1+\frac{\phi R}{i\omega\rho_0}\mathrm{G}(s)\right]\left[\gamma-\frac{\gamma-1}{1+(\phi R)/(i\rho_0\omega Pr)G_C(s\sqrt{Pr})}\right]}} \tag{1-48}$$

where

$$\Re = R\phi G_c(s)\,, \tag{1-49}$$

$$G_c(s) = \frac{-\frac{s}{4}\sqrt{-i}\frac{J_1(s\sqrt{-i})}{J_0(s\sqrt{-i})}}{1-\frac{2}{s\sqrt{-i}}\frac{J_1(s\sqrt{-i})}{J_0(s\sqrt{-i})}}\,, \tag{1-50}$$

$$s = \alpha\sqrt{\frac{8\omega\rho_0}{R\phi}}\,, \tag{1-51}$$

$$Z_m = C_m\rho_m\,, \tag{1-52}$$

$$k_m = \frac{\omega}{c_m}\,, \tag{1-53}$$

$$i = \sqrt{-1}\,, \tag{1-54}$$

ρ_m is the effective density, c_m is the effective speed of sound, k_m is the effective wavenumber, ω is the frequency, ρ_0 is the density of the material, R is the flow resistance, ϕ is the ratio of the flow area to the cross sectional area, J_0 and J_1 are zero order and first order Bessel functions, c_0 is the speed of sound in the material, Pr is the Prandtl number, i is an imaginary number, γ is the ratio of specific heats for the fluid, and α is a shape factor to account for non-circular cross sections in the capillaries.[31] More on the modeling of porous media may be found in reference [32].

1.4.5 External walls

The external walls of a muffler can also be designed to have dissipative and reactive qualities. Transmission loss of an acoustic wave traveling through a wall is determined by the stiffness, damping, and mass of the wall. At frequencies lower than the natural frequency of the wall, the stiffness dominates the TL. At frequencies higher than the natural frequency, the mass of the wall dominates the TL. At frequencies near the natural frequency the mass, damping, and stiffness of the wall, all contribute similarly to the TL. In the low frequency region, the TL will decrease at 6 dB per octave. In the high frequency region the TL will increase at 6 dB per octave. Doubling the mass will additionally provide approximately 6 dB of TL in the high frequency range. Having a high stiffness, damping, and mass will all provide extra attenuation performance in the wall.

High frequency acoustic waves tend to cause more problems in wall structures, than lower frequencies. High frequency energy generation from the engine or flow can come in a couple of different forms. There are mechanical vibrations and acoustic waves that arise from the firing or blade pass frequency, and there are pulsations that arise from vortex shedding in the pipe. The vortex shedding happens when there is an obstruction in the flow. These high frequencies may excite the natural frequencies in the muffler and create vibration and noise.[33] In walls exposed to acoustic waves, the most efficient noise and vibration transfer happens at coincidence frequencies. These are frequencies at which the wavelength of the acoustic wave matches the wavelength of one of the bending modes in the wall. The lowest coincidence frequency for a given wall is known as the critical frequency, and it is given by Equation 1-55.[34] The effective wavelength of the wave traveling towards the wall can be changed by the angle at which the wave is traveling at relative to the wall. The result of this is that above the critical frequency, every angle of propagation has some frequency that is coincident to one of the wall bending modes. This causes the shell to radiate noise much more efficiently at these frequencies. Equation 1-56 shows the calculation of coincidence frequencies for a given wall.[34] These effects are especially important when the size of the duct is large and the walls are more compliant than they would be in a smaller sized muffler.

$$\omega_c = c^2 \sqrt{\frac{m}{D}} \tag{1-55}$$

$$\omega_{co} = \frac{\omega_c}{sin^2 \phi} \tag{1-56}$$

where m is the mass per unit length of the wall, D is the bending stiffness of the wall, ϕ is the angle of propagation of the acoustic wave, ω_c is the critical frequency, and ω_{co} is the coincidence frequency.

It is obvious how the noise can affect acoustic performance, but the ways in which the vibration can affect acoustic performance are less so. Walls that are not rigid will decrease the impedance mismatch that is used to reflect waves back to the source. This will allow more of the wave to be transmitted through each of the muffler components. Also the vibration can change the resonance frequencies of the chambers that it is present in, which will result in a shifting of transmission loss performance away from the frequency bands that were originally intended. Lastly this vibration noise is able to bypass muffler components, and re-enter the exhaust flow downstream of the muffler.[25] This vibration may also radiate noise back inside and outside of the shell. Shell noise may have a significant contribution to the overall noise radiation of the system. All of these effects when added together can cause a severe decrease in transmission loss performance at high frequencies.

There are a few techniques to dampen this vibration and noise. The simplest way to do this is to add mass to the walls. This can be done by making the walls thicker, or by double wrapping the tube which in effect makes the wall twice as thick. Adding mass to the walls will heighten the rigidity and inertia of the walls allowing for less vibration.[27] The double wrapping is generally more effective because there is typically a small airspace in between the walls which will add some measure of performance to the muffler.[35] Another technique to dampen the vibration is to add extra layers of damping materials to the outside of the shell. The two techniques that involve adding additional layers to the outside of the pipe are extensional and constrained layer damping. In extensional damping, a layer of damping material is added to the outside of the shell. As the shell deforms, energy is dissipated through tensioning and compression of the damping material.[33] Constrained layer damping involves adding a damping layer to the outside of the muffler, and then constraining that layer with another layer of metal. During vibration, both the base layer and the constraining layer bend transversely. The damping layer undergoes pure shear deformation while the two layers around it are bending. This shear deformation causes much more energy dissipation within the damping layer than the bending in the extensional damping treatment.[36] Price and Smith provide a couple of design considerations for this type of damping treatment. The thickness of the constraining layer should be about 25-50% of the thickness of the base layer, and the damping layer should be as thin as is feasibly possible to increase the shear in the material. Damping layers are typically made from rubbers or viscoelastic materials.[33] In extensional damping, the damping layer should be relatively stiff, while in constrained layer damping the damping layer should be relatively soft, and the constraining layer should be more stiff.[37]

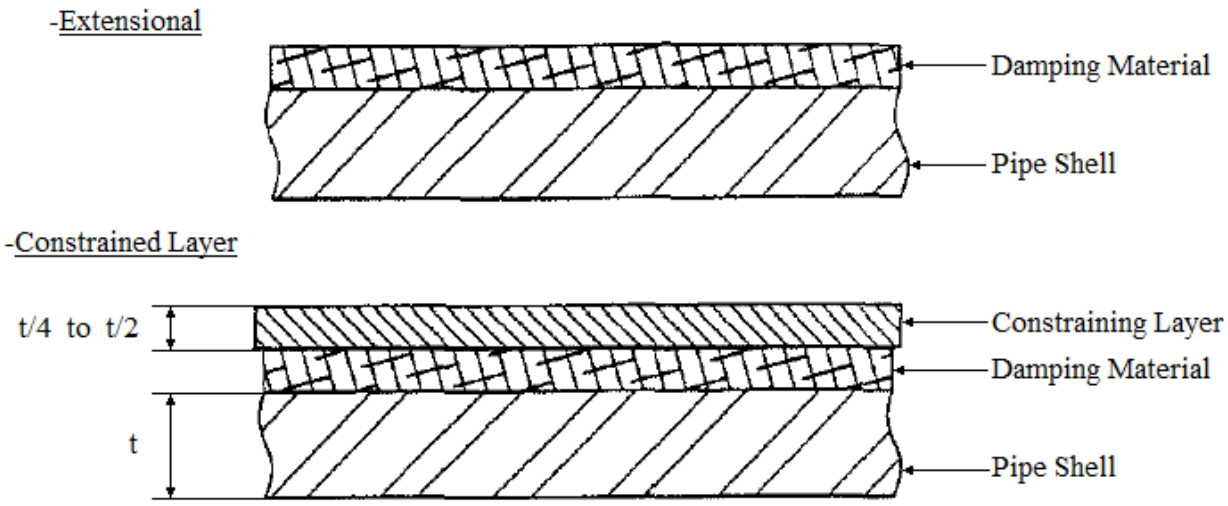

Figure 1.16: Illustrations of the extensional and constrained damping layer treatments.[33]

Typical damping materials are not practical for high temperature applications, because they have low melting and service temperatures. Commonly available damping materials that have high melting temperatures are silicon rubbers. Silicon rubber has a melting temperature of approximately 940°F and a maximum service temperature of approximately 600°F. Success has been had with higher temperatures, but the damping materials used tend to not be readily commercially available. When modeling a constrained layer damping treatment, care must be taken so that the mechanical properties of the damping layer are properly represented in the model.

2.0 VALIDATION OF PERFORMANCE EVALUATION TECHNIQUES

In order to cross check the performance testing and prediction procedures, measurements were made for mutual validation of testing procedures and FEA modeling of muffler performance. Three different muffler models were chosen. These muffler models will be referred to as models A, B, and C. Model A is the smallest model, and model C is the largest model. All three models were tested for NR and IL performance. Model A was also tested for TL performance. Each model was measured *in situ.* For this particular case *in situ* refers to the fact that the mufflers were not measured in lab conditions, but instead in a field with significant ambient noise and weather conditions. These models were then simulated in LMS Virtual.Lab Acoustics using similar acoustic and ambient conditions to those in the field test. The results from each test were compared and analyzed for agreement. The frequency range of interest is from 0 to 20 kHz, but due to computational limitations much lower frequency ranges were achieved. These frequency ranges differ by muffler model and are detailed in the simulation considerations section.

2.1 MEASUREMENT OF MUFFLER PERFORMANCE

Acoustic measurements were taken with either the Ono-Sokki Portable FFT Analyzer 3650 or a data acquisition program in Matlab. The data acquisition unit used with the Matlab code was the NI 9233 four channel dynamic signal acquisition module with the NI USB-9162 hi-speed USB carrier. The Matlab data acquisition code is included in Appendix B. For each muffler unit, a short time history was recorded at each measurement position. Then the power spectrum of the measurement was calculated using either the FFT program on the analyzer or a short user-written program in Matlab. If there appeared to be problems with the data, then another test was performed in which the problem was corrected. One to three minutes of collection in each position was considered sufficient to obtain the data needed. However, the time history files can grow to be very large, so the measurements were kept as short as possible to avoid excessive computation times.

2.1.1 Insertion loss (IL)

Insertion loss is measured with a single microphone. The microphone is placed outside the exhaust system. The sound pressure level output of the system is measured before and after the installation of the muffler. The system without the muffler is referred to as the reference system and is represented in Equation 1-25 by the subscript *r*. The muffled system is represented by the subscript *m*. For this experiment there was no exhaust system used. Instead a simple piping system was used. The details of this system are presented in the experimental setup and construction sections.

For IL measurement, the microphone was placed at four positions around the exit of the piping system or muffler. Each position had a linear distance of three feet from the outlet of the system, and a specified angle from the exit plane of the piping system or muffler. Figure 2.1 shows the four positions in which the measurements were taken for this particular experiment. The angles of microphone placement were 0°, 45°, 90°, and 100° relative to the exit plane. This measurement was made using one of two different methods. The first method was completed by using a single microphone and four different measurements. The second method was completed by using a single microphone and a single measurement in which the microphone moves to the four positions throughout the measurement. The first method was used at the site of the corporate sponsor. The second method was used at the University of Pittsburgh site. Measurements for insertion loss were taken once for the silenced system, and once for the reference system in which the muffler was replaced by a simple straight pipe.

The measurement field exceeded the specifications presented in section 4.1. This included keeping the field free of reflecting surfaces for at 100 foot radius around the outlet, and taking the measurements at a time when background noise and wind noise were at minimal levels in the field. Some testing equipment around the muffler exit was unavoidable, but was kept to a minimum. The background noise was measured during the test for reference purposes. If a significant, external noise source suddenly entered the field of measurement during the test, the measurement was be stopped and restarted after the source has passed. At times these noise sources included the honking of horns, car doors slamming, and loud engines on motorcycles. The test fields were relatively near to roads, and these noises were sometimes loud enough to interfere with the measurement. A wind screen was also used on the microphone during the test to reduce any signal noise due to the presence of wind.

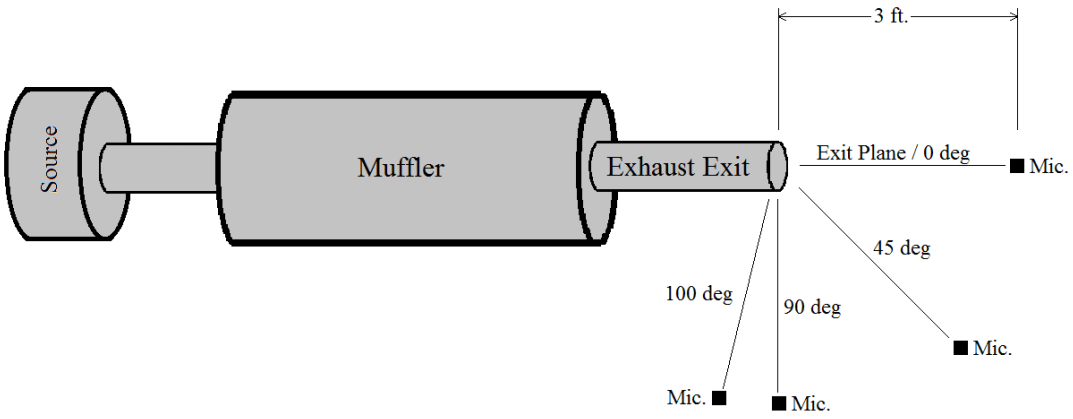

Figure 2.1: Microphone placements relative to muffler exhaust for insertion loss measurement

A measurement of the noise produced from shell vibration was also performed. This was done by placing the microphone at the approximate midline of the muffler at a distance of one inch from the shell. This close proximity allowed the noise from shell vibration to dominate the measurement. Knowing if significant noise radiates from the shell can prompt stricter design criteria for the shell walls. Since this measurement is made in the near field, it is not necessarily indicative of the noise that is radiated into the far field. However, this measurement can still be useful as an estimation despite being unable to produce an exact SPL value.

The acoustic wave source for this test will be white noise (random excitation) from speakers controlled by the spectrum analyzer. The true insertion loss of a muffler can only be determined by measuring the performance of the muffler in the exact system in which it will be installed. However, this measurement is only being taken for validation against LMS Virtual.Lab so measuring the IL in a real exhaust system is not necessary.

The following list is a short synopsis of the steps that were followed during the IL test. In step 4 the gains of the system are recorded. The gains in the microphone system need to be recorded so that the correct SPL may be calculated from the recorded data. The system gains in the speaker system need to be recorded so that the experiment can be repeated as closely as possible if need be. The background noise is recorded in step 2. If the background noise is almost as loud as the outlet noise from the muffler then the power output from the speakers needs to be raised. If this is not possible, then the test must be carried out and the results from the simulation must be post-processed using a noise floor, which will be explained in Section 2.4.1. Since only one microphone was used for all of the measurements, no calibration was necessary for the test.

Procedure:

1.) Choose and setup testing site according to guidelines in the microphone placement and testing environment section.
2.) Measure the background noise at the field of measurement.
3.) Check the system for clipping of data. Adjust gains and device input ranges accordingly.
4.) Record the output level of the speakers and the system gains.
5.) Measure the noise from shell vibration in the position specified in the microphone placement and testing environment section.
6.) Measure the sound pressure level at the positions specified in Figure 2.1.
7.) Average the SPL's together to obtain the averaged SPL for the system
8.) Repeat steps 6 and 7 for both the reference system and the silenced system.
9.) Use the sound pressure levels obtained to obtain the IL from Equation 1-25.

2.1.2 Noise reduction (NR)

Noise reduction is the measurement of the sound pressure level of a point upstream and downstream of the muffler, and is calculated by Equation 1-34. For the noise reduction test, the objective was to obtain a full noise reduction measurement of the muffler, and record sound pressure levels at different sections in the muffler. Since the inlet and outlet pipes have higher-order acoustic modes propagating within them, a spatial averaging of the SPL was necessary to determine the average noise reduction across the entire muffler. The Figure 2.2 shows the measurement scheme that was used on the inlet and outlet of the muffler to determine the averaged SPL. Each point in the figure represents a measurement position. The pressure spectra at these points are averaged to obtain an average pressure spectrum across the cross section of the pipe.

In order to obtain the SPL at a point inside the muffler, the microphones simply needed to be placed in a port. The measurement can be taken at one point, instead of several, because these measurements are only for comparison to the SPL from the LMS simulation at that point in the muffler. These measurements can also be used to calculate a loose estimate of noise reduction across certain components in the muffler.

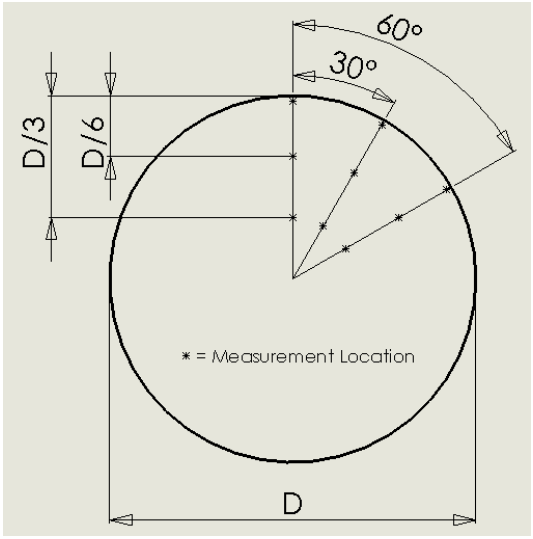

Figure 2.2: Measurement locations in cross section of muffler inlet and outlet

The following list is a short synopsis of the procedure involved in measuring noise reduction. All of the comments on the procedure that were made in relation to the insertion loss testing procedure in the last subsection apply here as well. Even though all the measurements made in this test are inside the piping system, a background noise measurement is still necessary because the background noise in the area will enter the muffler to a certain degree.

Procedure:

1.) Check measurement devices for clipping of data. Adjust gains and input ranges accordingly.
2.) Record all relevant gains and output levels in system.
3.) Record background noise in measurement area.
4.) Record SPL's upstream and downstream of the muffler using the measurement scheme in Figure 2.2.
5.) Average the values obtained from step 4 to obtain the averaged SPL
6.) Record SPL's at port locations in muffler.
7.) Determine the desired noise reduction using Equation 1-34 and the SPL's obtained from the previous steps.

2.1.3 Transmission loss (TL)

The measurement of TL was only performed on model A at the University of Pittsburgh. TL is a measurement of the incident and transmitted sound power from a muffler. Transmission loss is calculated by Equations 1-26 through 1-31 in the "Measurement of Acoustic Performance" section. Equation 1-26 is the definition of TL. Equations 1-27 through 1-29 deal with the calculation of the incident wave through the technique of wave decomposition. Equations 1-30 and 1-31 deal with the conversion of a power spectrum to the incident and transmitted power wave spectrums. These equations and the wave decomposition technique are detailed in the "Measurement of Acoustic Performance" section earlier in this document.

This method will be used to separate the incident wave from the reflected wave upstream of the muffler. Two microphones are placed upstream of the muffler. The spectral density at each point is measured from the microphones. These spectral densities are then applied to the aforementioned equations to obtain the incident wave spectral density. The spacing between the microphones determines the frequency range over which the measurement is valid. To cover the frequency range of interest three different microphone spacings will be needed. Applying Equation 1-33 we arrive at the ranges shown in Table 2.1. Since the limits are dependent on the flow rate, and the speed of sound, these limits are only valid for zero mean flow, one atmosphere and seventy degrees Fahrenheit. However there is enough overlap between the ranges that only the upper and lower limits of the entire range will be affected. The smallest spacing was limited by the size of the microphones, and the largest spacing was limited by the practicality of the measurement setup. The wave decomposition method relies largely on the phase difference of the measured wave at each position in the spacing. Therefor both measurements for a given microphone spacing must be taken simultaneously.

Table 2.1: Microphone spacing frequency ranges for decomposition method

Spacing	Lower Freq. Limit	Upper Freq. Limit
25.2 in.	26.9 Hz	214.9 Hz
3.24 in.	194.5 Hz	1556.0 Hz
0.75 in.	902.5 Hz	7220.0 Hz

An anechoic termination is used on the termination of the piping system. This termination reduces the reflection from the pipe termination as much as possible. This reflection reduction allows the

spectral density of the transmitted wave to be measured directly from the downstream pipe with one microphone, and calculated using Equation 1-31. Details on the concepts and construction of an anechoic termination can be found in the experimental setup section (2.2).

For both the incident and transmitted wave calculation, all measurements at the inlet and outlet of the pipe must follow the same type of spatial averaging scheme as presented in Figure 2.2. This can be somewhat challenging for the incident wave since both microphones being used must be moved to the same position simultaneously. However it is necessary so that higher order acoustic modes are taken into account during the calculations.

The following list is a short synopsis of the procedure for measurement of the TL of a muffler. In step 4, the microphone spacings that are referred to are those in Table 2.1. Step 10 says to splice the incident waves together. Since each spacing is only valid for a certain frequency range, the entire incident wave must be constructed from the three different measured waves from each bandwidth given in Table 2.1 and at each circumferential position on the pipe. Each measured wave will have its valid range excised and then inserted into the total incident wave.

Procedure:

1.) Check measurement devices for clipping of data. Adjust gains and input ranges accordingly.
2.) Record all relevant gains and output levels in system.
3.) Record background noise in measurement area.
4.) Record data in the nine microphone positions along the cross section of the pipe for both microphones upstream of the muffler.
5.) Repeat step four for each microphone spacing.
6.) Record data in the nine microphone positions along the cross section of the pipe downstream of the muffler.
7.) During each measurement make sure that microphone is moved along the cross section of the pipe. The microphone should be moved so that measurement time is split evenly across the positions shown in Figure 2.2.
8.) Determine the power spectral densities of each measurement.
9.) Calibrate the two upstream measurements against each other using the procedure in Equations 1-35 through 1-39.
10.) Using Equation 1-27 determine the incident wave from each of the upstream measurements.
11.) Splice together incident waves from same placement along perimeter so that each measurement is only used in its intended frequency range indicated in Table 2.1.

12.) Take the mean of the incident waves and then take the mean of the downstream measurements. This should be done using linear quantities instead of the logarithmic (dB) quantities.
13.) Using the downstream measurement as the transmitted wave, calculate the incident and transmitted sound powers using Equation 1-31.
14.) Plug the calculated sound powers into Equation 1-26 to determine the TL.

2.1.4 Conversion of test results

The microphones used for field tests take an acoustic pressure and turn it into and electrical voltage. This voltage is then captured by a data acquisition device, and recorded. For all of the tests except the model A IL test, the spectral analyzer was available so the voltage could be recorded in the frequency domain on a logarithmic scale. For the model A IL test, a time history was taken in MATLAB and then a Fourier analysis was performed in MATLAB to obtain the voltage in the frequency domain. The code for the time history analysis is included in Appendix B. The following equations take a voltage in dBV_{rms}, convert it to a linear scale, convert it to an acoustic pressure, and then convert the linear acoustic pressure to decibels. Equation 2-1 was not necessary for the model A IL test since the voltage was never recorded on a logarithmic scale.

$$V(f) = 10^{dBV_{rms}(f)/20} \tag{2-1}$$

$$p(f) = \frac{V(f)S}{G} \tag{2-2}$$

$$P_s(f) = 20Log_{10}(p(f)) + 94 \tag{2-3}$$

where f is the frequency, dBV_{rms} is the output from the spectral analyzer, V is the voltage from the microphone, p is the acoustic pressure, S is the microphone sensitivity in units of pressure per voltage, G is the gain from any signal conditioner in the system, and P_s is the power spectrum. This conversion from voltage to acoustic pressure will allow for comparison to the FEA results, which are calculated is acoustic decibels.

2.2 EXPERIMENTAL SETUP

This section will go into the details of the two different testing sites that were constructed to test the three different muffler models. The first testing site was at the University of Pittsburgh. At this site the IL, NR, and TL of muffler model A were measured. The other testing site was on the industrial sponsor's office complex. At this site the NR and IL of muffler models B and C, which were considerably larger, were measured. Multiple tests were taken at both sites.

2.2.1 Pittsburgh site

The Pittsburgh test site is where the smallest muffler was tested. The setup consisted of inlet and outlet pipes where measurements were taken, muffler model A, speakers, a coupling between the speakers and the pipe, the measurement equipment, and an anechoic termination for measurement of TL. All of these pieces are shown together and assembled in Figures 2.3 and 2.4. The only piece not mentioned yet is the reference pipe required for the measurement of IL. The reference pipe is just a straight PVC pipe that replaces the muffler in the piping system to create the reference system.

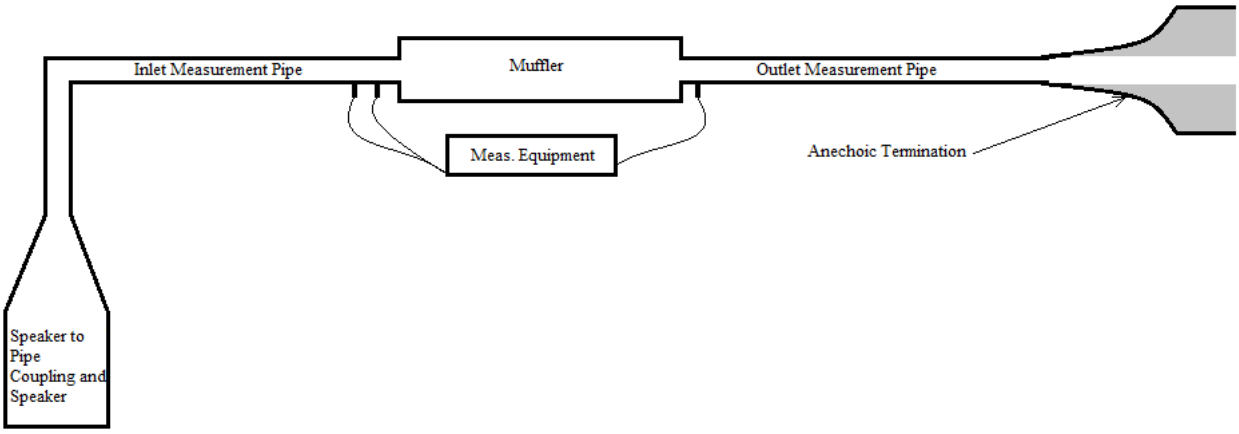

Figure 2.3: Top view of Pittsburgh testing site setup. Schematic not to scale

Figure 2.4: Photograph of testing Pittsburgh test site

The entire setup, with the exception of the muffler, was constructed from materials that are readily available at hardware stores and on industrial supply websites. The speaker to pipe coupling was made from a medium density particle board. The particle board pieces were joined together using a combination of wood screws and wood glue. The seams between the boards were then sealed using a silicone caulk to prevent acoustic leakage. A PVC pipe was then placed in the end of the coupling and attached using an epoxy and the silicone caulk. The inlet and outlet pipes were made from PVC pipe and PVC flanges that were joined using PVC cement. Then holes were drilled in the pipes at appropriate locations so that measurements could be taken. These holes were filled with modeling clay when not being used. The pipes, the muffler, and the speaker to pipe coupling were all joined together using bolts and silicone caulk. The silicone caulk acted as a substitute for a flange gasket.

The Anechoic Termination was built according to the dimensions and guidelines recommended in Appendix D of British Standard 0848-02:1985. Figure 2.5 shows the schematic that provides the guidelines for the construction of the termination from the standard. The frame of the anechoic termination was made from sheet steel. The sheet steel was cut and rolled into cones with different expansion ratios. These cones were tack welded closed and then tack welded together. The frame was then welded to a steel flange. The seams were then sealed with epoxy. The entire structure was wrapped in duct tape to help dampen any ringing that might result from subjecting the sheet steel to acoustic and vibrational excitation. Open cell foam was used as the dissipative material in the termination instead of mineral wool. The perforated metal was not needed since the foam was able to hold its own shape within the termination. The dimensions of the anechoic terminations are shown in detail in Appendix A. The anechoic termination is only need for the measurement of TL.

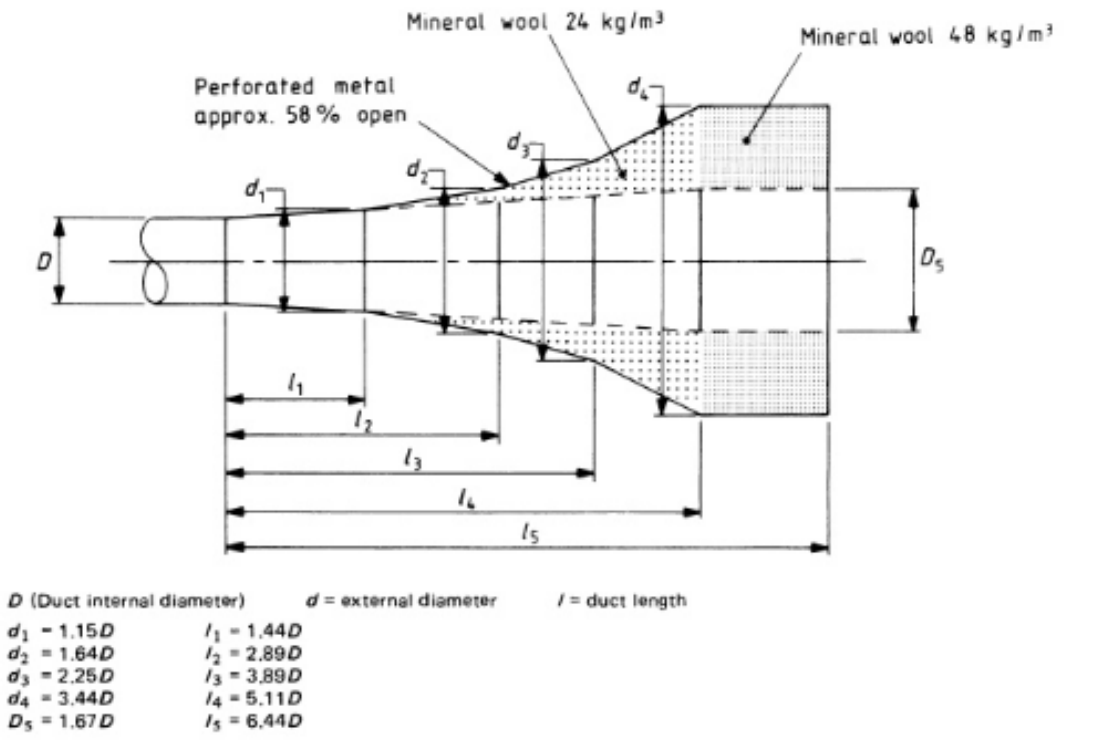

Figure 2.5: Construction guidelines for an anechoic termination[38]

2.2.2 Corporate sponsor site

The test site at the complex of the corporate sponsor was similar to the test site in Pittsburgh. At this site the two larger mufflers were tested for performance. A few key changes were made due to the size of muffler models B and C (Major dimensions 18.75'L x 4.5'D and 32'L x 7.9'D respectively). The reference pipes and mufflers were too large and heavy to be switched in and out of the system. Instead, the reference pipes and mufflers were setup in separate systems. Since there was only one set of speakers and four systems (two mufflers and two reference pipes), one speaker to pipe coupling was made for each system. These couplings were attached permanently to each system, and then the speakers were attached to the coupling when the test was being performed. This helped to reduce the time spent breaking down and setting up between tests. The speakers were moved between setups on a pallet using a forklift. Outlet pipes were not fabricated due to time and cost restrictions. The measurements that would normally be taken inside the outlet pipe were instead taken just inside the flange of the muffler outlet. No anechoic termination was needed since only NR and IL were measured. The mufflers, inlet pipes, and reference

pipes were all made from carbon steel. The speaker box and speaker to pipe couplings were both fabricated from plywood and wood screws. The seams in the plywood fabrications were sealed using an insulating foam sealant. The general organization of the measurement field is shown in Figure 2.6. Figure 2.7 shows the measurement setup for muffler model B.

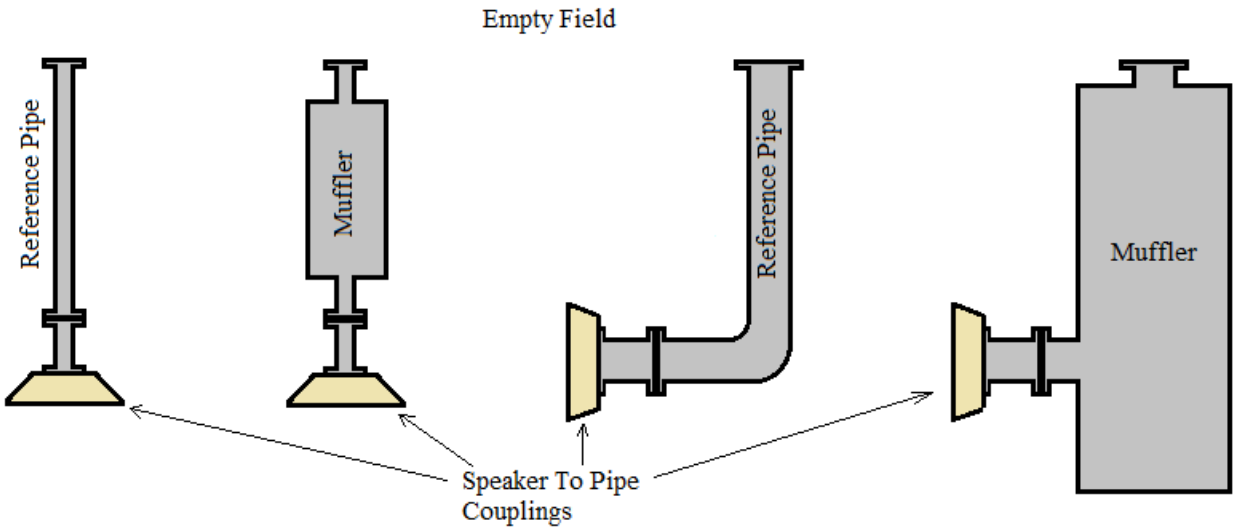

Figure 2.6: Top view of measurement field at corporate sponsor's compound. Schematic not to scale

Figure 2.7: Corporate site measurement setup of mid-size muffler model

2.3 MATHEMATICAL FORMULATION OF FINITE ELEMENT MODEL

2.3.1 Finite element formulation

The finite element formulation of an acoustic system starts with the Helmholtz equation. The Helmholtz equation is a simplification of the plane wave equation (Equation 1-15) that is obtained by assuming that the solution to the wave equation is separable. The homogeneous Helmholtz equation is given as:[39]

$$\nabla^2 p + k^2 p = 0. \tag{2-4}$$

As discussed in Section 1.2.2, the Galerkin method (Equation 1-24) is applied directly to the Helmholtz equation to obtain the weighted residual formulation of the Helmholtz equation. This equation is also known as the weak formulation of the Helmholtz equation, and is given as:[40]

$$\int_V (\nabla \tilde{p} \nabla p) dV - \omega^2 \int_V \left(\frac{1}{c^2} \tilde{p} p\right) dV = \int_V (j\rho_0 \omega \tilde{p} q) dV - \int_\Omega (j\rho_0 \omega \tilde{p} \vec{v} \vec{n}), \tag{2-5}$$

where V is the fluid domain, Ω is the boundary surface, $\tilde{p}$ is the weighting function, q is the acoustic source distribution, $\vec{n}$ is the unit normal vector, and $\vec{v}$ is the velocity vector .

Next, an approximation of the field variable is made. This was the procedure discussed in Section 1.2.1 in which the field variable of interest is estimated using the shape function N. In this case the field variable is acoustic pressure. The field variable approximation for an element is given as:[5]

$$p = \sum_i N_i p_i \ , \tag{2-6}$$

where i refers to the nodes within the element. This is the approximation that turns the model from a continuous system into a discrete system.

Using this approximation, the governing equations of the acoustic finite element model are obtained. Equation 2-7 shows the finite element model. Equations 2-8 through 2-11 show the formulation of the finite element model from the terms of the weak formulation of the Helmholtz equation. The acoustic stiffness and mass matrices (in Equations 2-8 and 2-9 respectively) are derived from the left side

of Equation 2-5. Excitation and boundary condition vectors (Equations 2-10 and 2-11 respectively) are derived from the right side of Equation 2-5. These equations are as follows:

$$([K] + j\omega[C] - \omega^2[M])\{p_i\} = \{Q_i\} + \{V_{ni}\} + \{P_i\}\,, \tag{2-7}$$

$$\{\tilde{p}_i\}^T[K]\{p_i\} = \int_V (\nabla\tilde{p}\nabla p)dV\,, \tag{2-8}$$

$$-\omega^2\{\tilde{p}_i\}^T[M]\{p_i\} = -\omega^2\int_V \left(\frac{1}{c^2}\tilde{p}p\right)dV\,, \tag{2-9}$$

$$\{\tilde{p}_i\}^T\{Q_i\} = \int_V (j\rho_0\omega\tilde{p}q)dV\,, \tag{2-10}$$

$$\{\tilde{p}_i\}^T\{V_{ni}\} + \{\tilde{p}_i\}^T\{P_i\} - j\omega\{\tilde{p}_i\}^T[C]\{p_i\} = -\int_\Omega (j\rho_0\omega\tilde{p}\vec{v}\vec{n})\,, \tag{2-11}$$

where K is the stiffness matrix, C is the damping matrix, M is the mass matrix, Q is the excitation vector, V_n is the normal velocity boundary condition vector, and P is the pressure boundary condition vector.

2.3.2 Boundary conditions

The general boundary condition for the Helmholtz equation is known as the impedance boundary condition. The impedance boundary condition is determined by specifying an acoustic impedance at the boundary of the system. The impedance boundary condition is given by:[39, 41]

$$Z(\omega) = \frac{p}{v_n}\,, \tag{2-12}$$

where v_n is the velocity normal to the boundary. This boundary condition can be satisfied by specifying an impedance, a pressure, or a normal velocity on the boundary.

Two special cases of Equation 2-12 that are commonly used in finite element simulations of mufflers are the rigid boundary: [41]

$$Z = \infty, \tag{2-13}$$

and the matched impedance boundary:

$$Z = Z_0 = \rho_0 c_0 \, . \tag{2-14}$$

The rigid boundary condition is generally used to model the shell of the muffler. The rigid boundary condition defines a surface that perfectly reflects the pressure wave back into the acoustic cavity. This condition is created by setting the normal velocity at a node equal to zero. The matched impedance boundary condition is used in two instances. This boundary condition produces no reflections at a boundary, and can be used to model the anechoic termination needed for the simulation of TL. This boundary condition also satisfies the Sommerfield radiation condition,[40] and can be used to model the free propagation of waves needed for the simulation of NR and IL. There are several more advanced techniques that have been developed that better approximate the anechoic termination and the free propagation of acoustic waves, however, they will not be covered in this paper. These techniques are explained in detail in reference [42]

2.4 SIMULATION CONSIDERATIONS

2.4.1 Noise floor

When not measuring in lab conditions, ambient noise can be very high at certain frequencies. Even in "quiet" environments, ambient noise tends to have high-level low-frequency content. When this is coupled with the fact that reactive mufflers produce high attenuation at low frequencies, it is easy to see how ambient noise can greatly contaminate or even dominate muffler performance measurements at low frequencies. FEA models of mufflers do not have this ambient noise inherently present the same way that a field measurement does. In order to compare FEA simulations to field measurements, the ambient noise from the field must be recorded, and then added into the data from the simulation. This can be done by simply converting the pressures of the simulation and the background noise measurement to a linear scale (if they are already in dB form), adding them together, and then converting back to a logarithmic scale.

This procedure will be referred to as "applying a noise floor," and is only applicable to points that are near, at, or past the outlet of the exhaust system. This is because the ambient noise measured in the field will only be similar to the ambient noise at the outlet of the muffler or inside the muffler just past the outlet. Applying a noise floor to other measurements earlier in the exhaust system is not necessary since the noise levels at these points are generally high enough to dominate the measurement.

2.4.2 Simulation input

In order for the application of the noise floor to have the desired effect, the outlet SPL from the FEA model and the outlet SPL from the field tests must have the same magnitude relative to the ambient noise. To accomplish this, the acoustic pressure at the inlet of the muffler during the field test must be used as the acoustic pressure at the inlet to the FEA model. The input pressure is applied to the inlet as the excitation vector, Q, in the finite element model of Equation 2-7. To achieve the same inlet acoustic pressures, the acoustic pressure from the fields test was recorded and converted into acoustic intensity. The higher order acoustic mode excitation boundary condition in LMS Virtual.Lab requires acoustic intensity as its input. Acoustic intensity can be calculated from recorded acoustic pressures using Equation 2-15:[43]

$$I = \frac{\hat{p}^2}{2\rho c} = \frac{p_{rms}^2}{\rho c} \tag{2-15}$$

Equation 2-15 is for the case of a plane wave traveling in the free field. While this was not the case of the wave that was measured, there were several different methods that were attempted to calculate the acoustic intensity. This method produced the most agreement between the measured SPL at the inlet and the simulated SPL at the inlet in the FEA model.

2.4.3 Frequency range

The Nyquist-Shannon sampling theorem states that in order for a frequency to be uniquely determined, the wave must be sampled at least twice per cycle.[44] This applies to both temporal and spatial sampling. The two samples per wavelength rule is a theoretical limit, and in reality much more samples are needed for sufficient accuracy. In FEA, the spacing of the nodes is very similar to a spatial sampling of the

domain. The node spacing is determined by element size. In this study, it was considered sufficient for good results to have four elements per wavelength.

Each of the muffler models differed greatly in size, and as a result the frequency ranges that were achievable also differ greatly. The FEA model size or mesh size is determined by two factors; the domain size and the element size. As the domain gets larger, so must the elements in order to maintain the computational cost. Taking the Nyquist-Shannon theorem into account, for a given computational cost, larger domains have smaller achievable frequency ranges. Despite having a very capable desktop to perform the simulations, the following were the maximum frequency ranges achievable for this study. The approximate maximum frequency that was achieved for each muffler is listed in Table 2.2 along with the major dimensions of each muffler. Since the NR and IL were measured from 0-20 kHz, the simulation maximum frequency ranges will be the limiting range in the validation. However, for the TL of model A, Table 2.1 shows that TL measurement was only valid from 26.9 Hz-7220 Hz. This will be the limiting range in the TL validation.

Table 2.2: Approximate maximum simulation frequencies and dimensions for the three muffler models

Model	Diameter	Length	Max. Freq.
A	1.2 ft.	5 ft.	9000 Hz
B	4.5 ft.	18.75 ft.	5000 Hz
C	7 ft.	32 ft.	3000 Hz

2.4.4 Fluid and catalyst modeling

In the FEA simulation, the fluid domain was modeled as Nitrogen. Nitrogen was considered to be a sufficient approximation to air. Data for Nitrogen, as well as many other fluids and gases, is available on the NIST website (http://webbook.nist.gov/chemistry/fluid/). The approximate temperature inside the muffler during the field test was used as the temperature for the Nitrogen in the FEA simulation.

The modeling of catalyst elements is covered in Section 1.3.4. The catalyst is modeled as a fluid with complex speed of sound and density. The complex fluid properties introduce damping into the system. This damping models the dissipative properties of the catalyst. The complex speed of sound and density can be calculated using Equations 1-32 through 1-39.

2.4.5 Atmospheric absorption

Most muffler models are small enough that atmospheric absorption may be neglected for audible frequencies. However, since the muffler models considered in this study are much larger than many mufflers, absorption can become a significant factor in the attenuation properties of the muffler. This is especially true for higher frequencies. Just like with the catalyst, absorption may be introduced by adding an imaginary component to the speed of sound and the density of the fluid. Damping is a modeling parameter that can be adjusted to improve model agreement. However, the levels of damping should be verified experimentally or taken from previous research. A modest damping of .05% was introduced to simulations of muffler models B and C (the two larger models). However, this is only an estimation since a standard for acoustic absorption in air could not be found in literature.

2.5 RESULTS OF VALIDATION

2.5.1 Noise reduction and internal sound pressure levels

NR was measured for all three models. As stated in the testing methodology, the NR was measured at the inlet and outlet of the muffler models. These NR measurements were also accompanied by measurements of the SPL at specific points inside the muffler. Both the NR and the SPL's at these points were simulated in the LMS Virtual.Lab software. The comparison of the measurements and the simulation for all three muffler models is presented below.

2.5.1.1 Model A Figures 2.8 through 2.11 show the comparisons of SPLs at different measurement points in the muffler. Figures 2.12 through 2.14 show the noise reduction between the different measurement points. Figure 2.15 shows the NR across the entire muffler. An analysis of all of the results is included in the discussion (Section 2.6).

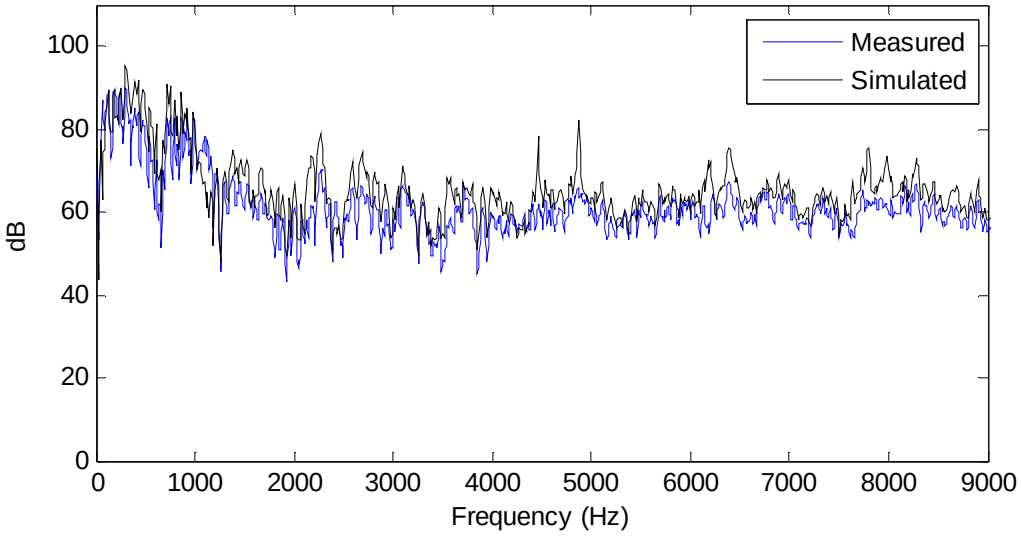

Figure 2.8: Comparison of SPLs at inlet for model A

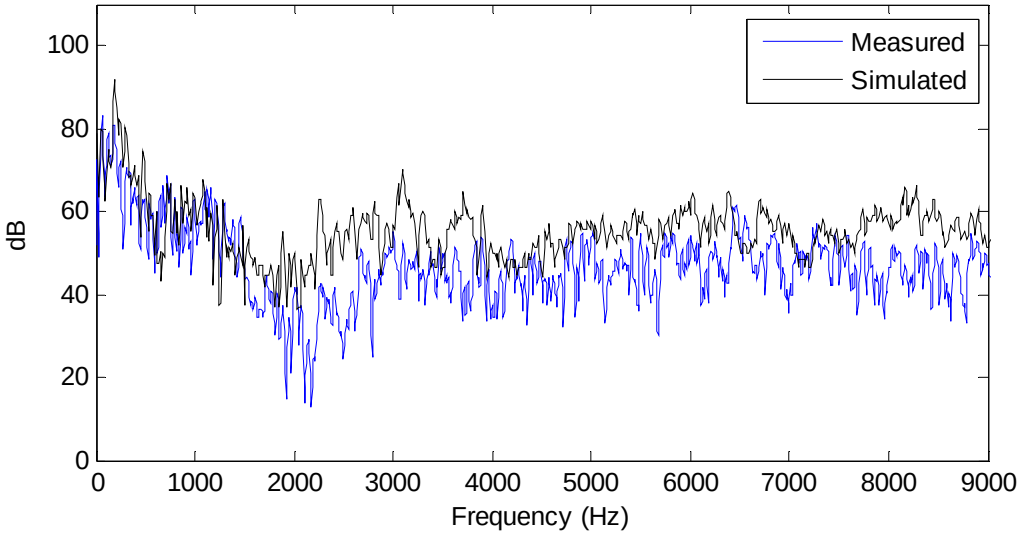

Figure 2.9: Comparison of SPLs at a point before catalyst for model A

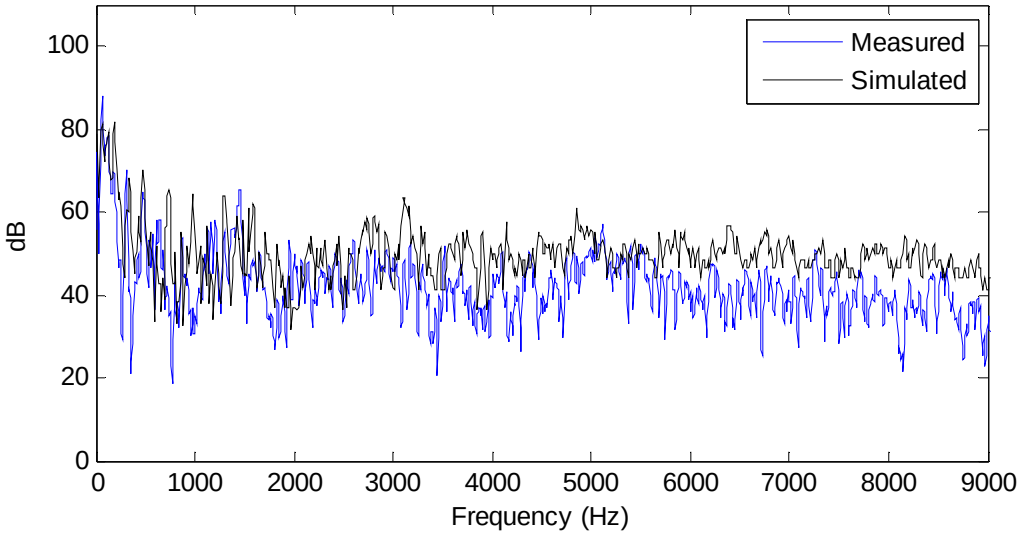

Figure 2.10: Comparison of SPLs at a point after the catalyst for model A

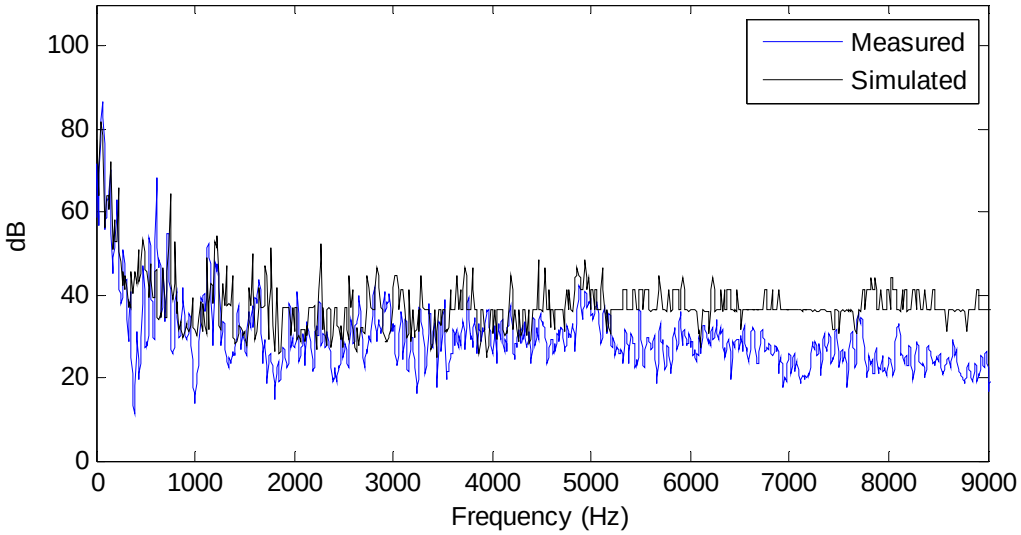

Figure 2.11: Comparison of SPLs at outlet for model A

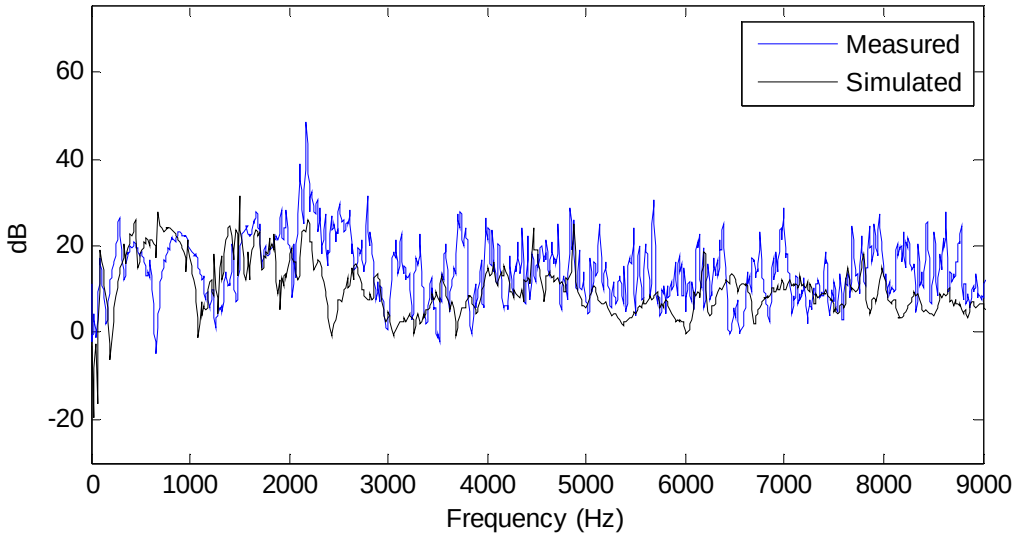

Figure 2.12: Comparison of NR between inlet and point before catalyst for model A

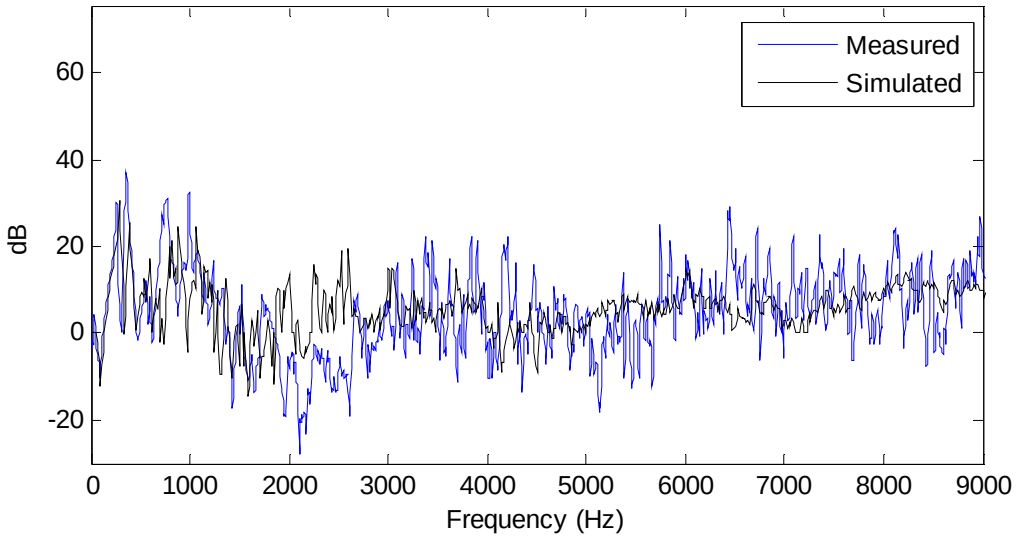

Figure 2.13: Comparison of NR between point before and point after catalyst for model A

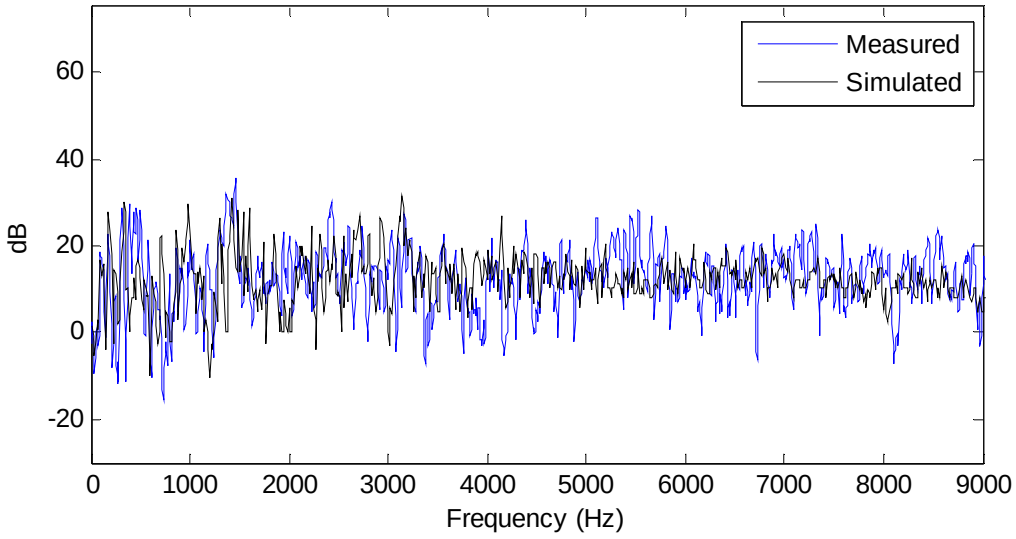

Figure 2.14: Comparison of NR between point after catalyst and outlet for model A

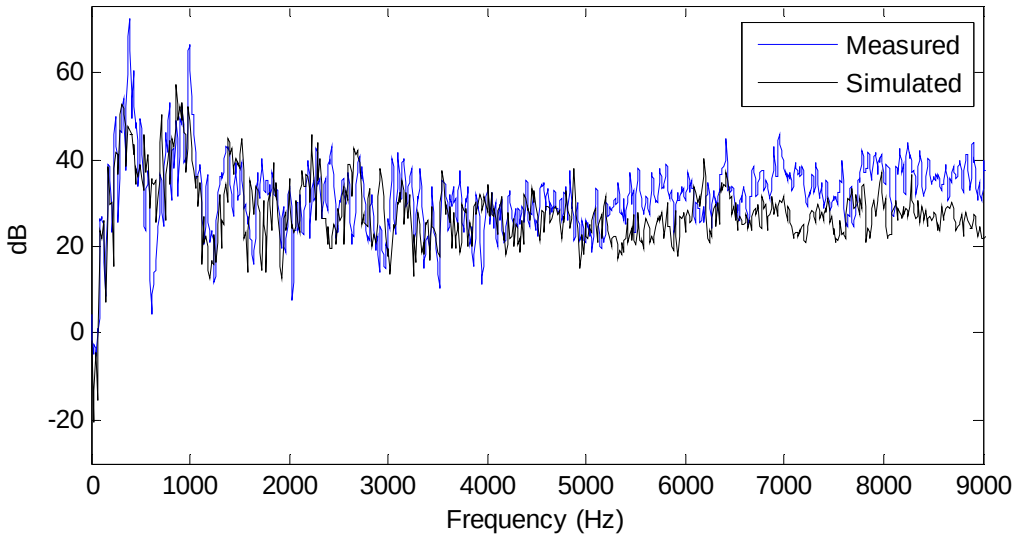

Figure 2.15: Comparison of NR over entire muffler for model A

2.5.1.2 Model B Figures 2.16 through 2.20 show the comparisons of SPLs at different measurement points in the muffler. Figures 2.21 through 2.24 show the noise reduction between the different measurement points. Figure 2.25 shows the NR across the entire muffler. An analysis of all of the results is included in the discussion (Section 2.6).

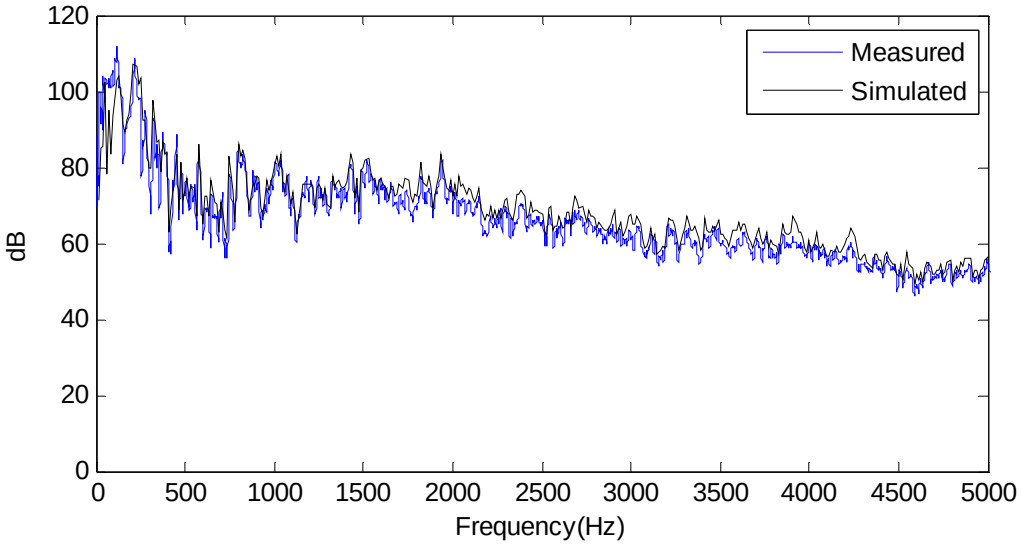

Figure 2.16: Comparison of SPLs at inlet for model B

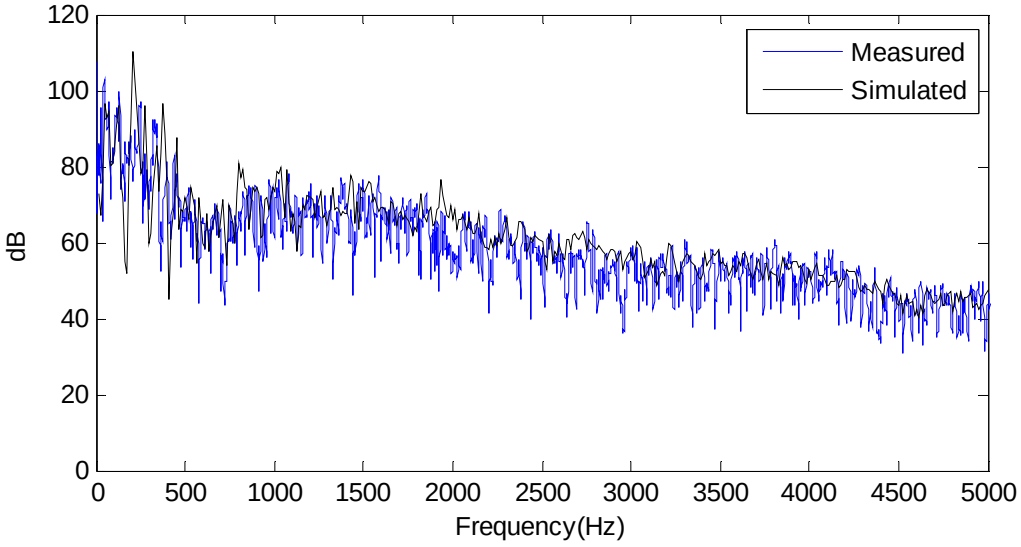

Figure 2.17: Comparison of SPLs before catalysts for model B

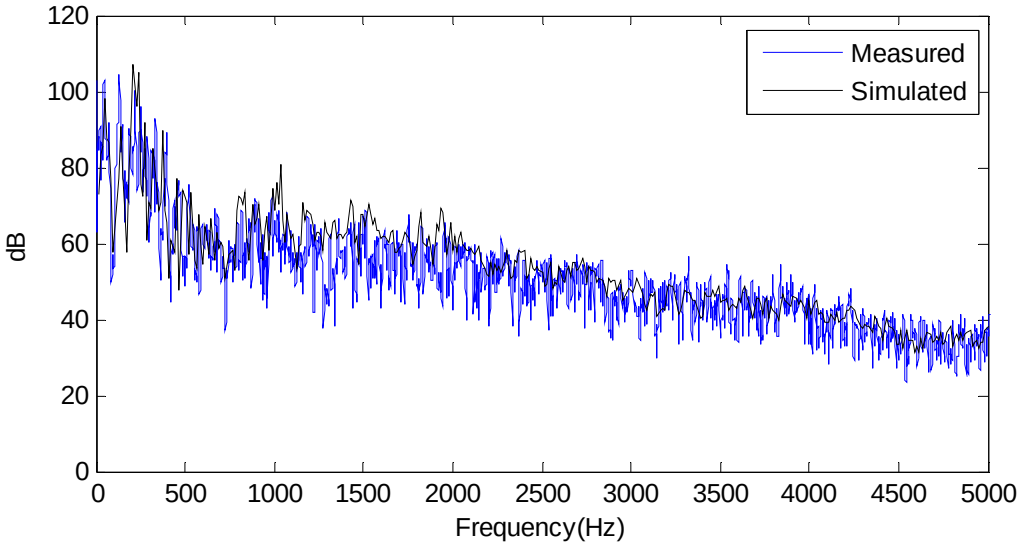

Figure 2.18: Comparison of SPLs after catalysts for model B

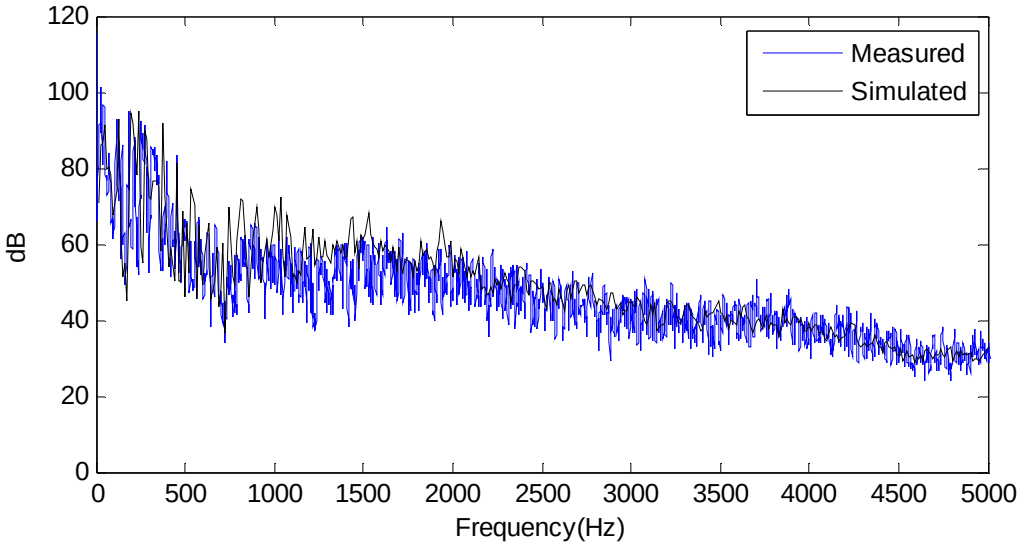

Figure 2.19: Comparison of SPLs in chamber 3 for model B

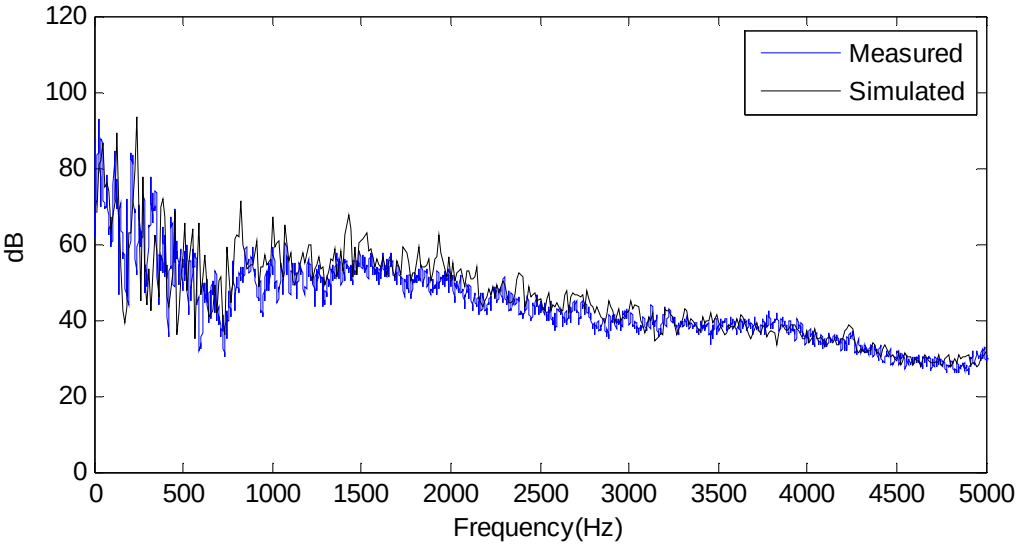

Figure 2.20: Comparison of SPLs at outlet for model B

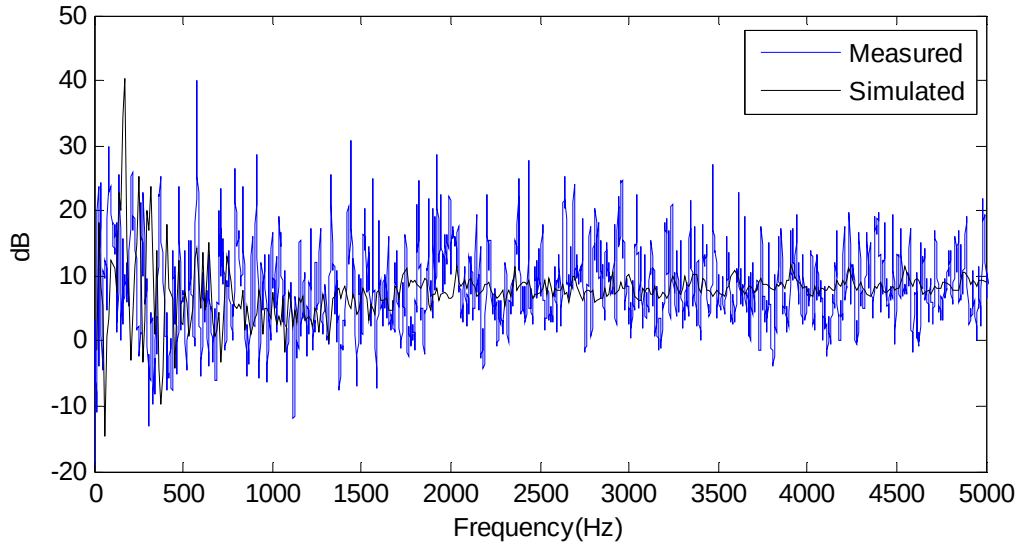

Figure 2.21: Comparison of NR between inlet and point before catalysts for model B

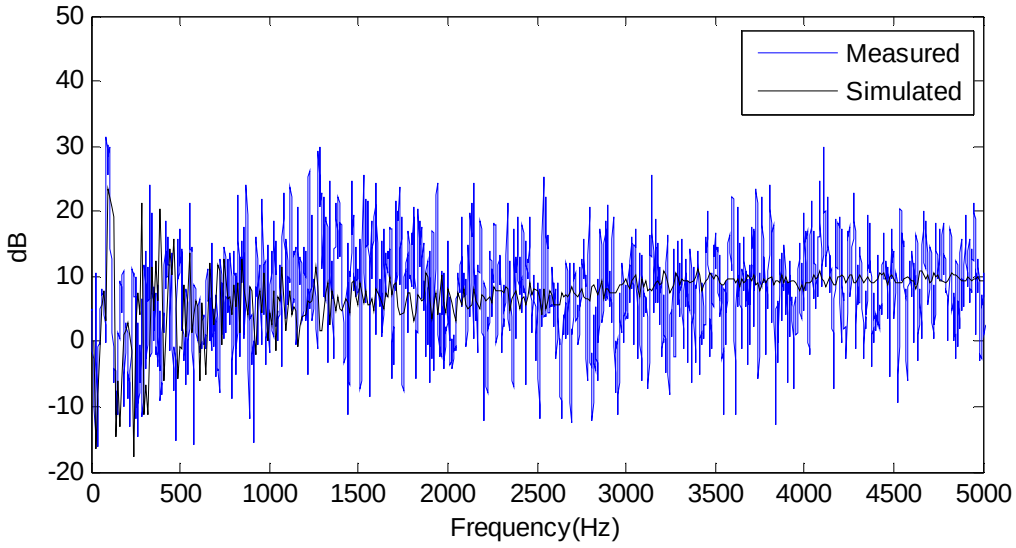

Figure 2.22: Comparison of NR between point before and point after catalysts for model B

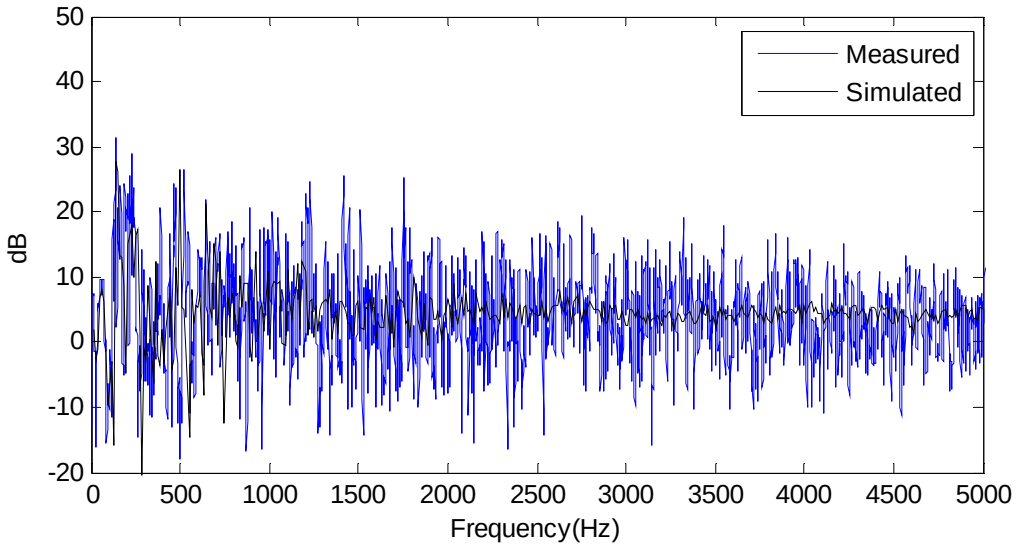

Figure 2.23: Comparison of NR between point after catalysts and chamber 3 for model B

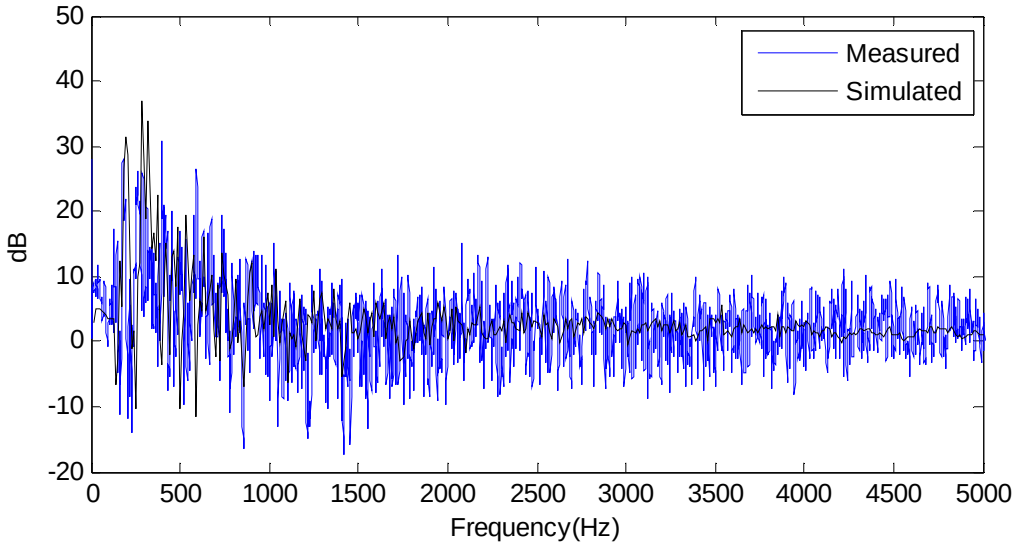

Figure 2.24: Comparison of NR between chamber 3 and outlet for model B

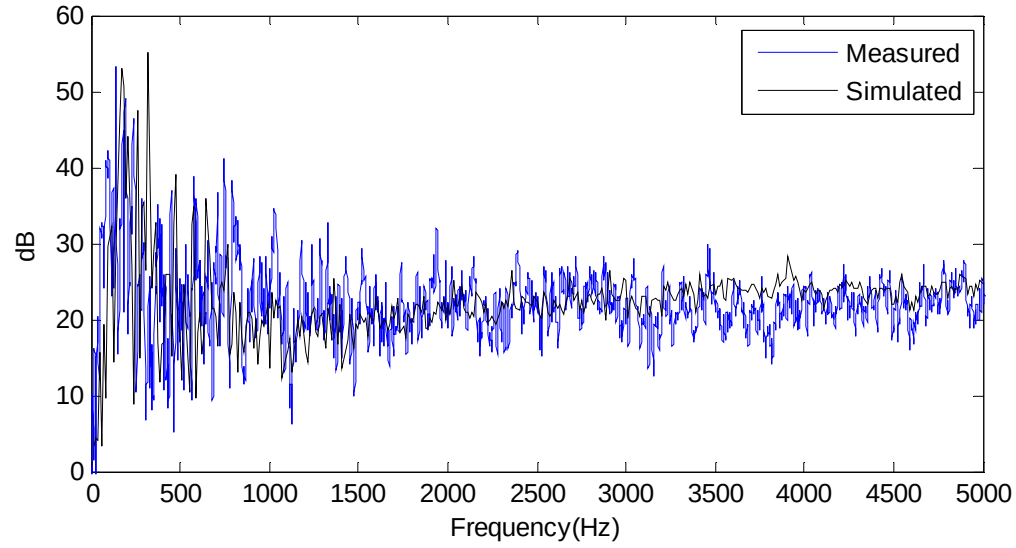

Figure 2.25: Comparison of NR over entire muffler for model B

2.5.1.3 Model C Figures 26 and 27 show the comparisons of SPLs at the inlet and the outlet of the muffler. Figure 28 shows the NR across the entire muffler. There were no internal measurements made for Model C. An analysis of all of the results is included in the discussion (Section 2.6).

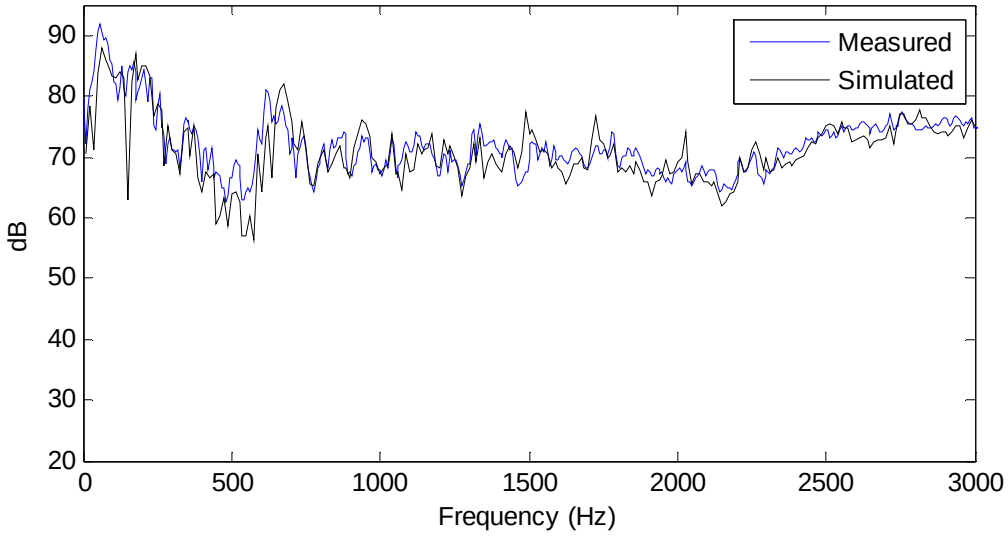

Figure 2.26: Comparison of SPLs at inlet for model C

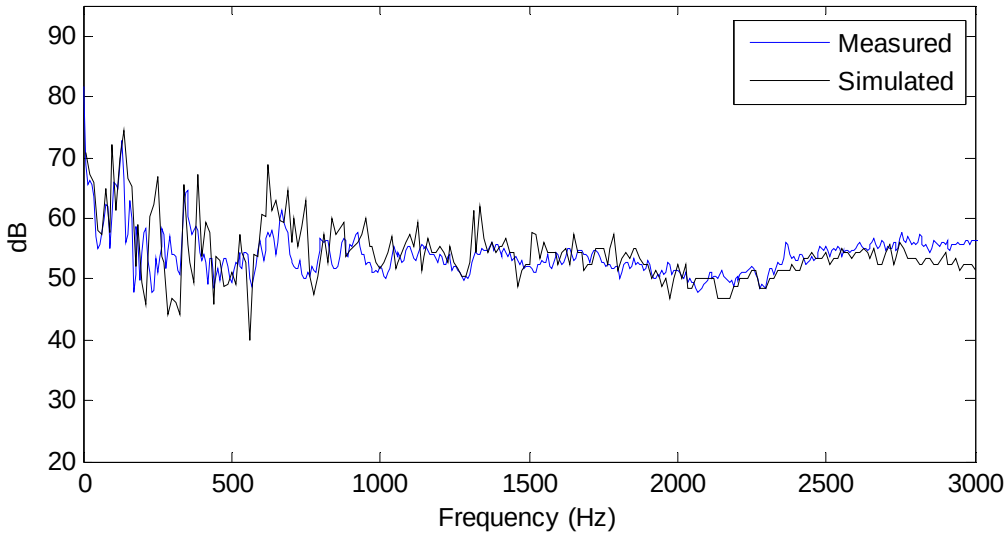

Figure 2.27: Comparison of SPLs at outlet for model C

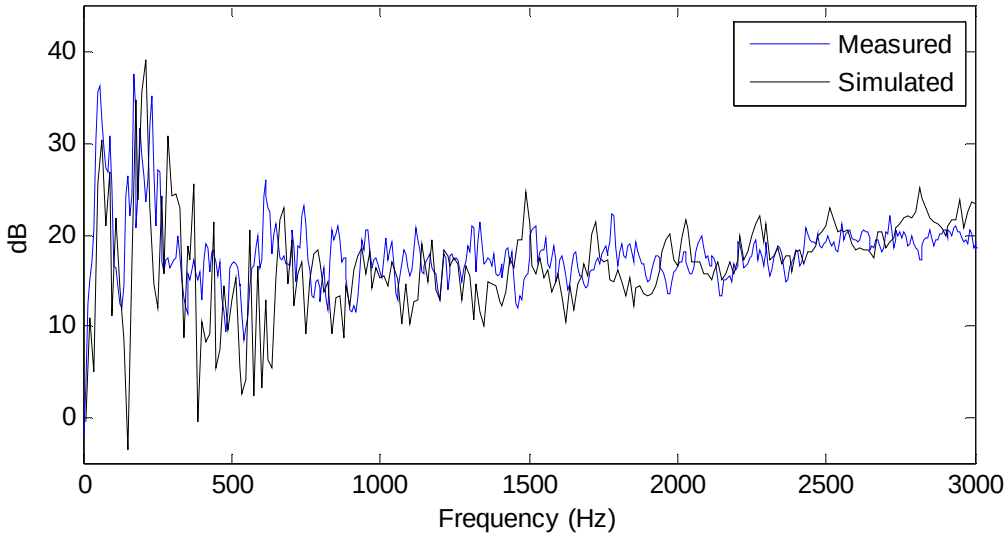

Figure 2.28: Comparison of NR over entire muffler for model C

2.5.2 Insertion loss and external sound pressure levels

IL was measured for all three models. As stated in the testing methodology, the IL was calculated using SPLs measured in the field outside of the piping systems for the muffled and reference system. Both the muffled and the reference systems were simulated in the LMS Virtual.Lab software. The comparison of the measurements and the simulation for all three muffler models is presented below.

2.5.2.1 Model A Figures 2.29 and 2.30 show the comparisons of SPLs for the muffled and reference systems respectively. Figure 2.31 shows the IL of the model A. An analysis of all of the results is included in the discussion (Section 2.6).

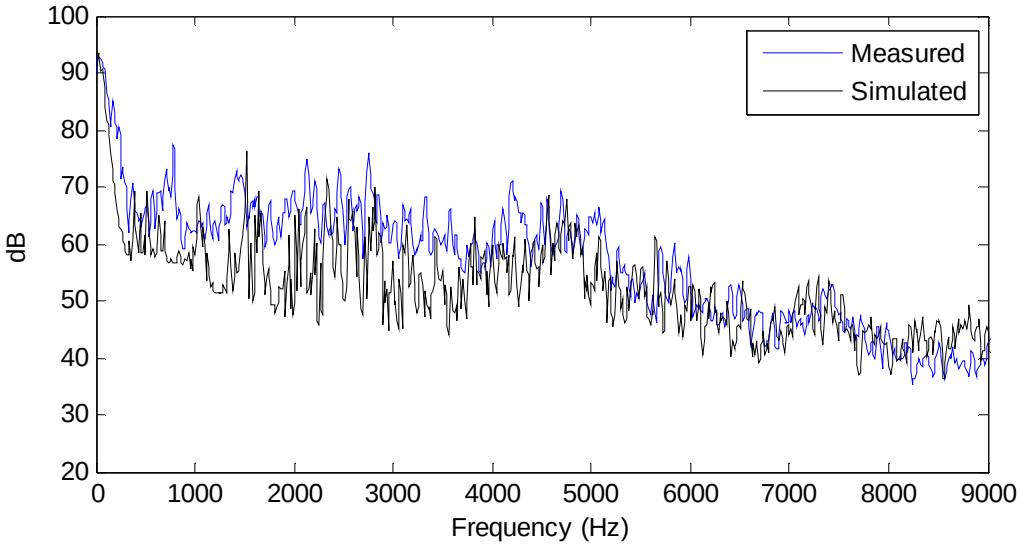

Figure 2.29: Comparison of SPLs of muffled system for model A

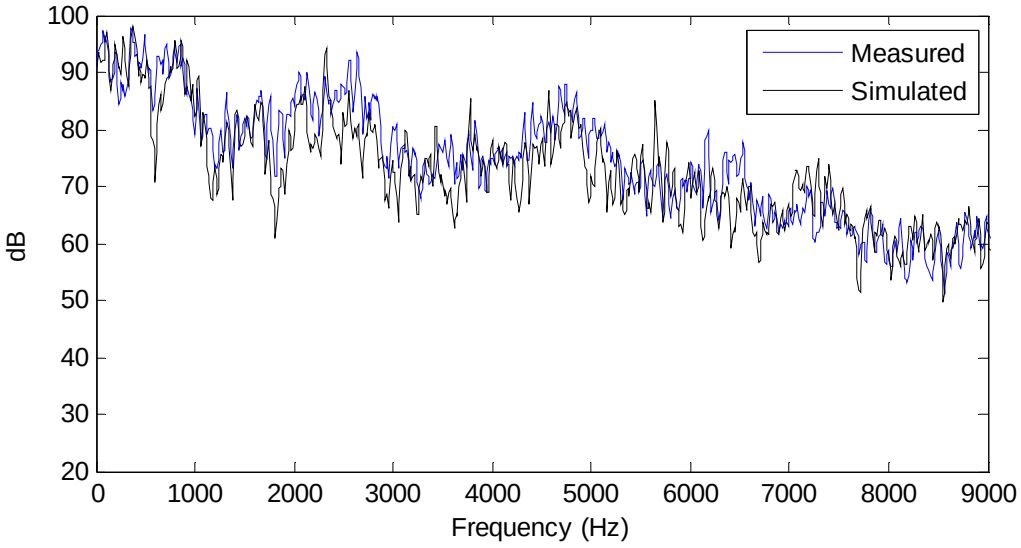

Figure 2.30: Comparison of SPLs of reference system for model A

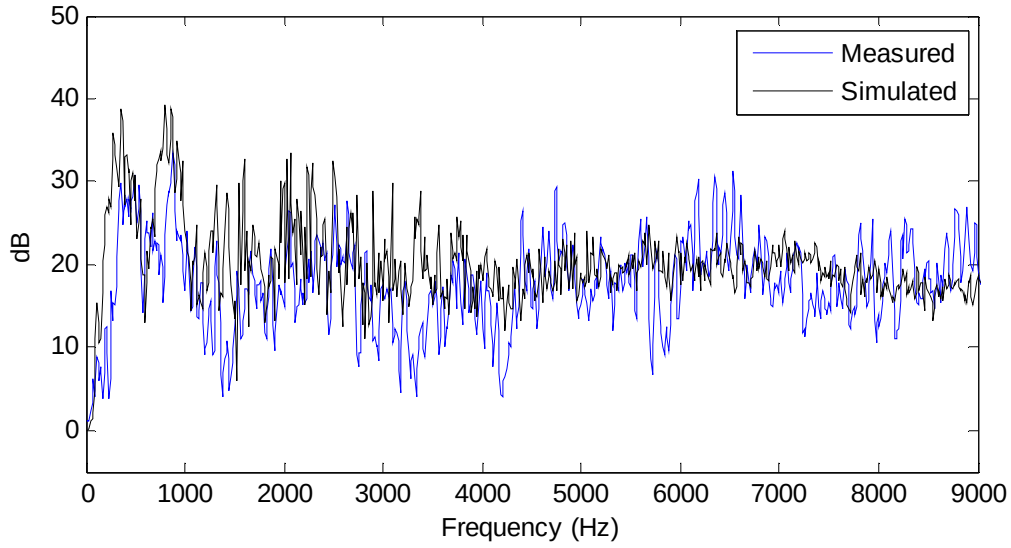

Figure 2.31: Comparison of IL for model A

2.5.2.2 Model B Figures 2.32 and 2.33 show the comparisons of SPLs for the muffled and reference systems respectively. Figure 2.34 shows the IL of the model B**.** An analysis of all of the results is included in the discussion (Section 2.6).

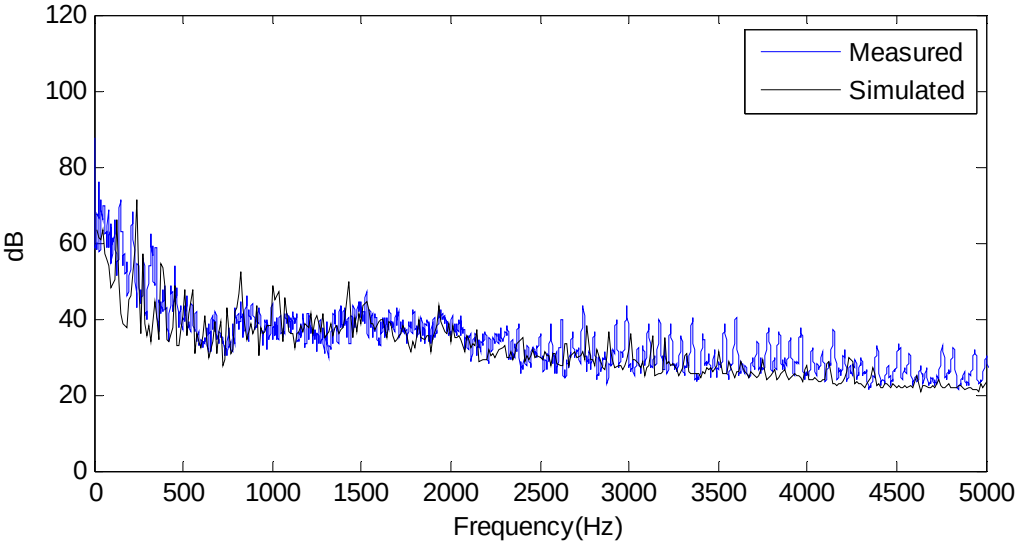

Figure 2.32: Comparison of SPLs of muffled system for model B

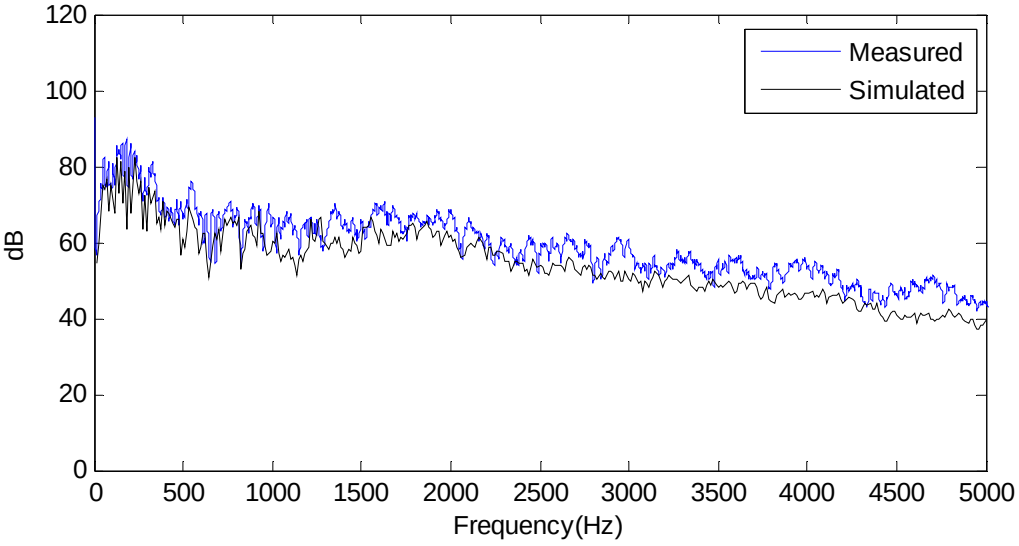

Figure 2.33: Comparison of SPLs of reference system for model B

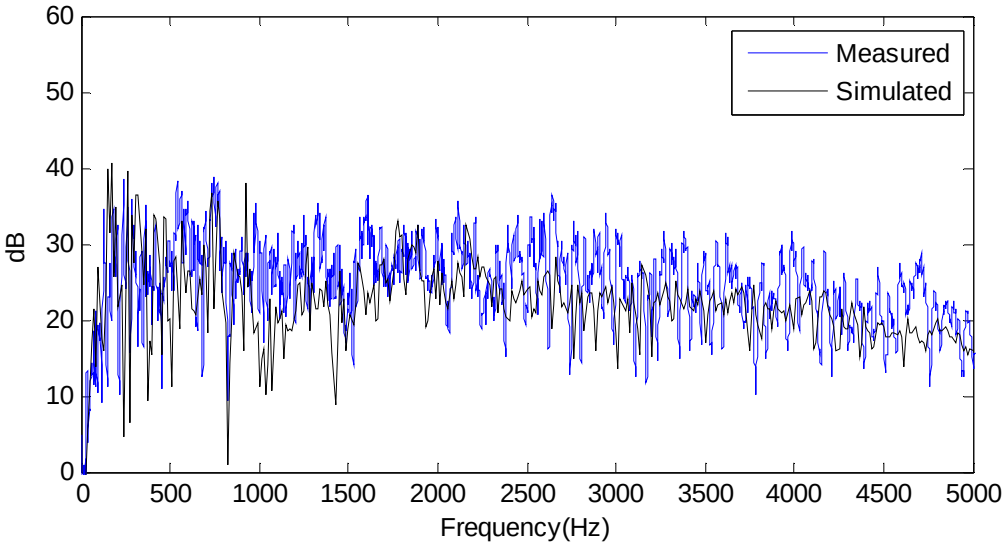

Figure 2.34: Comparison of IL for model B

2.5.2.3 Model C Figures 2.35 and 2.36 show the comparisons of SPLs for the muffled and reference systems respectively. Figure 2.37 shows the IL of the model C. An analysis of all of the results is included in the discussion (Section 2.6).

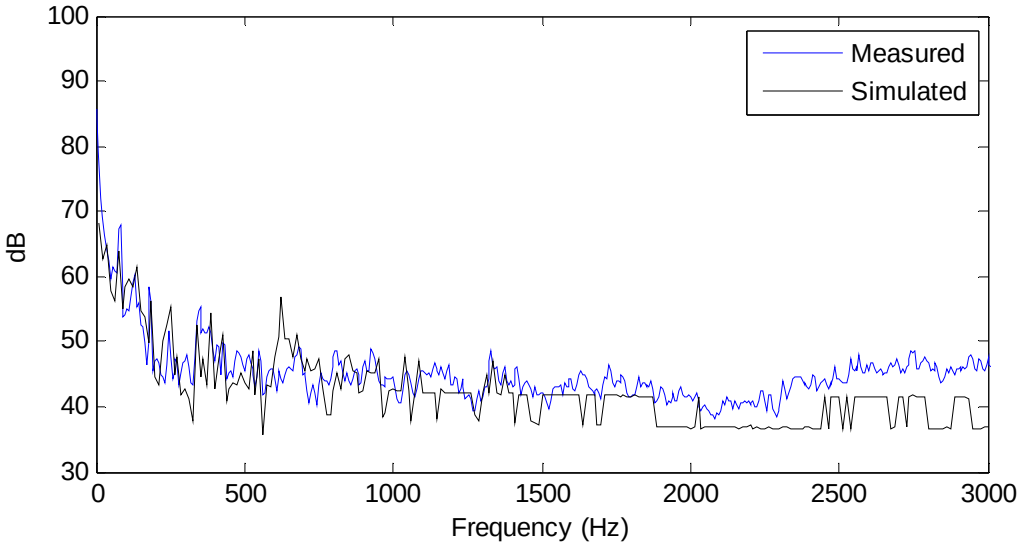

Figure 2.35: Comparison of SPLs of muffled system for model C

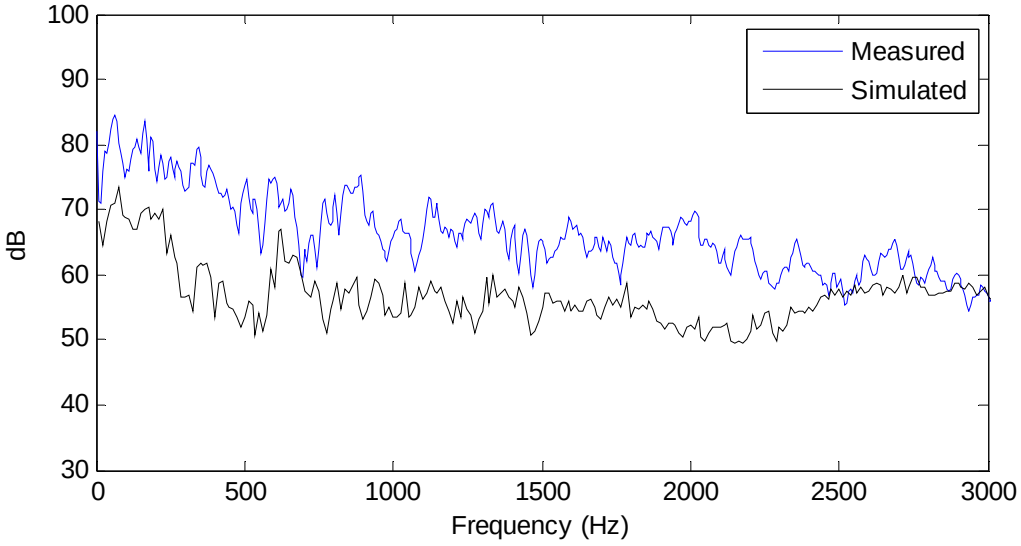

Figure 2.36: Comparison of SPLs of reference system for model C

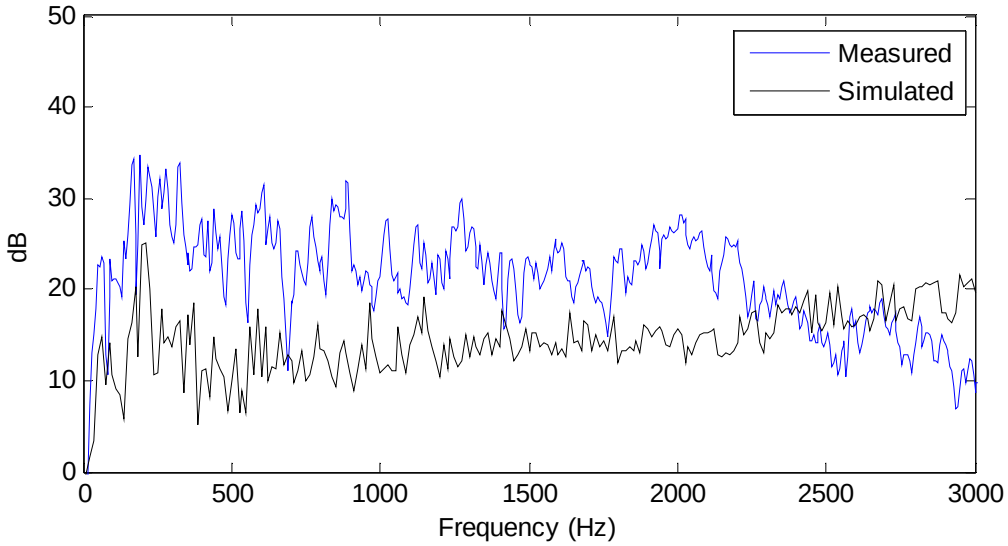

Figure 2.37: Comparison of IL for model C

2.5.3 Transmission loss

TL was only measured for model A. The incident and transmitted waves were obtained through the methods that are explained in earlier sections. The noise floor was not applicable for reasons that will be explained later in this section. Figures 2.38 and 2.39 show comparisons of the incident and transmitted waves respectively. Figure 2.40 shows the TL performance for model A. An analysis of all of the results is included in the discussion (Section 2.6).

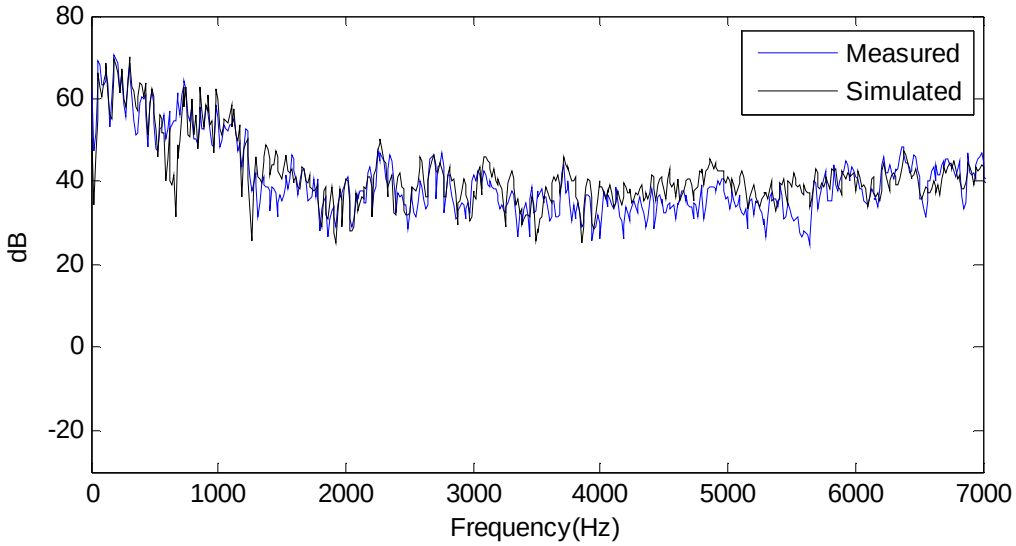

Figure 2.38: Comparison of incident sound powers for model A

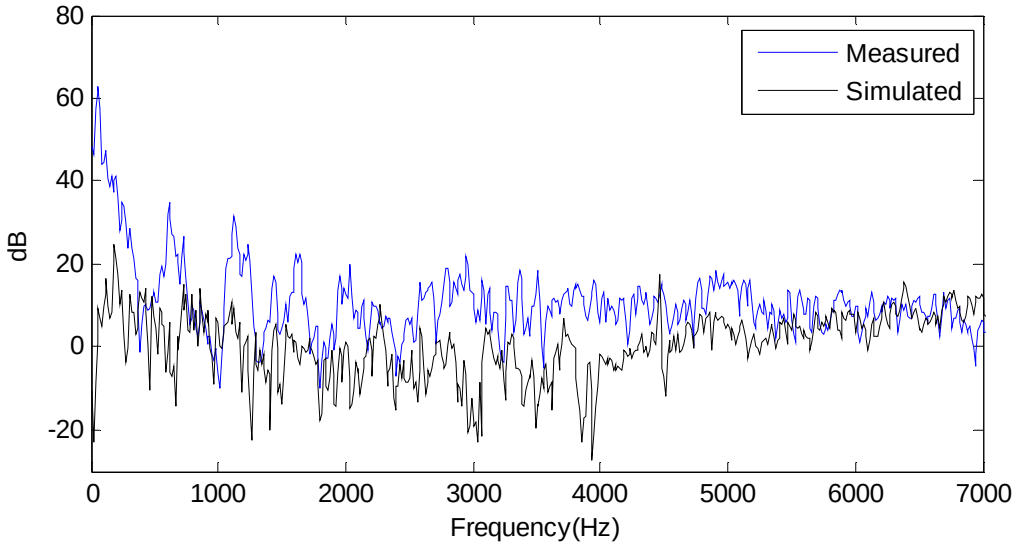

Figure 2.39: Comparison of transmitted sound powers for model A

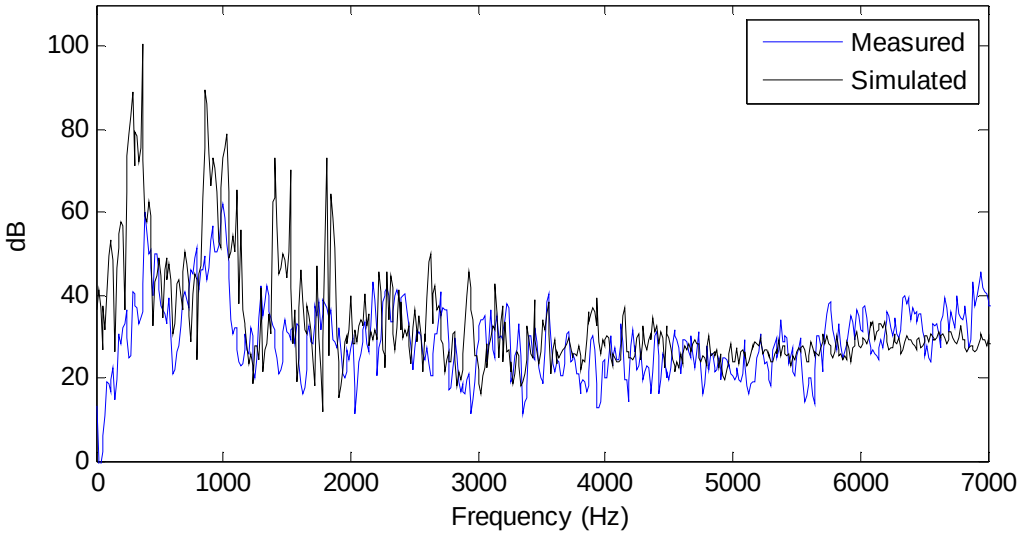

Figure 2.40: Comparison of TL for model A

2.6 DISCUSSION

2.6.1 Comparison of results

It is clear from comparing Figures 2.15, 2.25, 2.38, 2.31, 2.34, 2.37, and 2.40 that, of all three performance metrics, IL is the performance metric that achieved the worst agreement between the field measurements and the FEA simulation. The IL comparisons are shown in Figures 2.31, 2.34, and 2.37. This poor agreement was expected since IL has the most external factors significantly affecting the field measurement. These external factors can be computationally expensive and complicated to model.

One factor that has the potential to cause significant disagreement between the measurements and the simulations was the presence of reflective bodies outside the muffler during the field measurements. Even though reflective bodies in the measurement field were kept to a minimum, certain reflectors were unavoidable such as the ground and the microphone operator. These bodies produce acoustic reflections which affect the measurements. To fully reproduce this effect, the bodies would need to be created in the domain and the reflective properties would need to be properly modeled. Attempting to model these features would increase the size and complexity of the FEA model, and greatly add to the computational

cost of the model. The frequency ranges studied for each muffler model would have been reduced greatly if these factors were added into the FEA model, so as a result, they were not modeled.

Other factors that affected the accuracy of the IL models were errors due to atmospheric absorption, ambient noise, and leakage from the experimental setup. Since the IL measurement, out of the three performance metrics, is the measurement that is taken the furthest from the noise source, the agreement between the FEA model and the measurements will be the most susceptible to errors in the atmospheric absorption used in the FEA model. The ambient noise is comprised of wind, machinery, vehicles, animals, and various other common environmental noises. While much of this error was addressed by the application of the noise floor, none of these noise sources are constant throughout the entirety of a testing process so there is still some error that results from the ambient noise. The leakage from the experimental setup can greatly affect the IL measurement. The experimental setup at the Pittsburgh site produced much less leakage in the coupling and piping of the system than the system at the corporate site did. This was in part because of the difficulty that lay in producing an interchangeable system that fit both muffler models B and C. As a result the agreement between the IL simulation and measurements for model A is much better than the agreement for models B and C.

The performance metric that achieved the most agreement between the FEA simulation and the field measurements was the NR. The NR comparisons are shown in Figures 2.15, 2.25, and 2.28. The NR is the most accurate performance metric for many reasons which correspond to the reasons why IL was unable to achieve good agreement. The NR measurements are all taken inside the muffler. This means that all relevant reflective boundaries are modeled in the FEA simulation. The NR measurements are also less susceptible to errors that originate from the atmospheric absorption, ambient noise, and leakage noise.

The internal SPL measurements that accompanied the NR measurements help to identify more possible sources of error in the FEA simulation. One source of error that is already known, and is further evidenced from the figures is the idealistic treatment of the shell walls. The muffler shell was treated as a rigid boundary. A rigid boundary is the boundary condition given in Equation 2-13. This is a boundary that is perfectly reflective. When the shell wall is modeled as a rigid boundary, all of the energy is kept within the shell and is only allowed to escape through the outlet and atmospheric absorption. In reality the walls absorb and reflect some of the sound, and allow some of it to travel through the shell where it then breaks out to the atmosphere, or in to other parts of the duct. These effects are neglected by the rigid boundary in the FEA model. Figure 2.9, 2.10, 2.17, 2.18, and 2.19 all show similar patterns. We see more pronounced peaks and over prediction of the SPL throughout the frequency range of the plot. This is believed to be because the dissipation and radiation from the shell wall reduces those peaks in the real system. The calculation of a realistic muffler shell is very computationally expensive, and would not have been possible with the computing capabilities available for this research.

Another source of error that is revealed by the internal SPL comparisons is the modeling of the catalyst. Figures 2.9, 2.10, 2.17, and 2.18 all represent measurements made immediately on either side of the catalyst in both models A and B. These figures show a much more pronounced disagreement between the measurements and the simulation than we see in many of the other internal SPL comparisons. This is especially true in figures 2.9 and 2.10 which correspond to the catalyst in model A. This error could possibly be fixed by looking for other methods that have been used to model catalysts in FEA simulations.

A procedural error that likely accounts for a portion of the error in NR and internal SPL measurements is the coordination of where the measurements were taken in the muffler to where the pressure data was taken from in the FEA model. These positions were mostly approximated and not exact. As a result there could be error due to the data being taken from different places in the propagating mode shapes in the muffler shell.

The TL comparison in Figure 2.40 achieved poor agreement below 2000 Hz, but good agreement above 2000 Hz. However, the disagreement at low frequencies stems from the fact that the noise floor was not able to be applied to the TL simulations. There is also a certain amount of disagreement that is a result of the fact that the anechoic termination used was imperfect. The noise floor could not be applied because the TL calculation is based upon the muffler's incident and transmitted sound powers while the ambient noise measurement is a SPL, and thusly cannot be directly added. Even if this was not the case, the noise floor would still not be applicable to the TL measurement. The anechoic termination introduces damping to the outlet measurement tube. This significantly alters the sound field inside the tube, and there is not a readily available transfer function for the ambient noise passing through the anechoic termination into the outlet pipe. The absence of this transfer function renders an ambient noise measurement made in the field irrelevant for any measurements made in the outlet tube. In order to apply the noise floor, the ambient sound power in the outlet tube would need to be determined.

2.6.2 Noise floor efficacy

The *in situ* nature of the measurements mad in the field test created a number of sources of disagreement in the validation of the measurements and the FEA program. A prominent source of disagreement was the presence of significant levels of ambient noise. Validations of FEA simulations with measurements have, up until now, typically been done with measurements made in very controlled conditions.[45] Settings for these measurements include quiet laboratories and anechoic chambers. These measurements typically produce high agreement with idealistic FEA simulations. While these settings help to measure ideal performances, they generally do not reflect the performance that is actually attainable *in situ*. *In situ*

measurements are not only more realistic, but they are also more economical. Renting out or buying an ideal testing environment can be very difficult and expensive for any size muffler. For large scale industrial mufflers, this practice is altogether impractical. The application of a noise floor to the FEA simulations offers a way to produce more agreement between the FEA models and the *in situ* measurements for NR and IL performance.

In this study, the ambient noise in the measurement fields reached very high levels in the low frequency ranges. As a result, this is where the noise floor was the most effective in increasing agreement. Figure 2.41 show the ambient noise measurement made at the Pittsburgh testing site and how that measurement compares to the results of the IL FEA simulation. It is clear from the figure that the noise floor will have its greatest effects in approximately the 0-3 kHz range. This is the range in which the ambient SPL is greater than or on the same approximate magnitude as the SPL from the outlet of the system. Above this range the noise floor will not have much effect at all. It is emphasized that the frequency range and efficacy experienced in this research is only for this research. In other studies, the noise floor may have effects in different frequency ranges or no effect at all. The effects of the noise floor will differ based on the level of the input noise, the level of the background noise, and the effectiveness of the muffler.

The case in which the application of the noise floor was most effective, was for the IL of muffler model A. The noise floor was so successful in this case because the Pittsburgh testing site did not have the ability to produce a lot of sound power. As a result, the muffled noise source was very quiet and the measurement was highly contaminated by ambient noise at many of the low frequencies. Figure 2.41 shows the application of the noise floor to the FEA simulation for the IL of muffler model A. Figures 2.42 and 2.43 show the simulated Il before and after the application of the noise floor and how it compares to the measured IL. There is a dramatic difference between the simulated IL for Figure 2.42 and 2.43. It is clear that the simulation models the *in situ* measurements much more closely after the noise floor is applied to the simulation. As mentioned before the greatest difference produced in the predicted performance is in the 0-3 kHz range.

It should be noted that the error patterns that we see in Figure 2.42 are similar to thos in the TL performance for muffler model A in Figure 2.40. In both figures we see over predicted peaks in the lower frequency ranges. From this comparison it is clear that the agreement between the field measurements and the FEA simulation could be drastically improved by applying the noise floor to the TL FEA simulation.

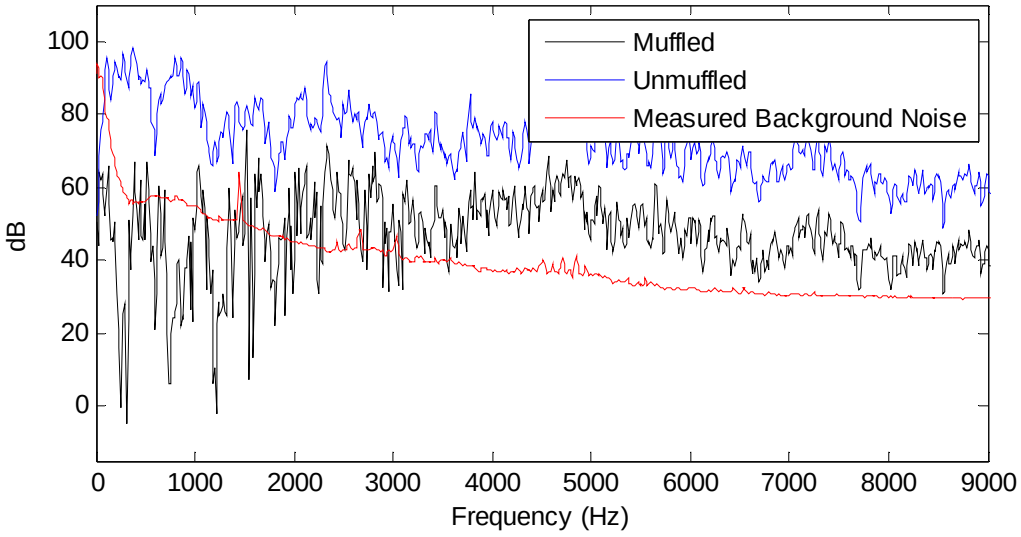

Figure 2.41: Model A IL simulation results before application of noise floor and measured ambient noise

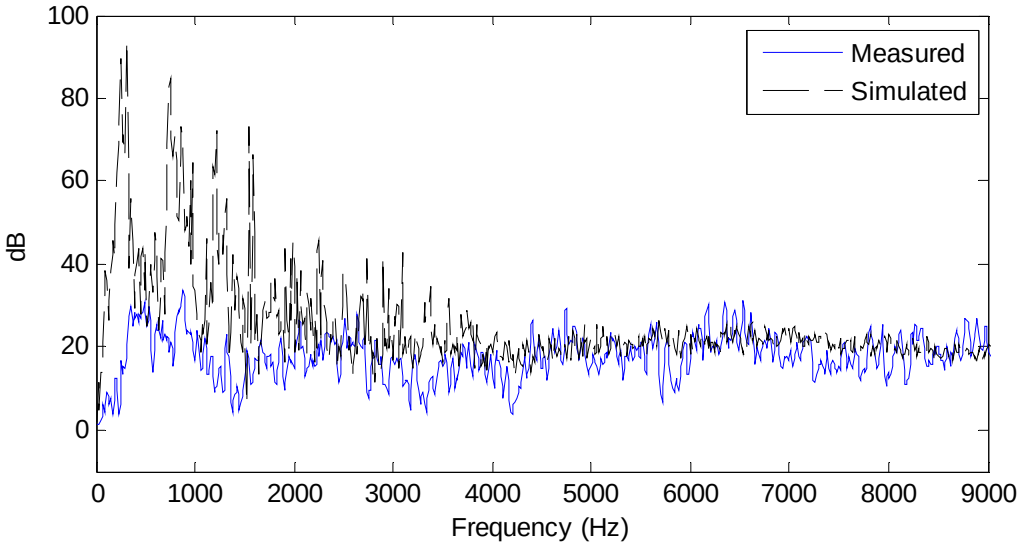

Figure 2.42: Model A comparison of IL before the application of the noise floor

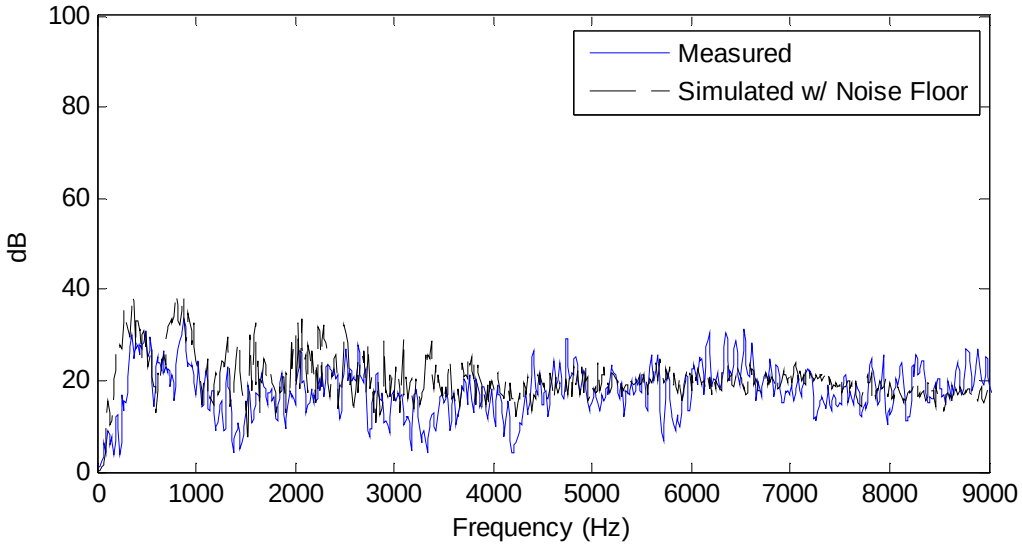

Figure 2.43: Model A comparison of IL after the application of the noise floor

3.0 PARAMETRIC STUDY

The one-dimensional acoustic performance of many types of muffler design elements has been well documented. However, the three dimensional propagation of acoustic waves causes the performance of the reactive elements to diverge from one-dimensional theory. The three-dimensional performance of these elements is a very complex subject, and not much research has been conducted in regards to the design of mufflers for three-dimensional acoustic propagation. In order to determine the effectiveness of these design elements in a three-dimensional acoustic field, it was necessary to perform a parametric study for each one across a frequency range that extends well past several resonances relating to the dimension under study. For each muffler model considered in this study, several dimensions were chosen for examination. These dimensions were chamber lengths, baffle tube lengths, baffle tube positions, number of baffle tubes, as well as a number of other dimensions or features of interest in each muffler. In order to determine if the general behavior of the elements is constant over the three different mufflers, many of the dimension types studied overlapped from muffler to muffler. The plan for each study will consist of targeting a specific part of the muffler geometry, varying the characteristic dimension of that part while holding all other dimensions constant, and observing the changes in the TL performance of the muffler. This will then be repeated for a number of other dimensions in the muffler as well.

3.1 MODEL STUDY PLANS

For muffler model A, the main dimensions considered in the study of this model are chamber and baffle tube length. The dimensions and features studied that were unique to this model were the major diameter of the muffler, the presence of perforations in the baffle tubes, and the presence of an open area under the catalyst. These dimensions are shown in Figure 3.1 and then briefly described in Table 3.1. The reason varying the major diameter was only considered for this model is because increasing the major diameter greatly increases the size of the finite element model. Significantly increasing the diameter of

the larger models would prove to be very costly computationally. Computational cost also drove the number of models that were completed for each model. A large majority of the total number of models were focused on this muffler rather than for the other models. This was because of the speed with which a model of the muffler model A could be executed compared to the two larger models. For models B and C, a relatively low number of models were completed due to time constraints. The dimensions focused on in these models are the chamber and baffle tube lengths, as well as baffle tube number and radial position. The features studied for muffler model B are shown in Figure 3.2 and described in Table 3.3. The features studied for muffler model C are shown in Figure 3.3 and described in Table 3.5. Tables 3.2, 3.4, and 3.6 detail the different size ranges for each feature. All simulations were run at a temperature of 538 Celsius using the LMS Virtual.Lab Acoustics software. 538 Celsius, or 1000 Fahrenheit, represents an average temperature at which exhaust systems operate.

3.1.1 Model A studied features

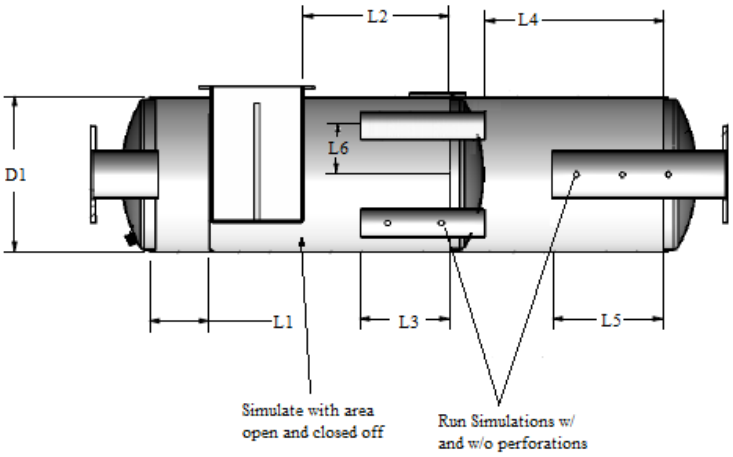

Figure 3.1: Parameters to be studied for muffler model A

Table 3.1: Description of parameters for study of muffler model A

Parameter	Description
L1	Length of chamber one
L2	Length of chamber two
L3	Length of chamber two baffle tubes
L4	Length of chamber 3
L5	Length of outlet baffle tube
L6	Distance of baffle tubes from axis
D1	Total diameter of muffler

When varying D1, L6 should be kept in the same relative position with respect to the diameter of the muffler i.e. The ratio L6/D1 should be held constant. Using this method, the feature of interest should be isolated. The varying of the L6/D1 ratio will be tested separately when the L6 test is performed.

Table 3.2: Parameter ranges and step values for study of muffler model A

Parameter	Start value	End value	Step	Permutations
L1	1"	10"	1"	10
L2	10"	22"	2"	7
L3	0"	10"	1"	11
L4	14"	36"	2"	12
L5	0"	14"	2"	8
L6	2"	5"	.5"	7
D1	15"	21"	2"	4
Baffle tube perfs	Present	Not Present	N/A	2
Extra area below cat	Open	Closed	N/A	2
			Total:	63

3.1.2 Model B studied features

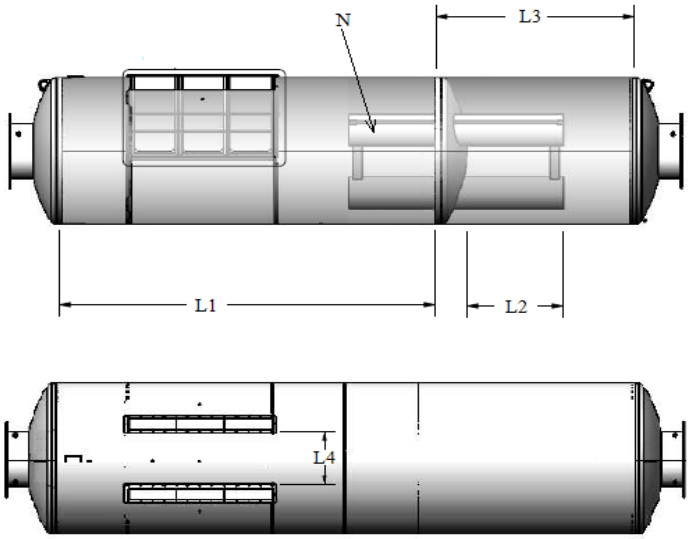

Figure 3.2: Parameters to be studied for muffler model B

Table 3.3: Description of parameters for study of muffler model B

Parameter	Description
L1	Length of chamber one
L2	Length of chamber two baffle tubes
L3	Length of chamber two
L4	Distance between catalyst chamber
N	Number of Baffle Tubes

Table 3.4: Parameter ranges and step values for study of muffler model B

Parameter	Start value	End value	Step	Permutations
L1	100”	140”	20”	3
L2	20”	50”	15”	3
L3	40”	60”	10"	3
L4	15”	25”	5"	3
N	2	4	1	3
			Total:	15

3.1.3 Model C studied features

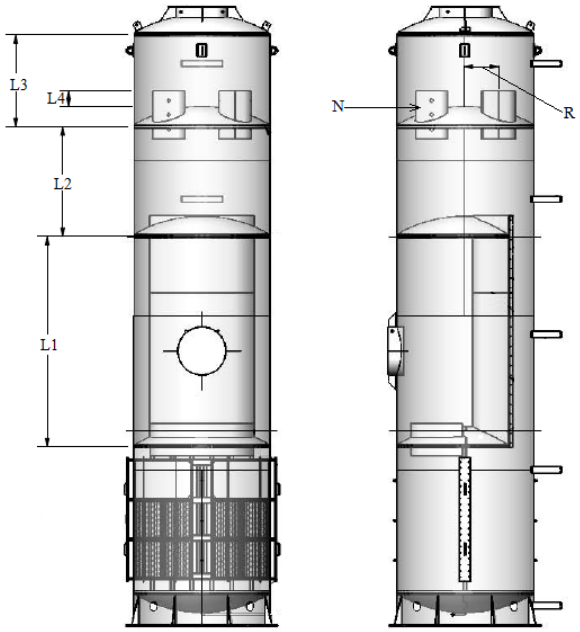

Figure 3.3: Parameters to be studied for muffler model C

Table 3.5: Description of parameters for study of muffler model C

Parameter	Description
L1	Length of chamber one
L2	Length of chamber two
L3	Length of chamber three
L4	Length of chamber three baffle tubes
N	Number of baffle tubes
R	Radius of baffle tubes from center axis

Table 3.6: Parameter ranges and step values for study of muffler model **C**

Parameter	Start value	End value	Step	Permutations
L1	100″	120″	20″	2
L2	40″	80″	20″	3
L3	40″	60″	10"	3
L4	0″	30″	15"	3
N	2	4	1	3
R	20.5″	29.5″	4.5″	3
			Total:	17

3.2 PARAMETRIC STUDY RESULTS

The following section will present the results from the parametric study on the three muffler models. Due to the large volume of data that was obtained during the study, a shortened version of the results will be presented. The significant findings for each feature type will be shared, followed by figures that illustrate and support the finding.

3.2.1 Chamber and baffle tube length

The majority of the features examined in the parametric study for all three models were chamber and baffle tube lengths. The variation of the lengths of baffle tubes and expansion chambers both had the same outcome in that the variation of these features did not produce a usable result. The peaks and troughs in the TL figures would differ from model to model, but not in a way that was predictable. The combination of three-dimensional acoustics and complex geometries causes each chamber to have a very large number of resonances. When the resonances from two different chambers coincide with one another, they cause the resonances of the two chambers to shift. This phenomenon becomes common when there are so many resonances present in every chamber. The large number of resonances combined with the shifting of these resonances makes it very difficult to predict the effects that the variation of the chamber will have.

One useful observation that can be made from this data is that expansion chambers and baffle tubes do not produce very large attenuation past the first several resonances of the feature. For muffler

model A the effects became negligible after approximately 5 kHz. These limits were approximately 1.2 kHz for muffler model B, and 0.8 kHz for muffler model C.

Figure 3.4 shows the TL curves obtained from the variation of the length of an expansion chamber (L1) for muffler model A. Figure 3.5 shows the TL curves obtained from the variation of the length of baffle tubes (L4) for muffler model C. Each figure only shows three iterations to prevent the figures from being crowded.

There was one special case of the baffle tube variation that produced a predictable result. In muffler model A, L5 was an extended outlet baffle tube. This particular baffle tube will produce a peak in TL performance at the first resonance that is expected from plane wave theory. This result is most likely resulting from the baffle tubes proximity to the outlet. This feature does not experience any interference from other chambers before it leaves the muffler. The result is the ability to target a certain frequency by "tuning" the outlet baffle tube. The resonance that results from this feature is the resonance that is expected from a baffle tube of length L5 with the additional length that results from the curvature of the end plate of the muffler (approximately three inches for muffler model A). An illustration of this effect is shown in Figure 3.6 and Table 3.7.

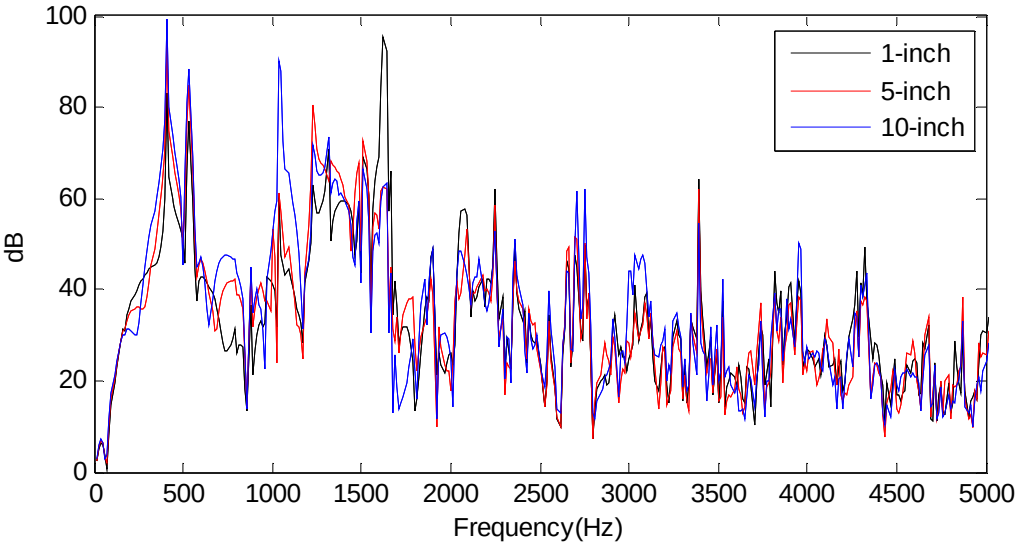

Figure 3.4: TL curves for different lengths of L1, the length of chamber 1, in muffler model A

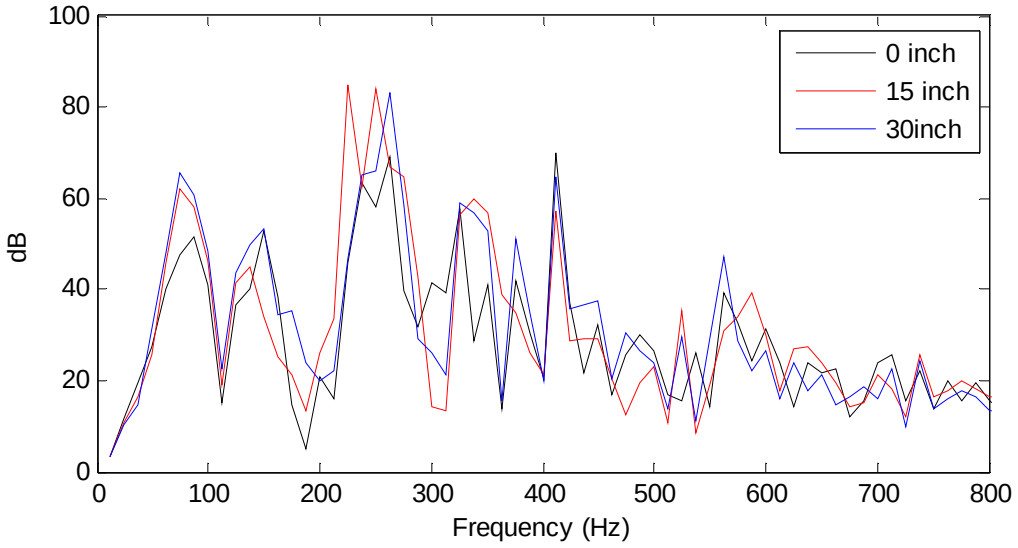

Figure 3.5: TL curves for different lengths of L4, the length of the baffle tubes in chamber 3, in muffler model C

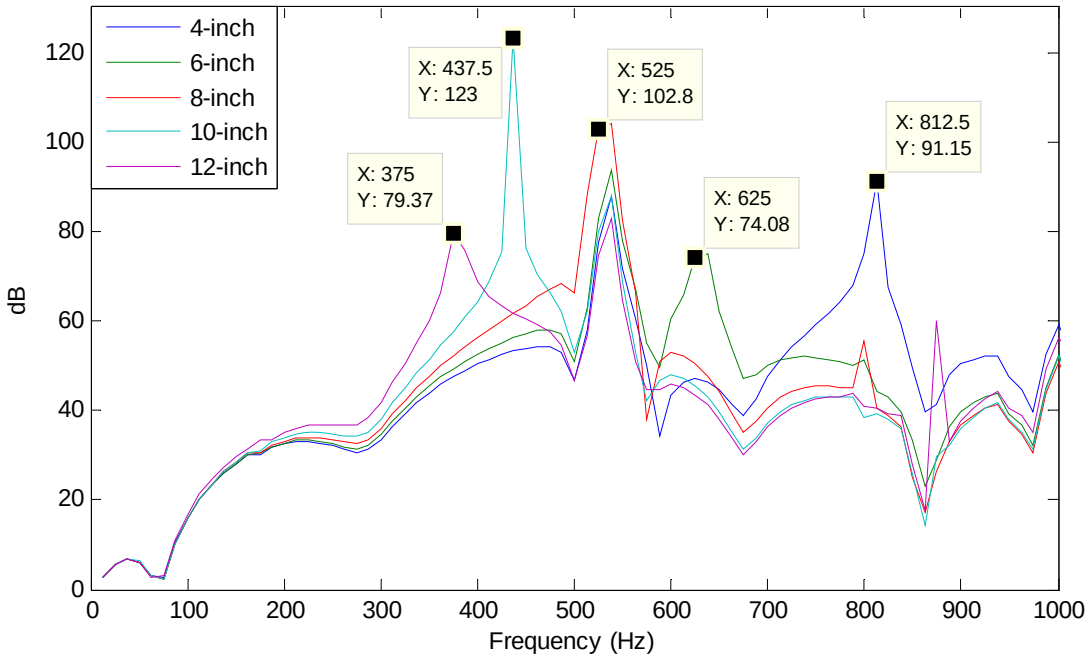

Figure 3.6: TL curves and resonances for lengths of L5, the length of the outlet baffle tube, in muffler model A.

Table 3.7: Expected resonances for L5, the length of the outlet baffle tube, values in Figure 3.6.

L5	Tube Length	Expected Resonances
4	6.98	806.69
6	8.98	627.03
8	10.98	512.81
10	12.98	433.8
12	14.98	375.88
14	16.98	331.61

3.2.2 Baffle tube radial position

The baffle tube radial position (L6 for muffler model A and R for muffler model C), has a large potential to affect the performance of the muffler when three-dimensional acoustic propagation is involved. As explained in Section 1.3.2, the placement of the baffle tubes at the inlet and outlet of a chamber control which modes are excited and transmitted in the chamber. Moving the baffle tubes outward toward the shell prevents many higher-order modes from being transmitted to the next chamber. For both muffler model A and muffler model C, the TL performance of the mufflers increased as the baffle tubes were moved towards the outer shell. This trend is not immediately apparent for muffler model C (Figure 3.8), but is apparent for muffler model A (Figure 3.7). While the TL performance is improved by moving the baffle tubes outward, the FEA simulations did not model the shell fluid interaction. The baffle tubes transmit the acoustic waves from chamber to chamber, and as a result have high acoustic pressure fluctuations at their exit. If these exits are closer to the shell, then the pressure fluctuations are more likely to excite the shell and produce radiated shell noise. This must be kept in mind when determining the best radial position for the baffle tubes.

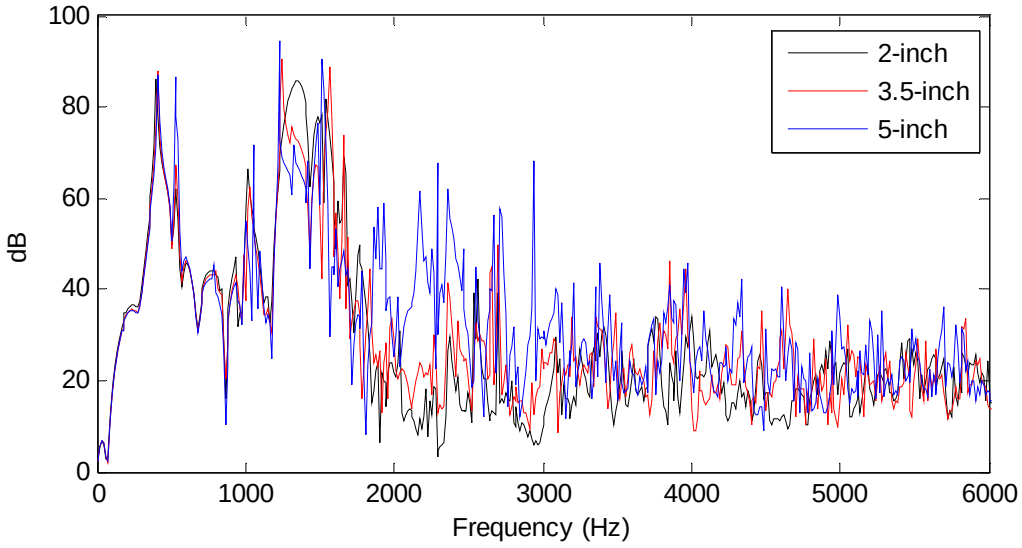

Figure 3.7: TL curves for different lengths of L6, distance of baffle tubes from axis, in muffler model A

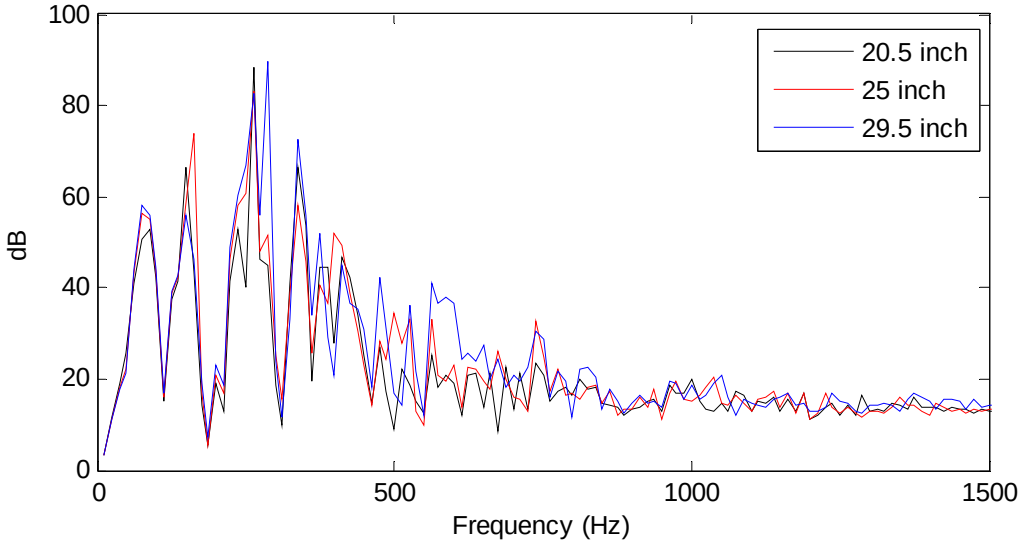

Figure 3.8: TL curves for different lengths of R, radius of baffle tubes from center axis, in muffler model C

3.2.3 Major diameter

The effects of an area expansion are detailed in Section 1.3.1. As expected, the TL performance improved as the area of the expansion chamber grew larger in relation to the area of the inlet pipe. Muffler model A was the only muffler for which major diameter was studied. Figures 3.9 and 3.10 shows the two extremes of the diameters studied for muffler model A. Figure 3.9 shows the first half of the 9 kHz range and Figure 3.10 shows the second half of that range. The range is split into two figures so that an appropriate amount of detail is visible in each figure. There is a pronounced and consistent increase in the TL performance from approximately 0-1000 Hz. This improved performance continues for most of the 9 kHz but is less pronounced and less consistent. This is most likely due to the presence of three-dimensional effects.

For the 15 inch muffler diameter we see peaks in the TL performance around 2600-2700 Hz. These peaks are not present in the 21 inch muffler. However, we see peaks in the TL performance at 1600-1700 Hz for the 21 inch muffler, which are not present in the 15 inch muffler. Large peaks in the TL performance like these are usually associated with the region just before the cut on of three-dimensional propagation. These peaks correspond to the (1, 1) mode for each size diameter. While three-dimensional effects generally start before this mode, it would not be entirely surprising that three-dimensional effects might start at this point due to the complex geometries of the mufflers.

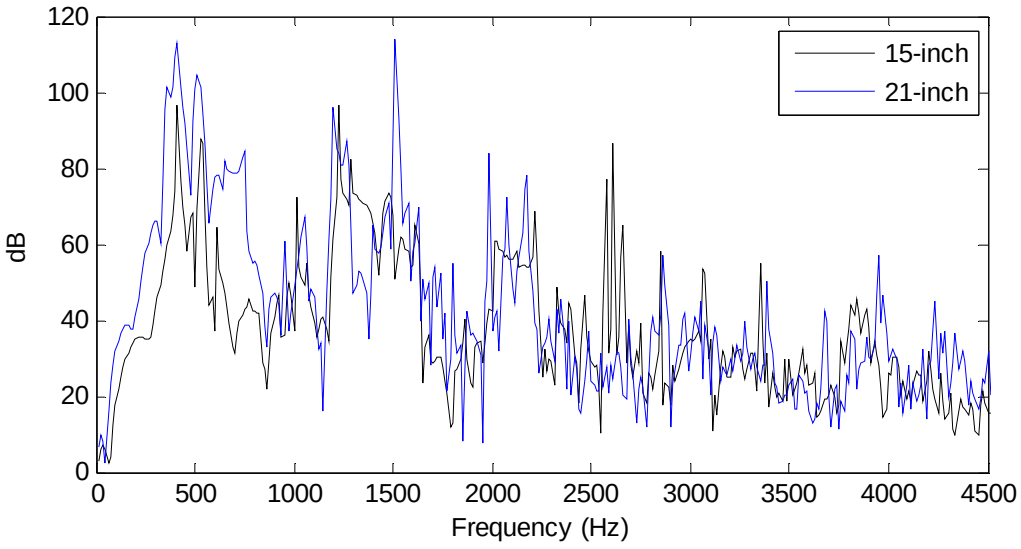

Figure 3.9: TL curves for the smallest and largest major diameters for muffler model A (0-4500 Hz)

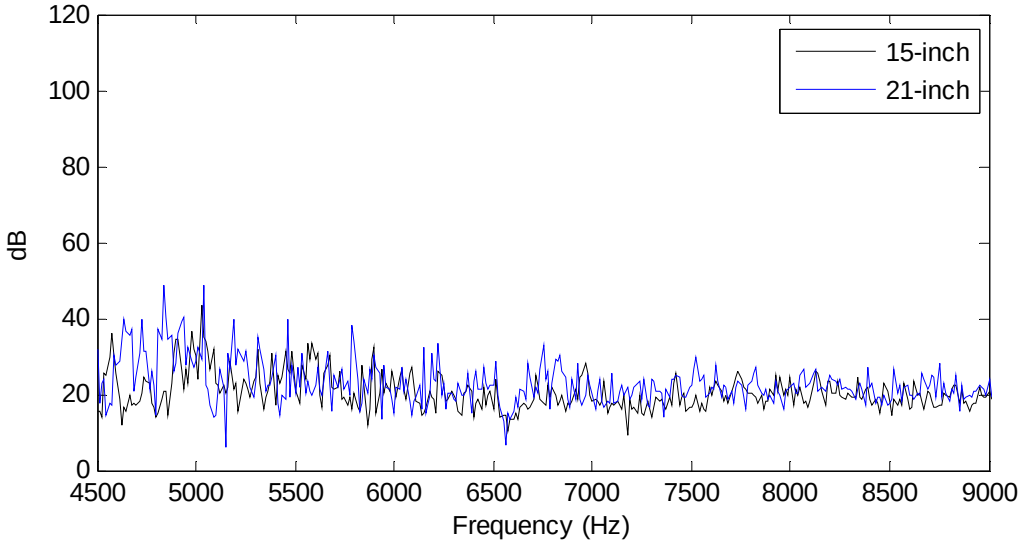

Figure 3.10: TL curves for the smallest and largest major diameters for muffler model A (4500-9000 Hz)

3.2.4 Number of baffle tubes

The number of baffle tubes used between two chambers was varied for muffler models B and C. For muffler model B, the best performance resulted from the use of two baffle tubes. The improved TL performance was most pronounced in the 0-300 Hz and the 1500-5000 Hz ranges. For model C, inspection reveals that there is not a configuration that clearly outperforms the others. Figures 3.11 and 3.12 show the TL curves for the variation of baffle tube number in models B and C respectively. However, to change the number of baffle tubes, a number of other dimensions needed to be changed as well. In order to keep the same flow area as before, the baffle tubes would need to be scaled and possibly moved outwards or inwards radially to adjust for the new baffle tube size. While observations could be made on the change in performance between the different configurations, more studies in which these extra dimensions are held constant need to be performed before any solid statements are made on the effects of the number of baffle tubes on TL performance.

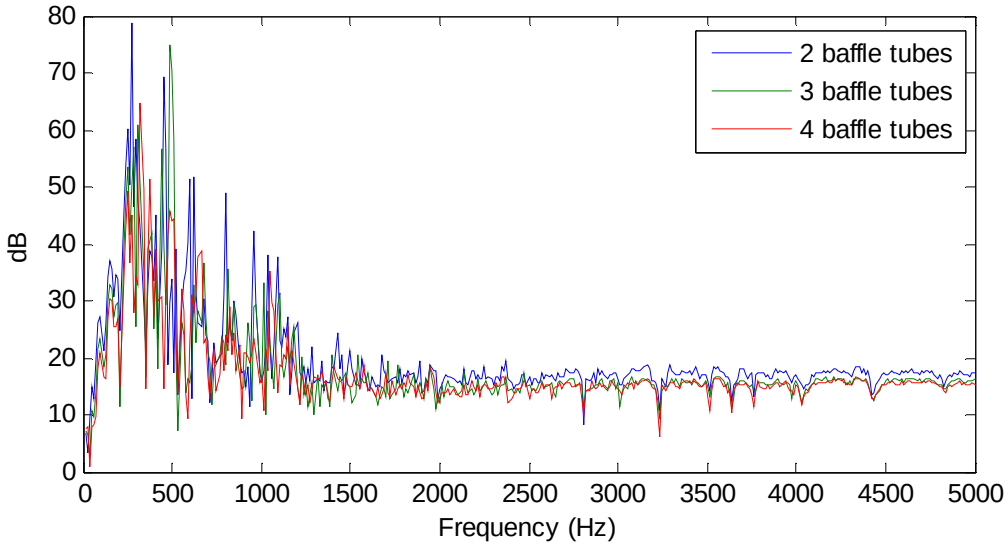

Figure 3.11: TL curves for the baffle tube configurations for muffler model B

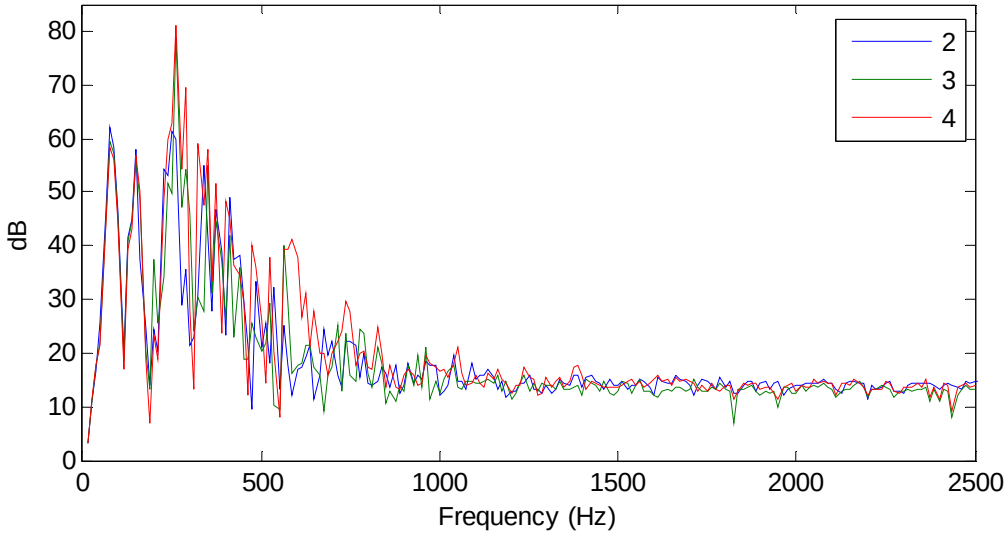

Figure 3.12: TL curves for the baffle tube configurations for muffler model C

3.2.5 Model A special features

There were two features studied that were specific to model A. These features are shown in Figure 3.1. The first feature was an open area beneath the Catalyst. This feature was simulated both open and closed off. The second feature was a series of perforations in the baffle tubes. These perforations serve as a path for exhaust gases that are trapped in the chamber to exit through the sides of the baffle tubes. Neither feature produced a large amount of insight about the muffler. One possible use for this area is to close it off with a plate that has an opening with a neck. This would effectively turn this volume into a Helmholtz resonator that could be used to target specific frequencies.

Figure 3.13 shows the different TL curves for the perforations in the baffle tubes. When the perforations were removed from baffle tubes the TL performance dropped in the 0-700 Hz range, but rose dramatically in the 700-1000 Hz range. Since we see a very significant increase in performance for the 700-1000 Hz range, it is recommended that the perforations in the tubes are left out and another method is found for improving the pressure drop performance. Figure 3.14 shows the different TL curves for the volume below the catalyst. Closing off the volume did not change the TL performance much at all. Thus the acoustic effects of this cavity should not be taken into account when designing the muffler.

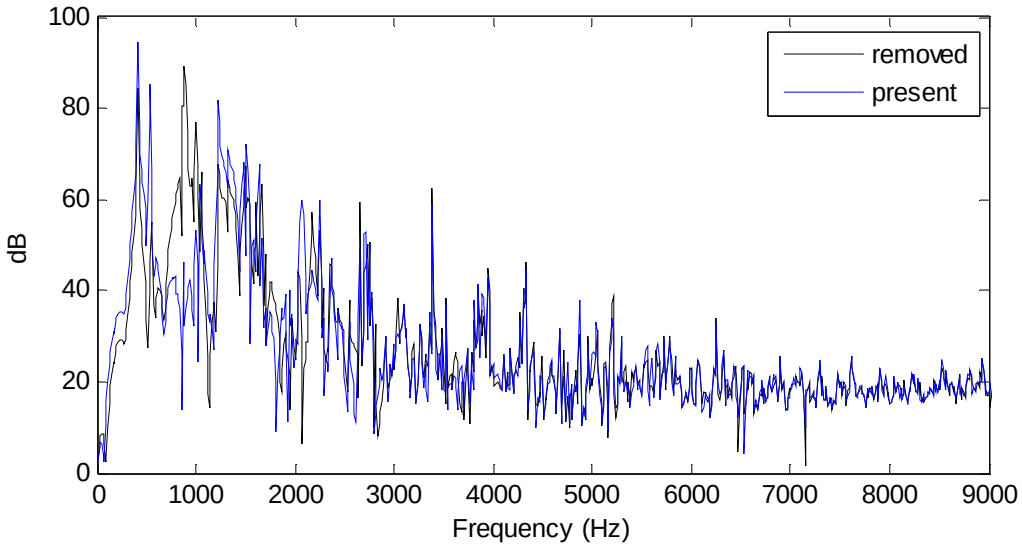

Figure 3.13: TL curves for the presence of baffle tube perforations for muffler model A

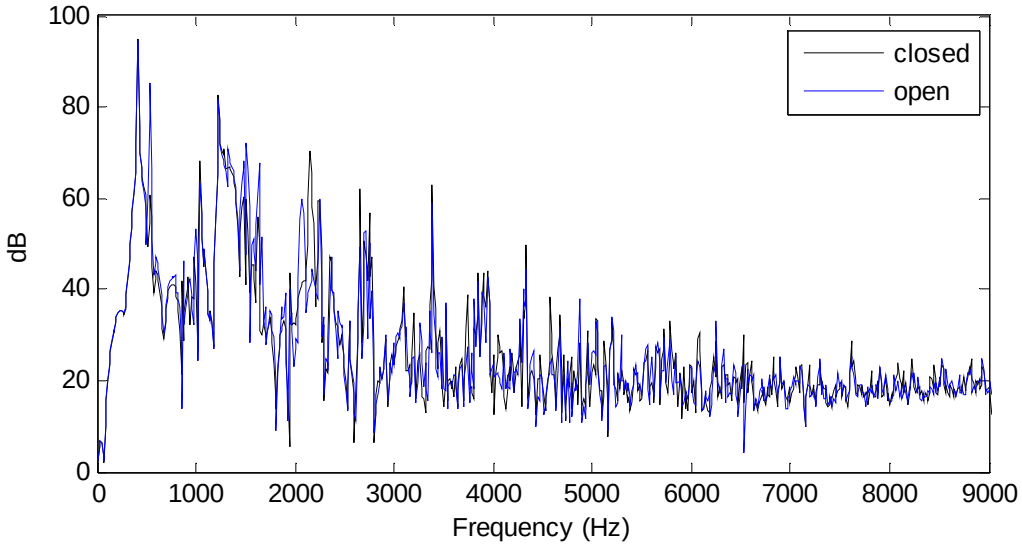

Figure 3.14: TL curves for the volume beneath the catalyst for muffler model A

4.0 CONCLUSIONS

As stated in the introduction, this research seeks to begin to develop a design and test process based upon three-dimensional muffler theory as opposed to the traditional plane wave theory. This was achieved by using the three-dimensional FEA program LMS Virtual.Lab Acoustics to investigate the effects of design features in the complex three-dimensional acoustic fields present inside the mufflers. The performance criteria considered during the study were NR, IL, and TL.

Before performing this investigation the FEA program had to be validated for relative accuracy. This was done by measuring the *in situ* performance of three large sized industrial mufflers and validating them against a three-dimensional FEA modeling program. The measurements were performed *in situ* due to time and cost restrictions, but offered a more realistic model of muffler performance. The method of applying a noise floor was developed to account for the contamination of the field measurements by ambient noise experienced during the test.

After the FEA program was validated, a parametric study was performed to achieve an understanding of the effects that each feature currently used in mufflers has on performance. The parametric study was performed by varying the characteristic dimension of different muffler features and observing the change in performance that resulted. Some of the most common muffler features were studied, and the three-dimensional performance effects of these features are covered in sections 3.2 above and 4.2 below.

4.1 VALIDATION CONCLUSIONS

As mentioned above, three large sized industrial mufflers were considered. All three mufflers had their *in situ* performances measured in field tests, and modeled using FEA. The FEA simulations and the *in situ* measurements were validated against one another. The frequency ranges that were studied for the validation were 0-9000 Hz for model A, 0-5000 Hz for model B, and 0-3000 Hz for model C.

The NR of the mufflers achieved the best agreement of all three performance metrics. For model A, the NR achieved good agreement up to approximately 5000 Hz. After this point the NR was under predicted by the FEA simulation by about 10 dB. For model B, the NR achieved good agreement from 0-3000 Hz. After this point the NR was over predicted by about 5 dB. It should also be noted that from 0-800 Hz the peaks were generally higher for the simulated NR. For model C, good agreement was achieved throughout the entire frequency range. However, some of the troughs below 700Hz were predicted to be too low in the simulation.

The IL of the mufflers achieved the worst agreement of the three performance metrics. For model A, the IL was over predicted from 0-3500 Hz by about 10 dB, but achieved good agreement for the rest of the range. For model B, the IL achieved good agreement in the 0-1000 Hz, 1700-2400 Hz, 3200-4500 Hz ranges. In the other ranges the IL was under predicted by about 5-10 dB. For model C, the IL was consistently under predicted by about 15 dB until 2500 Hz when it starts to over predict the IL.

The noise floor introduces a method for improving the accuracy of FEA simulations attempting to model *in situ* performance of mufflers. The accuracy of the NR and IL simulations was greatly improved after the application of the noise floor for all three muffler models. The greatest effects were generally seen in the 0-2000 Hz range. This is the frequency range where the ambient noise is at its highest.

The TL for model A was over predicted from 0-2000 Hz and had good agreement everywhere else. As explained in Section 2.6.1, the noise floor was not able to be applied to the TL simulation. The TL simulation could possibly have the noise floor applied to it, but a scheme would need to be devised to estimate the sound power present in the outlet pipe before the noise source of the testing system is turned on. The application of the noise floor would most likely increase the agreement between the FEA simulation and the measurements in the 0-2000 Hz range.

As discussed in Section 2.6.1, there are many sources of error that caused the validation to reach poor agreement in certain frequency ranges and comparisons. Many of these error sources could be improved upon in future research. One of the most important factors is that the experimental setups need to be improved. The speaker box and speaker to pipe couplings must be built to fit together better so that leakage from the system does not affect the measurements as much. Outlet pipes should also be added to

the setup at the corporate site. This will make the NR measurements less susceptible to errors from fluctuating ambient noise levels. Also one source of error that has not been mentioned yet is the frequency resolution. A significant amount of disagreement in the validation could be done away with by making the resolution of the measurements and the simulation the same. The simulations were all performed with a frequency resolution of 12.5 Hz. The measurements varied in frequency resolution from 1.25 Hz to 6.25 Hz.

Several improvements can also be made to the simulations to make them model the *in situ* performance more closely. The IL and NR agreements can be improved by modeling the source impedance and source characteristics for the system. Modeling these parameters and incorporating them into the FEA model, improves the acoustic interactions that take place on the inlet side of the FEA model. Experimental and numerical methods have both been determined for calculating these parameters.[15] This technique should be examined to see how much accuracy is added versus how much computational cost is added.

As mentioned in Section 2.6.1, the catalysts are a possible source of error. This is supported by the disagreement that appears in the models around the catalysts. There are other methods of modeling the catalysts acoustic properties that have been developed and are available in literature.[31] The catalyst could also have its accuracy improved by performing an iterative study to determine the properties that produce the most agreement between the measurements and the FEA models. Another possible source of error that could be improved is the damping that was added to the model. As discussed in Section 2.4.5, there was no standard found in literature for the amount of atmospheric absorption that should be added to the FEA model. There are also other sources of damping in the system that have not been accounted for in the FEA model such as modal damping and surface roughness of the shell. A more comprehensive literature search could be performed on this subject to find an accurate and verifiable method for implementing the correct absorption factor that takes all of these damping sources into account. Also, an iterative study may be run to determine the levels of absorption that produce the most agreement between the measurements and the FEA models.

An additional source of error that was discussed in Section 2.6.1 was the fact that the FEA simulations did not model the fluid structure interaction (FSI) between the shell and the gas. This modeling was not done because of the computational cost, and the inability of LMS Virtual.Lab Acoustics to perform these calculations without the help of an outside FEA package. There are a number of ways to pursue this interaction, each with varying degrees of accuracy and computational cost. A couple of examples include modeling the shell boundary as an impedance boundary, finding a software package that can directly calculate the FSI between the shell and the gas, or finding the coincidence

frequency of the muffler shell. All of these would give different levels of insight into the effect that the muffler shell has on the acoustic performance of the muffler.

In Appendix E the ideal simulation data is presented. This is the data from the FEA simulations before the noise floor is applied. This data shows loss levels that would be unrealistically high even if there was no ambient noise present in the field of measurement. It is believed that by introducing the shell interaction to the model, as discussed in the previous paragraph, the loss levels that result from the ideal simulations would drop to levels that much more closely match the performance that is expected out of mufflers of this type.

There are also a couple of general alterations that may be made to improve the quality of simulations and the time it takes to perform them. The first alteration has to do with mesh refinement in the FEA model. In this study, as previously stated, four elements per wavelength were considered sufficient for accuracy. However, a convergence study could be performed in order to determine the number of elements per wavelength that are actually needed for convergence in the FEA model. This would be done by picking a frequency and simulating continually smaller meshes until convergence on a single value is achieved for that frequency.

The next alteration is related to the number of frequencies analyzed in the simulation process. In Appendix E the concept of octave bands is explained. If an octave band approach is taken to the simulation data, then there only need to be a certain number of data points taken in each octave band. In this way the simulation time can be dramatically reduced. Instead of spacing the simulation frequencies linearly, they should be spaced logarithmically so that the same number of simulation points are taken in each octave band. This can reduce the number frequencies the FEA program must calculate for a given model exponentially, and possibly allow for a significantly more refined mesh to extend the valid frequency range in the simulations.

4.2 PARAMETRIC STUDY CONCLUSIONS

After the FEA program had been validated, a parametric study was performed to determine guidelines for designing mufflers with three-dimensional acoustic fields. A number of different features in the mufflers were studied. These include chamber and baffle tube lengths, the major diameter of the muffler, baffle tube radial position, and the number of baffle tubes used in a baffle. A large majority of

the models were completed using muffler model A as the base model. This was because model A is the smallest muffler model and simulations could be completed faster using this model.

The chamber and baffle tube lengths were found to have significant but unpredictable effects on the muffler performance. While the average muffler performance did not rise significantly, the peaks would shift left and right on the frequency scale. The only case in which these shifts could be predicted was in the case of the extended outlet baffle tube. This was believed to be because the resonance of this tube was not interfered with by the resonance of other chambers in the muffler.

The major diameter had the effect that was expected. As the muffler major diameter grew with respect to the diameter of the inlet pipe, the low frequency performance of the muffler improved. This was because the impedance mismatch between the expansion chamber and the inlet grew along with the discrepancy in the areas between those two sections.

The baffle tube radial position was also found to have significant effects on the muffler performance. As discussed in Section 1.3.2, the placement of the baffle tubes in the cross section of the baffle determines which modes are excited and transmitted through the chamber. By moving the baffle tube outwards we increase the chance that one of the higher order modes will have a node in that position. This would cause that particular mode to not be either excited or transmitted in the chamber depending on whether the baffle tube is at the inlet or outlet of the chamber.

The study of the number of baffle tubes did not isolate one dimension in the same way as the other studies, and as a result differing and inconclusive results were obtained. The features that were specific to model A also did not produce very significant results. It was found that the absence of the perforations improved the performance, but an explanation was not immediately available.

Although no new novel ideas for acoustic muffler design were devised, a better understanding of currently existing muffler elements was obtained. An even better understanding may be achieved through the completion of more studies. The least understood feature studied is the configuration of baffle tubes in the interior of the muffler (radial position, number, shape, perforations, etc.). New studies should be performed to focus on this particular feature as it seems to have a large impact on the muffler performance.

As mentioned numerous times, the conventional design of mufflers has been based on plane wave theory. Many of the features currently used in muffler design focus on the axial characteristics of that feature. This is because in plane wave theory the only direction of propagation is axial. However, three-dimensional propagation opens the door for a new school of thought regarding design. Now features that are based on radial dimensions can have significant impact as well. This is why so much change in performance was observed when altering the baffle tube configurations throughout the study. This very important concept should be kept in mind when investigating new muffler designs.

APPENDIX A

PITTSBURGH SITE EXPERIMENTAL SETUP DESIGNS

This section details the designs used for the fabrication of the Pittsburgh experimental setup.

A.1 SPEAKER TO PIPE COUPLING

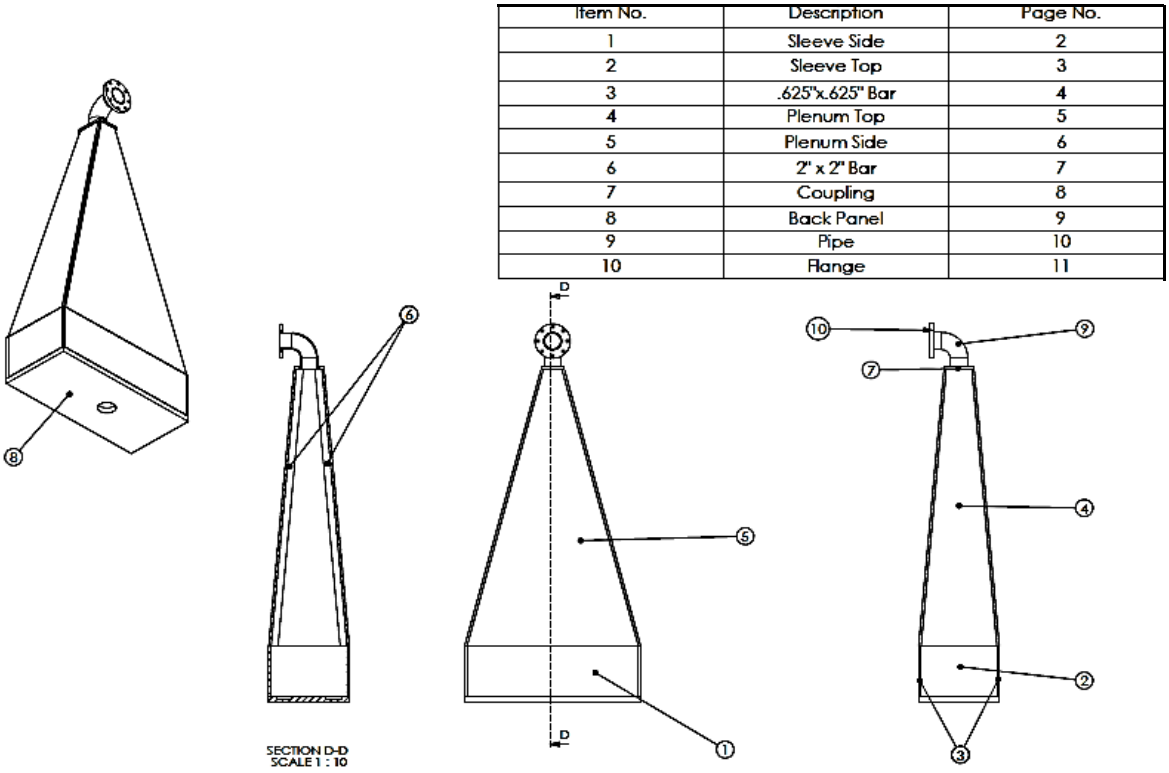

Item No.	Description	Page No.
1	Sleeve Side	2
2	Sleeve Top	3
3	.625"x.625" Bar	4
4	Plenum Top	5
5	Plenum Side	6
6	2" x 2" Bar	7
7	Coupling	8
8	Back Panel	9
9	Pipe	10
10	Flange	11

Figure A.1: Assembled speaker to pipe coupling

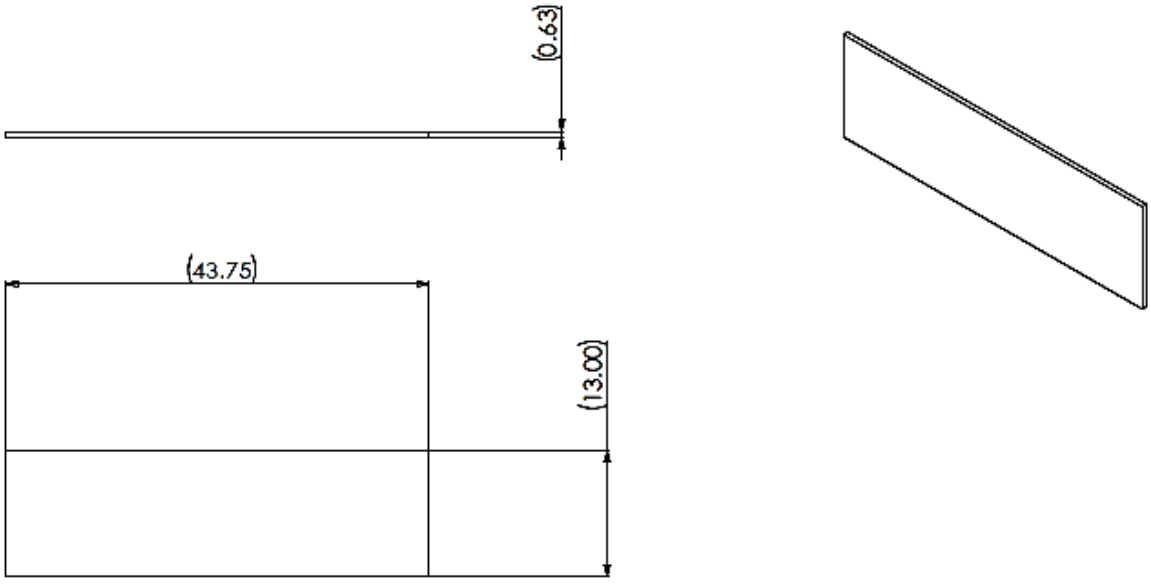

Figure A.2: Speaker to pipe coupling sleeve side panel

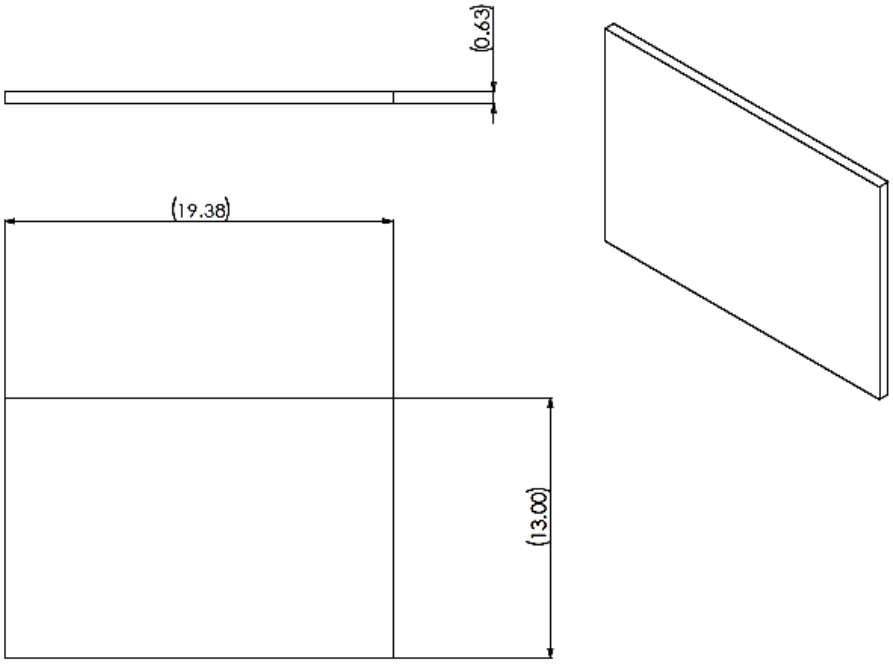

Figure A.3: Speaker to pipe coupling sleeve top panel

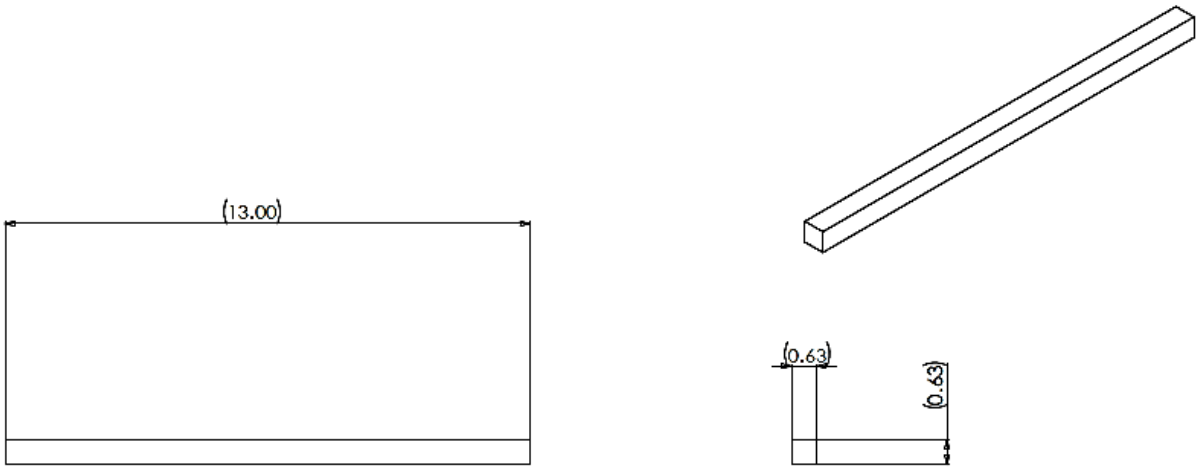

Figure A.4: Speaker to pipe coupling .625” x .625” bar

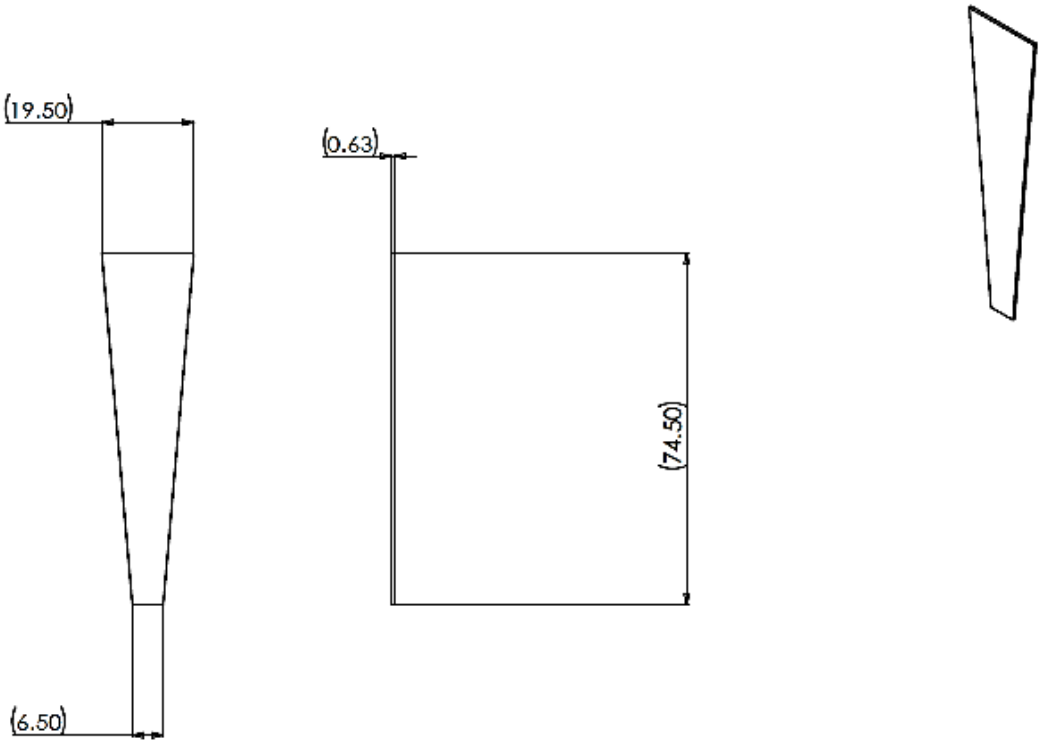

Figure A.5: Speaker to pipe coupling plenum top panel

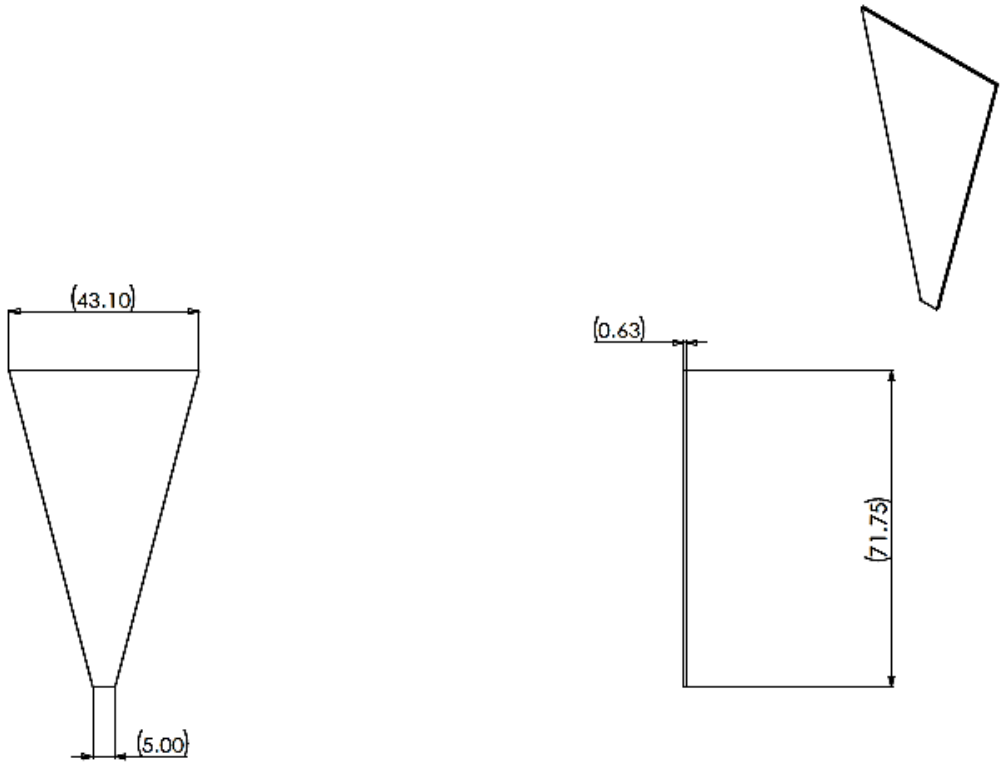

Figure A.6: Speaker to pipe coupling plenum side panel

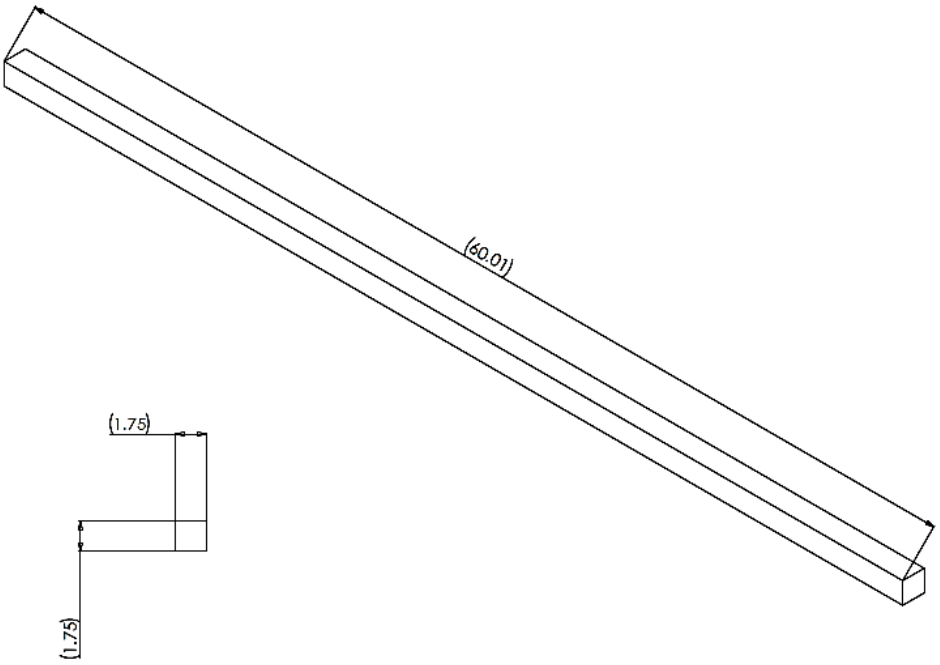

Figure A.7: Speaker to pipe coupling 2” x 2” bar

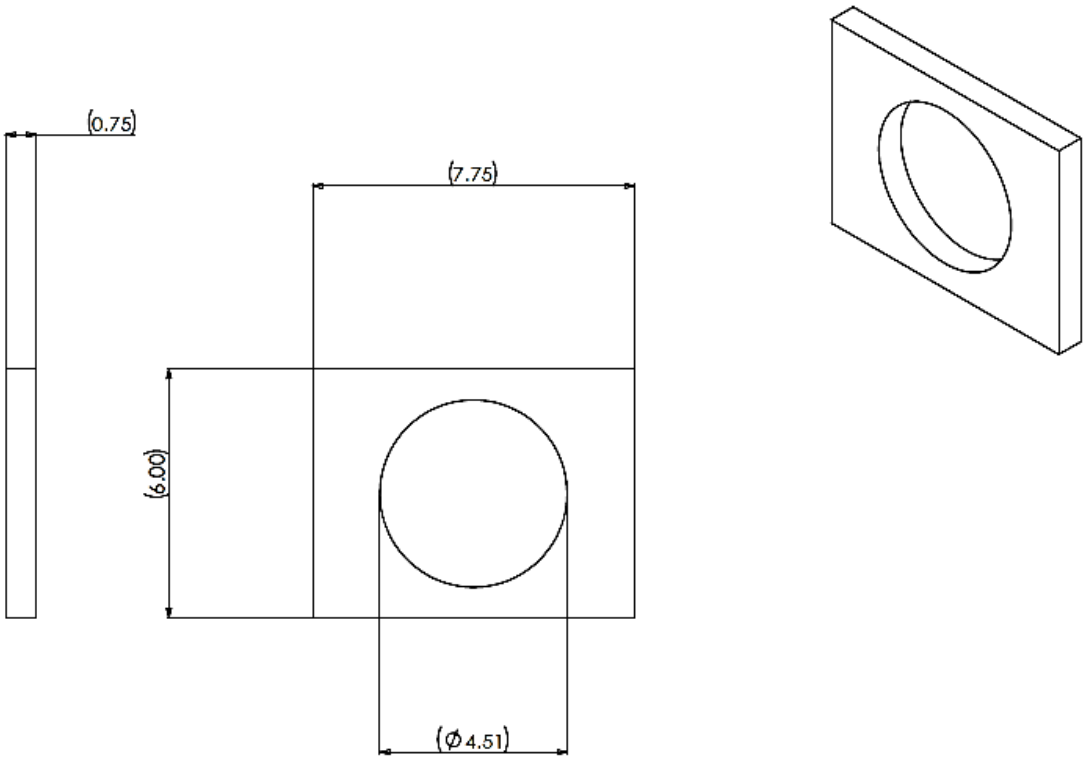

Figure A.8: Speaker to pipe coupling plenum coupling

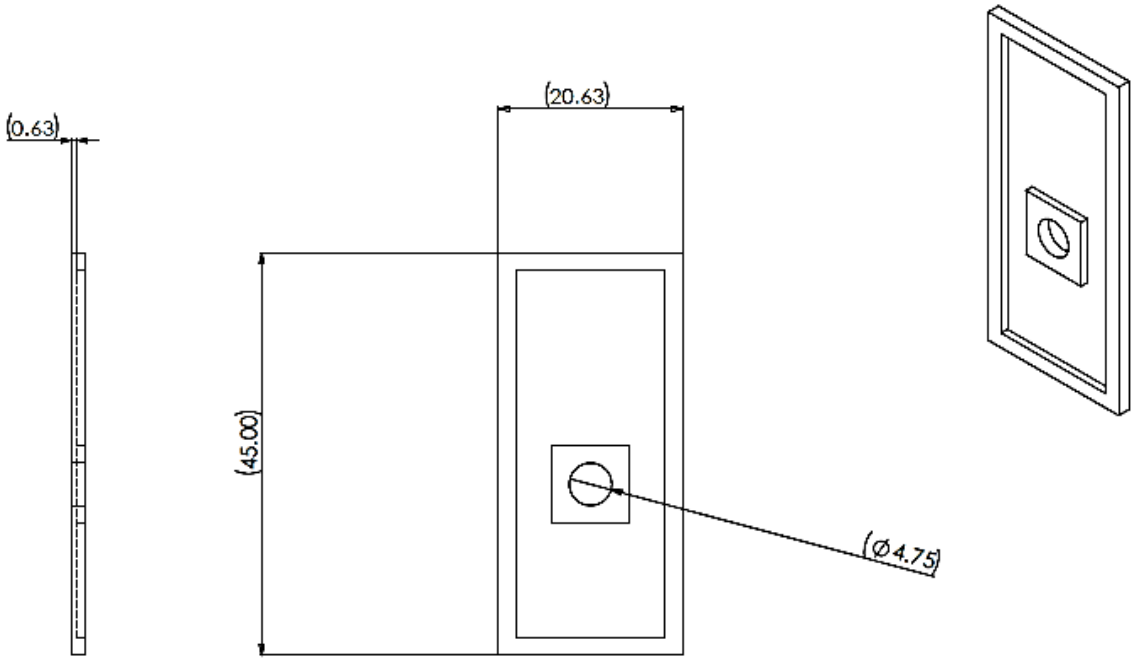

Figure A.9: Speaker to pipe coupling back panel

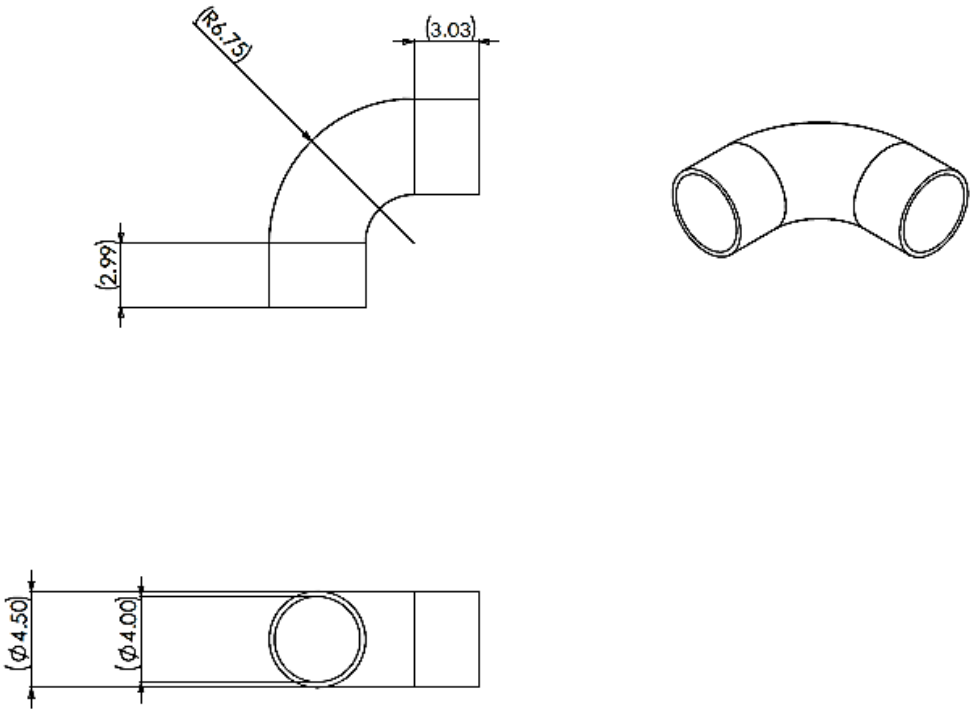

Figure A.10: Speaker to pipe coupling pipe

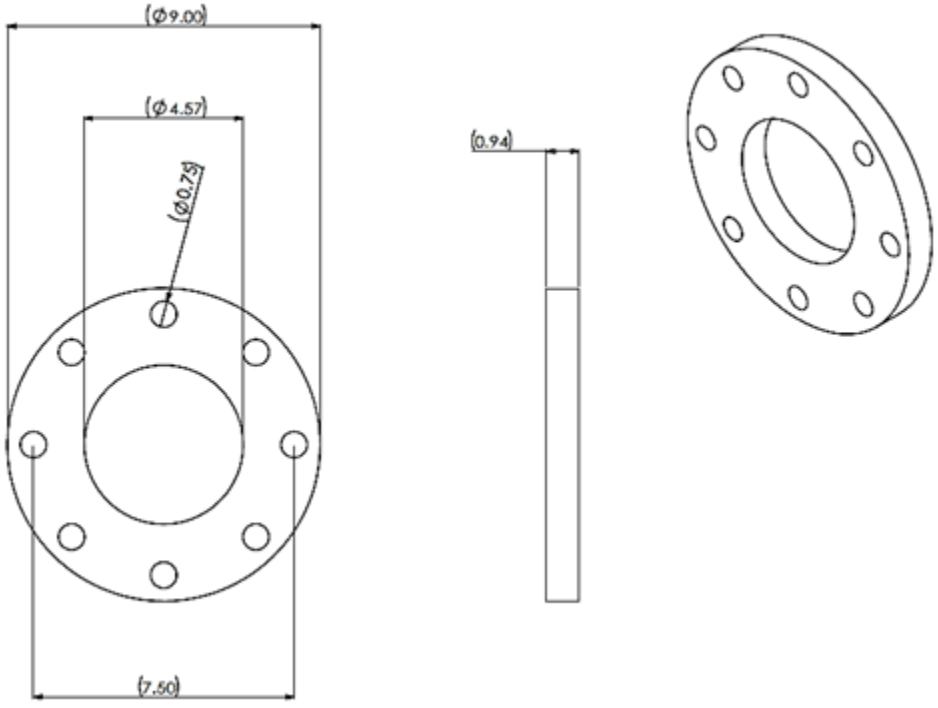

Figure A.11: Speaker to pipe coupling flange

A.2 ANECHOIC TERMINATION

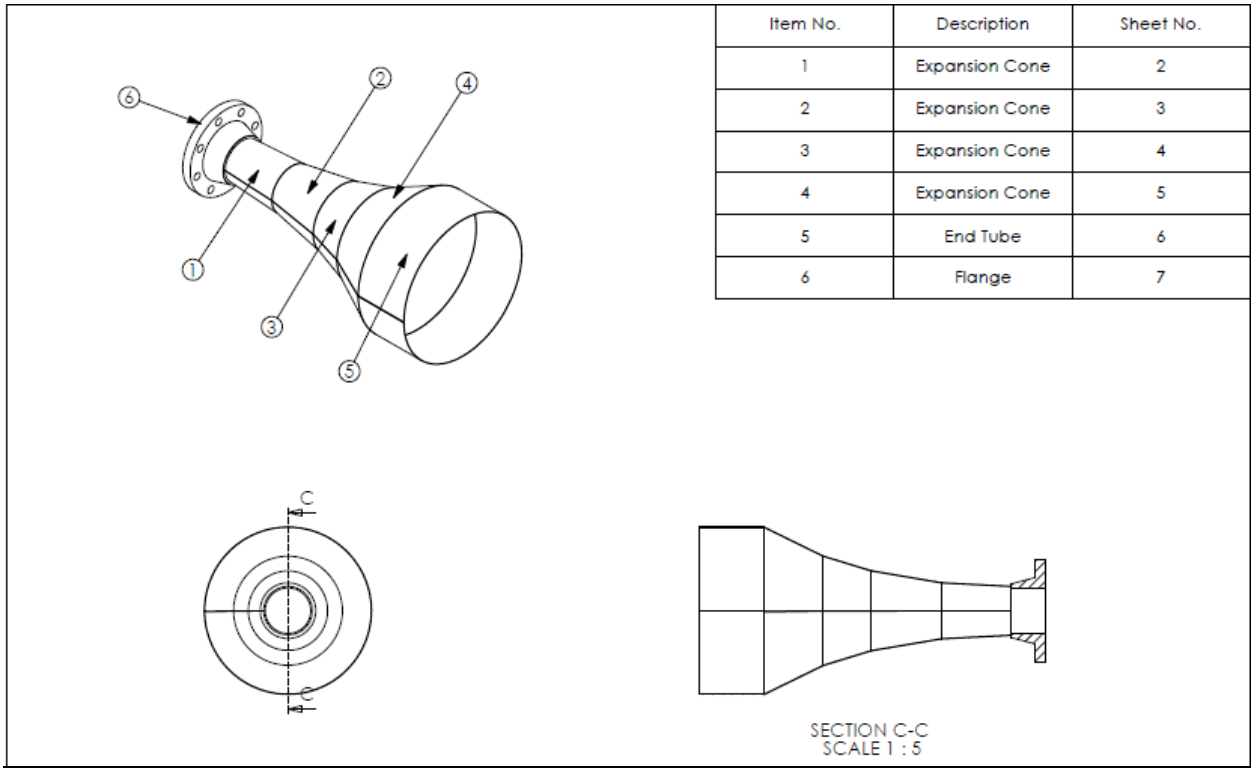

Figure A.12: Assembled anechoic termination

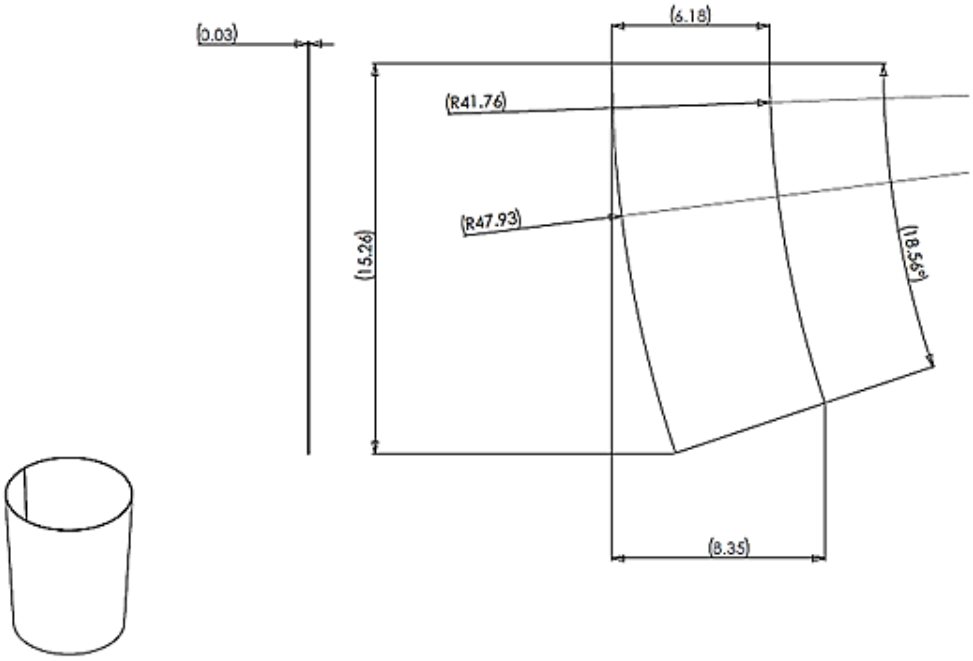

Figure A.13: Anechoic termination expansion cone 1

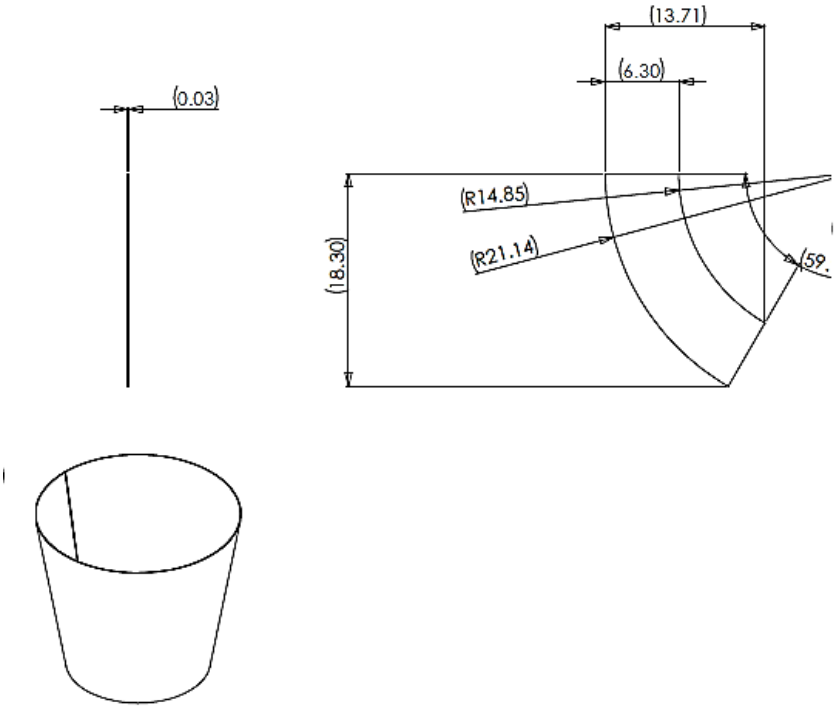

Figure A.14: Anechoic termination expansion cone 2

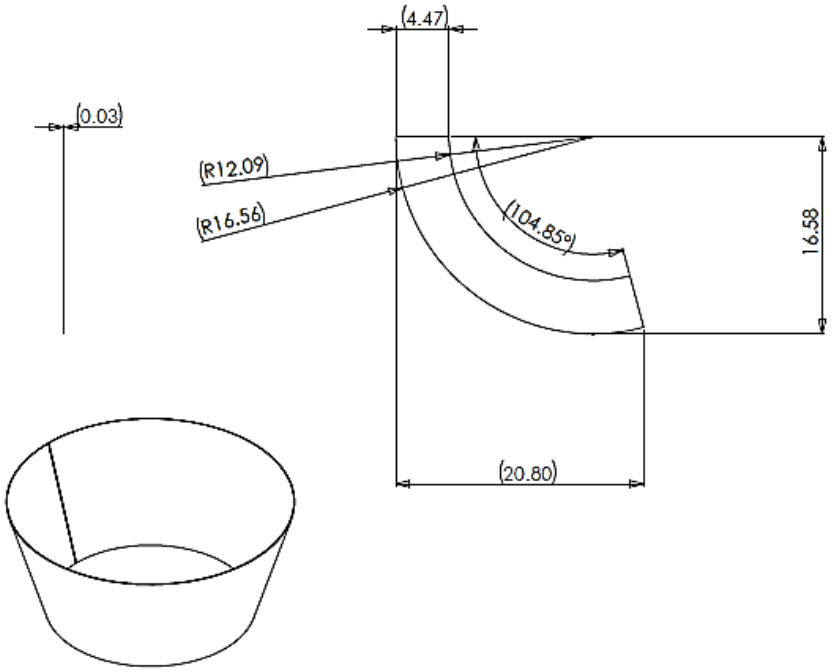

Figure A.15: Anechoic termination expansion cone 3

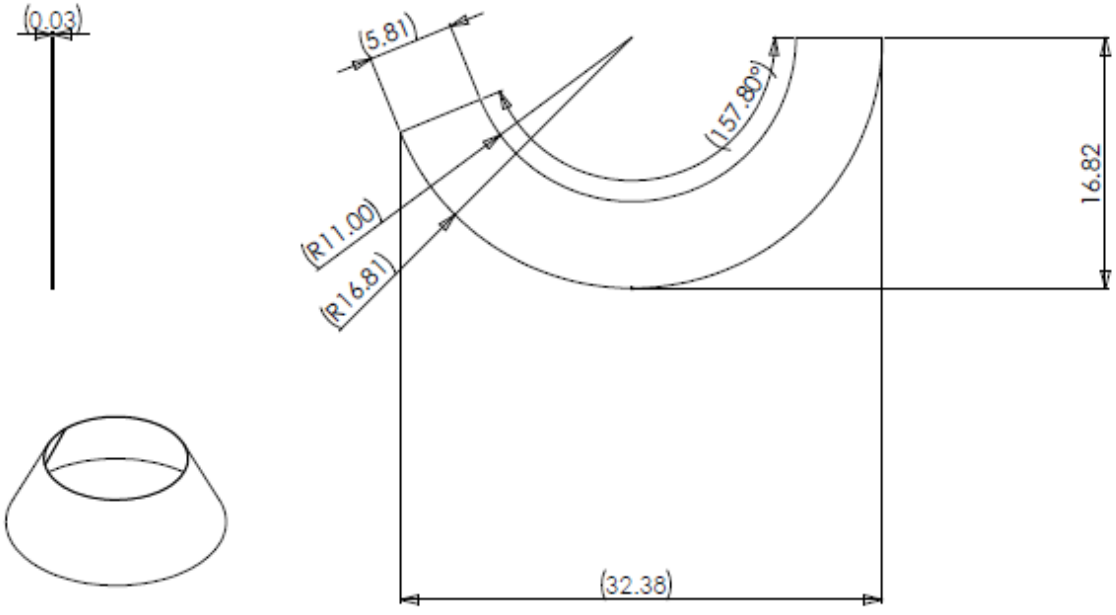

Figure A.16: Anechoic termination expansion cone 4

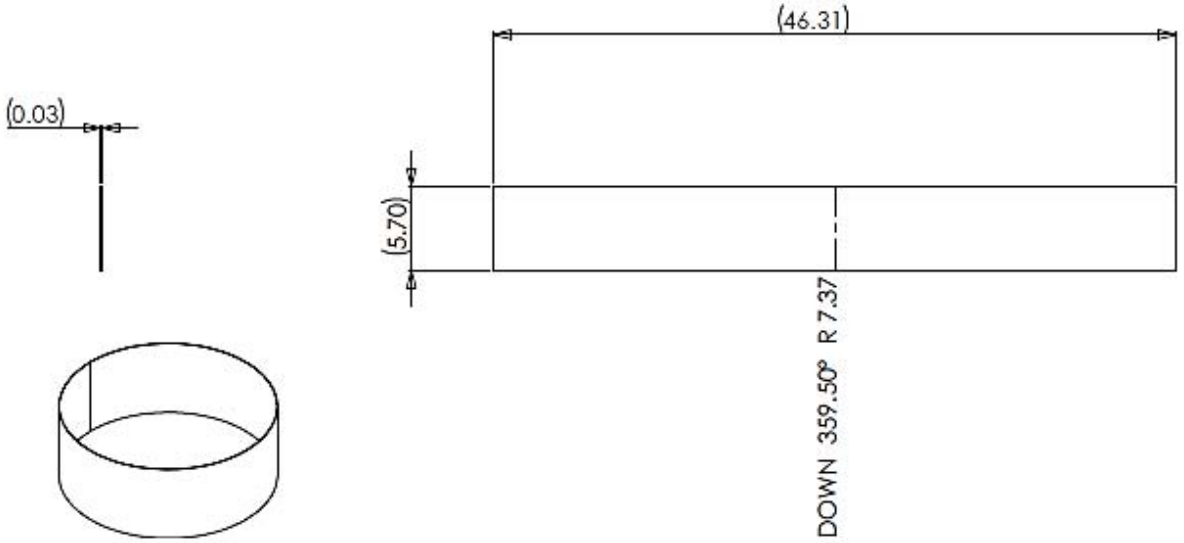

Figure A.17: Anechoic termination end tube

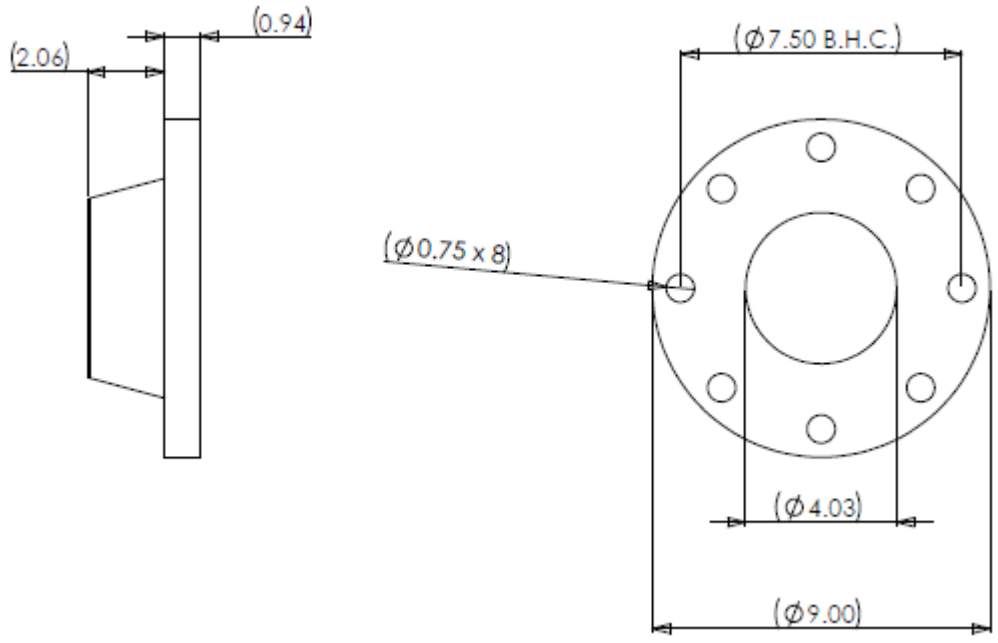

Figure A.18: Anechoic termination flange

A.3 EXPERIMENTAL SETUP PIPES

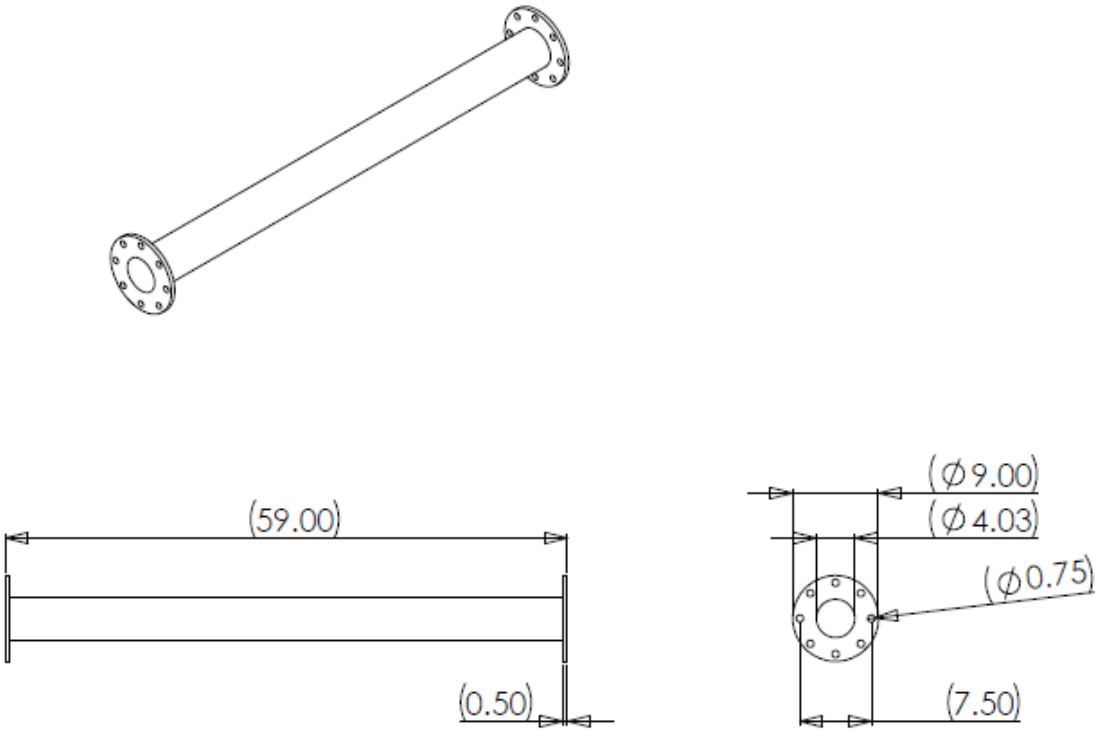

Figure A.19: IL reference pipe

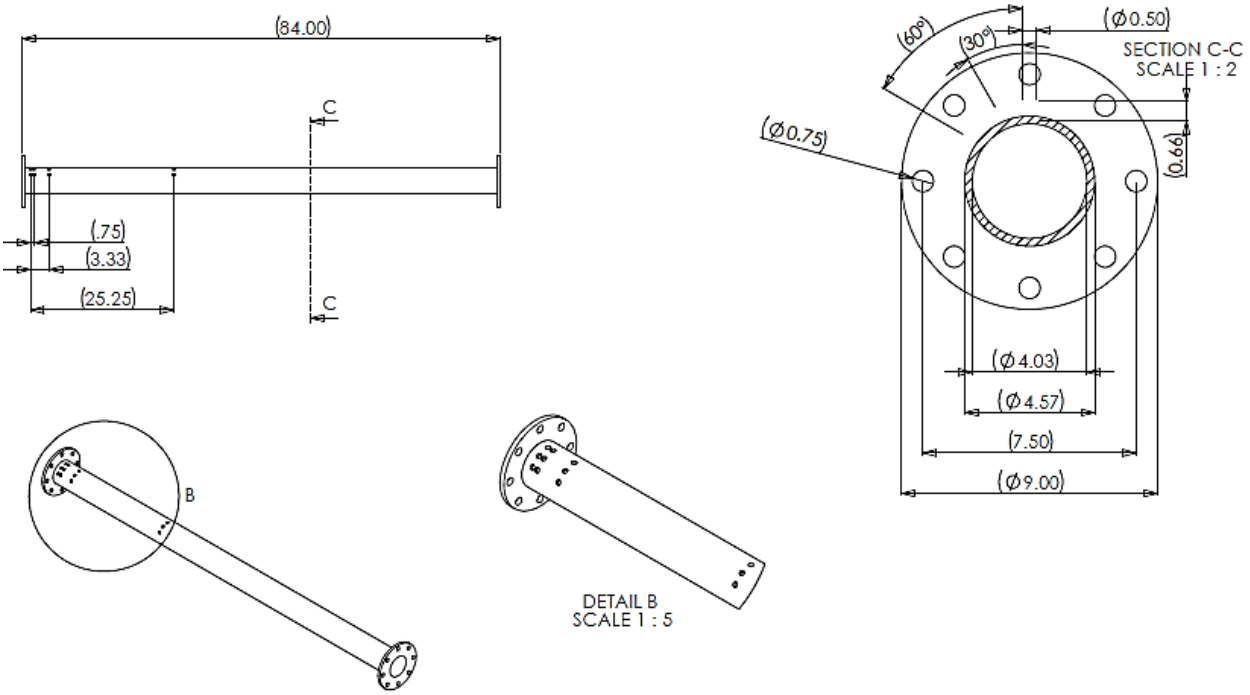

Figure A.20: Inlet measurement pipe

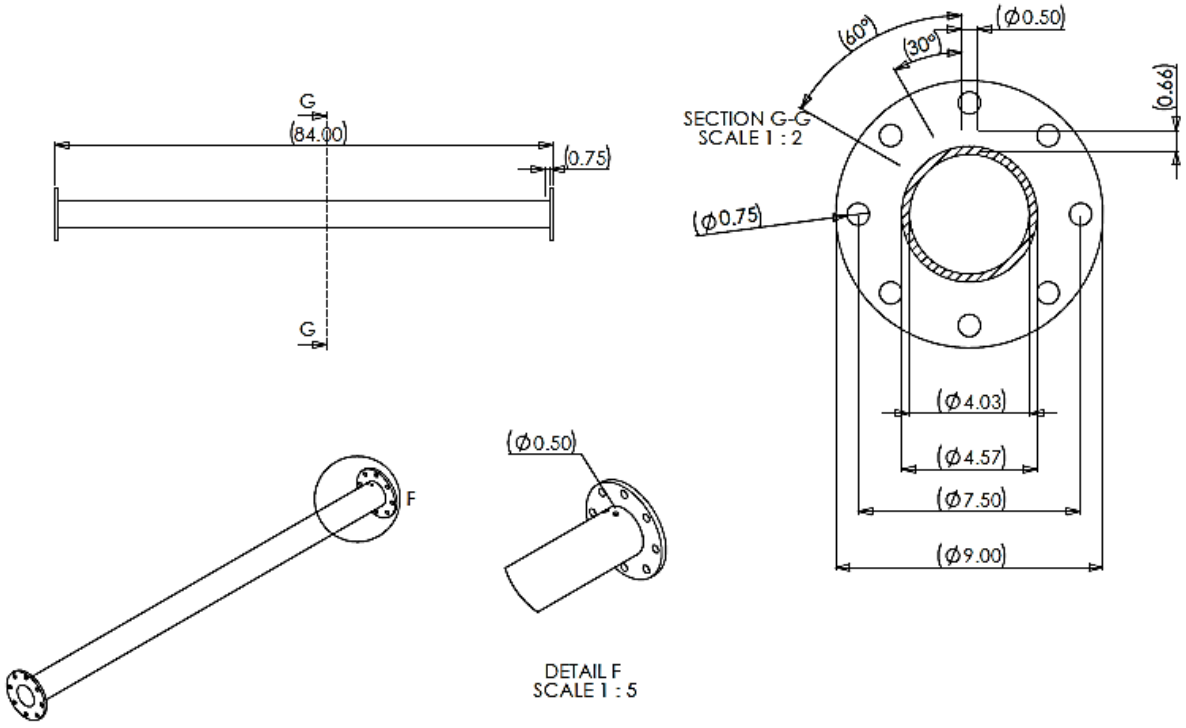

Figure A.21: Outlet measurement pipe

APPENDIX B

MATLAB CODES

The following appendix shows some of the Matlab codes that were written to capture, analyze, and post-process data throughout the course of this research. The Matlab codes that are not included are ones that are very routine and simple codes that were used to load and plot data.

B.1 CATALYST CALCULATIONS

```
clc
clear all

%these values are drawn from a spreadsheet. They should be the only pieces
%that change from test to test
R=;             % Flow Resistance
phi=;           % Open Area Ratio
Scoeff=;        % Value of S before the frequency vector is put in place
SOS=;           % Speed of sound in air at operating temp. and pressure
density=;       % Density at simulation temp. and pressure
gamma=;         % Ratio of specific heats at temp. and pressure
Pr=;            % Prandtl number at temp. and pressure


%setting up and solving catalyst equations form design element section
%of literature review

%setup a frequency vector
freq=linspace(10,20000,2000);

%calculate a vector for S* sqrt(-i)
%Matlab reccomends that 1i is used instead of i for the imaginary unit
```

```
%The equation for Gc(S) in the literture review calls for Bessel functions
%that are calculated as J(s*sqrt(-i)). the variable s*sqrt(-i) is setup
%below
S = sqrt(-1i) * Scoeff * sqrt(freq * 2 * pi);

%Calculate a vector for S*sqrt(Pr)*sqrt(-i)
%In the final equation for speed of sound Gc(S*sqrt(Pr)) is called for.
%This sets up a variable to for that equation
S2 = sqrt(-1i) * Scoeff * sqrt(freq * 2 * pi) * sqrt(Pr);

%calculate Gc(S) and Gc(S*sqrt(Pr))
Bes0 = besselj(0,S);      %Bessel function of first kind, order 0 for Gc(S)
Bes1 = besselj(1,S);      %Bessel function of first kind, order 1 for Gc(S)
Bes0_2 = besselj(0,S2);   %Bessel function of first kind, order 0 for
Gc(S*sqrt(Pr))
Bes1_2 = besselj(1,S2);   %Bessel function of first kind, order 1 for
Gc(S*sqrt(Pr))
X = Bes1 ./ Bes0;         %Next two lines divide the Bessel functions and put
them into an array ...
X_2 = Bes1_2 ./ Bes0_2;   %to make calculation later on easier
Gc   = (-S  ./ 4 .* X)   ./ ( 1 - ( (2 ./  S) )  .* X );    % calculation of
Gc(S)
Gc_2 = (-S2 ./ 4 .* X_2) ./ ( 1 - ( (2 ./ S2 ) ) .* X_2 );  % calculation of
Gc(S*sqrt(Pr))

%breakdown equations for speed of sound and density into smaller parts
fanr = R * phi * Gc;      % Numerator of fraction in first brackets of SOS
equation
fanr2 = R * phi * Gc_2;   % Numerator of fraction in the denominator of the
fraction in the second brackets of SOS eqaution
Y = 1i * freq * 2 * pi * density;  % Denominator of fraction in first
brackets of SOS equation
denom1 = 1 + (fanr ./ Y); % Entire term in first brackets of SOS equation
denom2 = gamma -( (gamma-1) ./ (1+fanr2 ./ Y / Pr) ); %Entire term in second
brackets of SOS equation
denom = sqrt(denom1 .* denom2); %Entire denominator of SOS equation

%calculate speed of sound and density
Cm = SOS ./ denom;
rhom = density - 1i * fanr ./ (freq .* 2 .* pi);

%plot results
figure(1)
plot(freq, real(Cm), freq, imag(Cm), freq, ones(length(freq))*SOS)
legend('real(Cm)','imag(Cm)','SOS')
xlabel('Freq (Hz)'), ylabel('Mag')

%save results
sos_vxc_param(:,1)=freq;
sos_vxc_param(:,2)=real(Cm);
sos_vxc_param(:,3)=imag(Cm);
rho_vxc_param(:,1)=freq;
rho_vxc_param(:,2)=real(rhom);
rho_vxc_param(:,3)=imag(rhom);
save sos_vxc_param
save rho_vxc_param
```

B.2 DATA ACQUISITION

```
clear
clc

%setup input object and create channel
ai=analoginput('nidaq','Dev1');
addchannel(ai,0);

%set sampling frequency and number of samples
Fs=50000;
samp=Fs*60;
set(ai,'SampleRate',Fs)
set(ai,'SamplesPerTrigger',samp)

%set gain and sensitivity of microphone system
gain=10;
sens=.045; %.045 V/Pa for 130d20, .05 V/Pa for 377B02

%Start data acquisition
start(ai)

%convert input voltage to pressure
data = getdata(ai)/gain/sens;

%Plot results and create time vector
plot(data)
t=linspace(0,samp/Fs,samp);

%create time and data array and save
test_name=horzcat(t',data);
save('test_namename','test_name')

%clear input object
delete(ai)
clear ai
```

B.3 TIME HISTORY ANALYSIS

B.3.1 Load and Analyze Data

```
clear
clc

%set FFT size
Nfft=4096;

%load time histories
load muff0half.mat
load muff0half2.mat
FsIL =50000;   % set sampling rate
x1 = muff0half(:,2);     % extract pressure data
x2 = muff0half2(:,2);     % extrcat pressure data

%obtain spectral data from spect function
[Pmuff1, Fmuff1] = spect(x1, Nfft, Nfft/2, hanning(Nfft), FsIL);
[Pmuff1_2, Fmuff1_2] = spect(x2, Nfft, Nfft/2, hanning(Nfft), FsIL);
```

B.3.2 Spect Function

```
function [H,f] = spect(x, y, Nfft, OLpts, window, Fs)

switch nargin
%call different cases of the built in Matlab command spectrum
case 1
   if nargout >= 1
      [H,f] = spectrum(x);
   else
      spectrum(x)
   end
case 2
   if nargout >= 1
        [H,f] = spectrum(x, y);
   else
        spectrum(x, y)
   end
case 3
   if nargout >= 1
        [H,f] = spectrum(x, y, Nfft);
   else
        spectrum(x, y, Nfft)
   end
case 4
   if nargout >= 1
```

```
        [H,f] = spectrum(x, y, Nfft, OLpts);
    else
        spectrum(x, y, Nfft, OLpts)
    end
case 5
    if nargout >= 1
        [H,f] = spectrum(x, y, Nfft, OLpts, window);
    else
        spectrum(x, y, Nfft, OLpts, window)
    end
case 6
    if nargout >= 1
        [H,f] = spectrum(x, y, Nfft, OLpts, window, Fs);
    else
        spectrum(x, y, Nfft, OLpts, window, Fs)
    end
end
```

B.4 APPLICATION OF NOISE FLOOR

```
clear
clc

%load in saved matlab variables from time history analysis
load meas_vxc_cold
load meas_background

%load data from excel files. If you wanted to load a .csv file you change
%these lines to: e.g.
%variable_name=load('data.csv');
%These commands load the data in to an automatically sized matrix
muffsim=importdata('Muffled.xls');

%using the command 'importdata' will load the data and the header lines.
%These commands extract just the data. If there are no header lines in the
%loaded file then these lines are not necessary
muff_sim=muffsim.data(:,2);

%In this section I implement the noise floor. I run a loop that executes
%N times. N being the length of the vector in question. The if statements
%allow me to create the doctored data. back(n) accesses the nth entry in
%the vector back. n counts up in the loop from 1 to the length of the
%vector
for n=1:length(muff_sim)
        muff_sim_nf(n)=20*log10(10^((muff_sim(n)-94)/20)+10^((back(n)-
94)/20))+94;
        nomuff_sim_nf(n)=20*log10(10^((nomuff_sim(n)-94)/20)+10^((back(n)-
94)/20))+94;
end
```

APPENDIX C

LMS VIRTUAL.LAB ACOUSTICS SIMULATION PROCEDURE

This Appendix is an overview of the procedure used to model the muffler and setup a FEA simulation in LMS Virtual.Lab Acoustics.

C.1 MODELING PROCEDURE

While the typical model of a muffler is of the solid shell of, the FEA analysis is performed on the fluid (air volume) interior of the muffler, so this is the portion that must be modeled for importation into the LMS program.

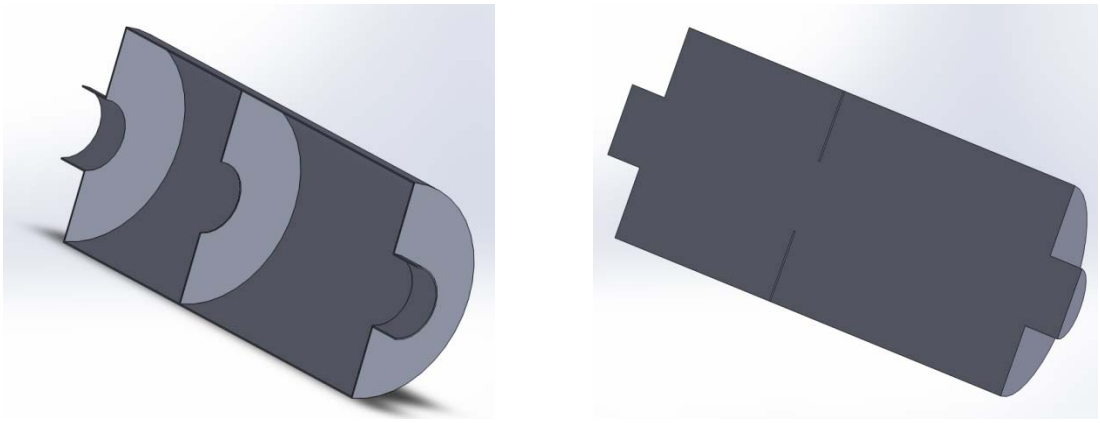

Figure C.1: Illustration of both shell (left) and fluid domain(right) of a simple muffler

The fluid model can be created from the shell model with ease in most solid modeling programs. In Solidworks, a simple way to perform this is by "capping" the shell model, creating a large solid block around the shell model, subtracting out the shell using the combine feature, and then deleting the extra material around the interior fluid domain. This process is illustrated in figure 2.

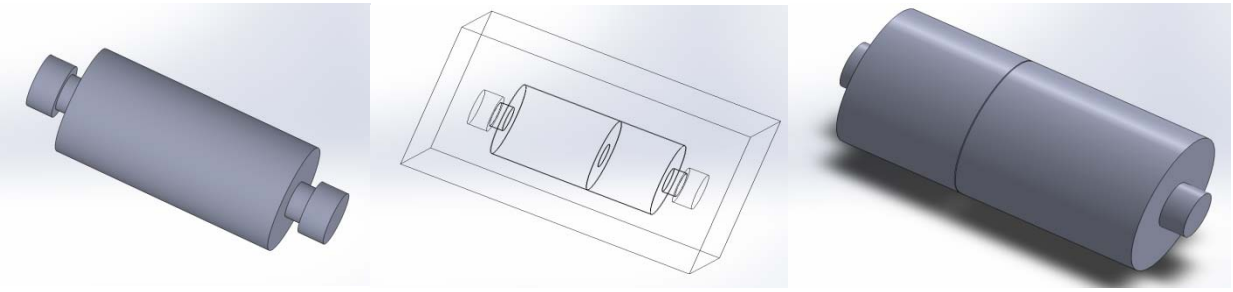

Figure C.2: showing the capped muffler (left), the encompassing solid block (middle), and the final fluid domain (right)

If the model is for a parametric study, or for validation of field noise reduction (NR) measurements, it is ready to be imported into LMS at this point. However, if the model is for validation of field insertion loss (IL) measurements, more manipulation is required. The model manipulation that is required at this point will depend on the test setup that is used for the field measurements. If there is additional outlet pipe added to the muffler then the fluid on the inside of this pipe should be modeled as well. Next, a mushroom or hemispherical like cap should be added to the end of the setup to represent the opening of the pipe into the atmosphere. For a flanged ending, a hemispherical cap should be added. For an un-flanged ending a mushroom like cap should be added.

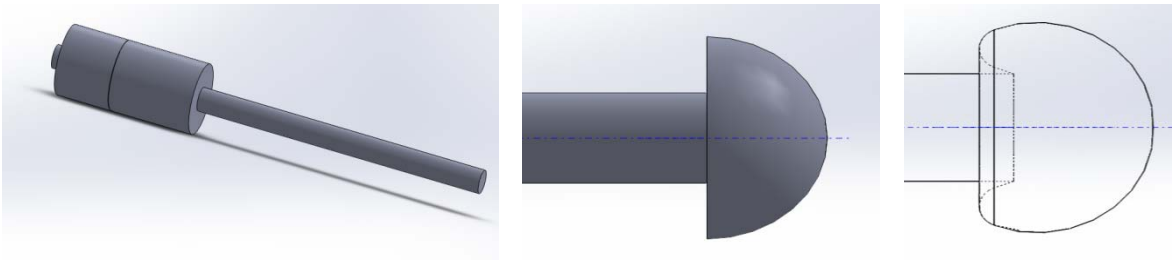

Figure C.3: Modifications to model for IL measurement validation. Extra fluid domain for the outlet pipe (left), hemispherical cap (middle), mushroom like cap (right)

Also, the measured reference system should be modeled. A hemispherical or mushroom cap should be added to the outlet of the reference system as well. LMS does not import Solidworks files so all files should be saved in STEP format.

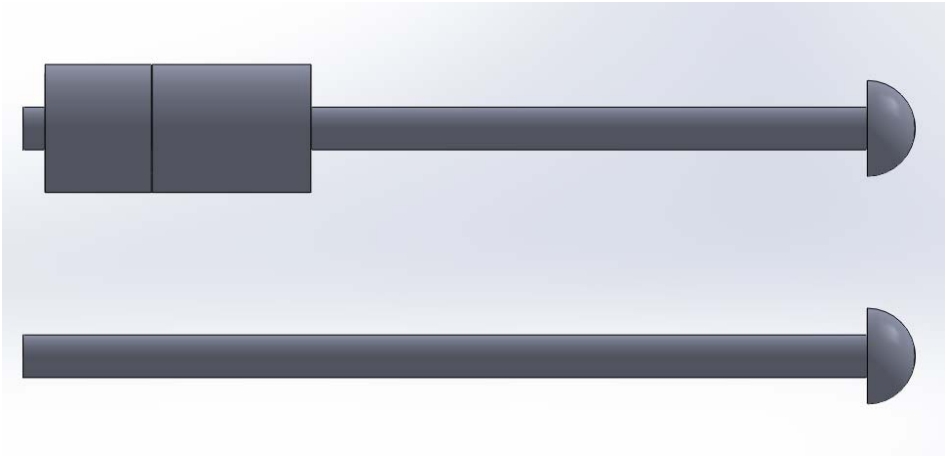

Figure C.4: Example of a muffler fluid domain and it's corresponding reference system

C.2 SIMULATION PROCEDURE

This section will describe the steps necessary to setup and run a simulation of the acoustic performance of a muffler in LMS Virtual.Lab Acoustics.

1.) Import Model in to LMS
   a.) File → Open

2.) Enter Mesh Coarsening Module
   a.) Start → Structures → Mesh Coarsening

3.) Create Surface Mesh
   a.) Insert → Pre/Acoustic Meshers → Pre/Acoustic Meshers → Tessellation Mesher
   b.)The grid support is the imported solid model which can be selected in the analysis tree under the links manager
   c.) The step value is the size of the element. This value should be chosen based upon the highest frequency of interest. There should be a minimum of four elements per wavelength.
   d.) The sag value determines how closely the mesh will model curved surfaces in the model. This value should always be considerably smaller than the step value.
   e.) Once all the parameters have been chosen select apply

4.) Merge Coincident Nodes
   a.) Tools → Nodes → Merge Coincident Nodes
   b.) Choose "Merge Nodes Within The Selection"
   c.) Choose the tessellation mesh for selection groups
   d.) Use 0mm for the tolerance
   e.) Check all three boxes "Exclude Nodes of Same Element", "Merge Impacted Coincident Elements", "Preview the Nodes Before the Merge"
   f.) Select apply

5.) Enter Acoustic Harmonic FEM Module
   a.) Start → Acoustics → Acoustic Harmonic FEM

6.) Create Volume Mesh
   a.) Tools → Meshing → Tetrahedron Filler
   b.) Choose the "Tessellation Mesh" in the analysis tree for the mesh parts
   c.) Choose "Linear Elements"
   d.) Use one for the size progression
   e.) Select apply

   Note:
   The tetrahedron filler mesh process can be unreliable. There are procedures that may be employed if the tetrahedron filler does not work. While these are not guaranteed to work either, the success rate for meshing can be greatly improved when all of the methods are considered. The procedures are enumerated below. Trying either method or a combination of the two may produce a surface mesh that will work with the tetrahedron filler.

Workaround 1: Fix Mesher

Going back to the Mesh Coarsening module you can apply the fix mesher to the tessellation mesh created in step 3. Then applying the tetrahedron filler to the fix mesher may produce the desired mesh.

a.) Start → Structures → Mesh Coarsening
b.) Insert → Pre/Acoustic Meshers → Pre/Acoustic Meshers → Fix Mesher
c.) Select the tessellation mesh from the analysis tree as the grid to fix and select apply.
d.) Repeat steps 5 and 6 with the fix mesh substituted for the tessellation mesh.

Workaround 2: Splitting the Surface Mesh

In this method a tessellation mesh is created with elements twice as large as the desired size. This will sometimes produce a working mesh. This mesh can then be split in half. The tetrahedron filler can then be applied to the split mesh.

a.) Start → Structures → Mesh Coarsening
b.) Follow step 3 to create a tessellation mesh that has twice the desired element size.
c.) Start → Structures → Finite Element Analysis Pre/Post → Nodes & Elements
d.) Tools → Mesh Modifications → Split 2D Elements
e.) Select the tessellation mesh as the group selection and apply
f.) Repeat steps 5 and 6 with the resulting tessellation mesh

Wokaround 3: Changing the Mesh size

This method just involves repeating step 3. A different value should be used for the step and sag values each time step 3 is repeated.

7.) Set Mesh Parts Type
a.) Tools → Set Mesh Parts Type
b.) Deactivate the tessellation mesh
c.) Set the tetrahedron filler mesh as acoustical mesh
d.)Select ok
e.) Right click on the tessellation and select hide to hide the surface mesh

8.) Create Acoustic Mesh Preprocessing Set
a.) Insert → Acoustic Mesh Preprocessing Set
b.) Choose the tetrahedron filler mesh as the mesh parts
c.) Select ok
d.) Right click on the acoustic mesh preprocessing set and select update

9.) Make Mesh Groups
a.) Insert → Mesh Grouping → Auto-update Group Set
b.) Right click on the Default Group Set → Mesh Grouping →Auto-update Group
c.) Select the type of auto update group necessary and create

Note:
For the Inlet and Outlet groups a feature angle group can be used. This type of group allows you to select a starting element and then choose all elements in the surrounding area that have a normal vector pointing in a direction within a specified angle of the normal angle of the starting element. For a flat surface a feature angle of ten to fifteen degreed is appropriate. For a curved surface a feature angle for seventy to eighty degrees is appropriate. The input groups will be "Nodes and Elements", then under the "Type Specific" tab the feature angle and starting element can be chosen.

For the catalyst, three different types of mesh groups must be used.

1.) The trap group will create a group of elements, faces, edges, or nodes inside of a three dimensional shape specified by the user. The input groups will be the "Nodes and Elements". Under the type specific tab the user can specify the dimensions of the trap. For the catalysts, the trap should encompass the catalyst as tightly as possible with an indefinite depth. Traps should be made for two perpendicular axes of each trap.
2.) The intersection group will create a group where two previously defined mesh groups share elements, nodes, etc. The input groups will be the mesh groups that the user wishes to isolate the intersection of. This group should be made by the two groups that intersect a catalyst on two different axes. This will isolate the catalyst.
3.) The union group will join separate mesh groups into the same mesh group. The input groups will be the mesh groups that the user wishes to join. Once an intersection group has been created for each catalyst, they may be joined together into a single group using a union group.

For the fluid medium (typically air), a difference group will be used. This type of group allows the user to create a mesh group using the remainder of one group being subtracted from another group. The Base group will be the "Nodes and Elements". The parts to subtract will be the union group created for the catalyst.

10.) Add Field Point Meshes to the Model

a.) Insert → Field Point Meshes → Spherical Field Point Mesh
b.) Enter in the coordinates that approximate the positions of the microphone during the test. These are the points where the simulation results will be saved in the model. The radius of the field point mesh should also be about the same size as the microphone.

Note:
The field point meshes are only needed for when the simulation is meant to be compared to a measurement or a realistic environment. For purely theoretical models the TL may be calculated automatically during the simulation when using the boundary condition in the next step.

11.) Add Duct Modes Boundary Condition

a.) Insert → Acoustic Boundary Conditions and Sources → Acoustic Boundary Condition and Source Set
b.) Right click on Acoustic Boundary Conditions and Sources → Add an Acoustic Boundary Condition
c.) Choose physical data type as annular/circular distributed duct modes
d.) Select ok
e.) In the analysis tree, expand annular/circular distributed duct modes boundary condition
f.) Double click on faces and choose the Inlet mesh group as the face

g.) Expand the data sources down to the edited load function, double click on the edited load function

h.)Either import a function using the import a file button under the commands tab, or create your own function by typing values into the data cells at the bottom and pressing enter

Note:

The input for this particular boundary condition is in units of acoustic intensity (W/m^2). If the model is for a parametric study, the input intensity can be a uniform value across the frequency range of interest. One Watt per square meter should be sufficient.

However, if the model is for validation of a real system, in order to get accurate pressure values at the field point meshes, the measured input from the field test must be used in the simulation. Generally the output from the test will be an array of dBV_{rms} versus frequency. To calculate the test input intensity, Equations 2-1, 2-2, and 2-15 must be used on the recorded input intensity from the field tests.

12.) Add the Outlet Condition

a.) In the analysis tree right click on Properties → New Acoustic Properties

b.) for a model with a flat outlet choose the anechoic end duct property and select the outlet mesh group as the application region

c.) for a model with a hemispherical or mushroom like outlet choose the automatically matched layer property, select the outlet as the application region, and pick the AML surface as the radiation surface for far-field calculation.

13.) Add Material to Analysis Tree

a.) In the analysis tree right click on Materials.1 → New Materials → New Fluid Material

b.) Enter in the sound velocity and density for the ambient fluid at the appropriate temperature

c.) Add materials for both the air and the catalyst

d.) For the catalyst it will be necessary to import a file with the information for a frequency dependent

Note:

1.) For larger models it may become necessary to apply some fluid damping to the model. This can be done by adding imaginary values to the speed of sound and density. Generally .025% -.05% damping is appropriate.

e.g. The speed of sound in air at 20 degrees Celsius is 343 m/s. With .05% damping the speed of sound in air at 20 degrees Celsius is 342.83 +.17i m/s

2.) When validating against a field test, the sound velocity and density for the ambient fluid should approximate the conditions in the field as closely as possible.

3.)To create the files that contain the frequency dependent speed of sound and density for the catalyst, Equations 1-32 through 1-39 must be used.

14.) Apply Material Properties to Model Mesh

a.) In the analysis tree right click on Properties.1 → New Acoustic Properties → New Acoustic Fluid Property

b.) Choose the appropriate mesh group for the “Application Region” and the appropriate material for the “Fluid Material”

15.) Add Mean Flow boundary condition

a.) Insert→ Mean Flow Boundary Conditions→ Mean Flow Boundary Condition Set
b.) Right click on the mean flow boundary condition set in the analysis tree and select add a mean flow boundary condition
c.) Select flow velocity and constant values as the physical data and mathematical types
d.) In the analysis tree, under the mean flow boundary condition, expand locations and double click on faces select the inlet as the support
e.)Now double click on constant values and set the desired flow velocity at the inlet
f.) Repeat steps b through e, but select the physical data type as flow potential and apply it to the outlet.

16.) Calculate Mean Flow

a.)Insert→FEM Analysis Cases→ Potential Flow Analysis Case
b.)Use the previously created mean floe boundary condition set
c.)Right click on the potential flow solution set and select update

17.) Add Analysis Case

a.) Insert → FEM Analysis Cases → Acoustic Response Analysis Case
b.) Use an existing boundary condition set and click on the "Acoustic Boundary Conditions and Sources" in the analysis tree
c.) Use no acoustic mode set
d.) Use no panel set
e.) Use no mean flow
f.) Choose ok

18.) Set Analysis Parameters

a.) Expand the acoustic response analysis case and double click on acoustic response solution set
b.) Choose to save the result at field points as vectors
c.) Unselect to save the potentials at acoustic nodes as vectors (this will not allow you to view the results at arbitrary points in the model, but it will significantly reduce the calculation time)
d.) Set the start, end, and step values for the frequency range, choose sweep ,and then click add
e.) Select the solving parameters tab; choose multi process frequency level and the direct solver
f.) Select the job and resources tab, and set the appropriate number of processes, and the maximum allocated memory

Note:

The number of processes will be determined by the size of the model, the number of processors and the available memory on the computer. Each process needs to have enough available memory to calculate the entire model.

$$Size\ of\ model \times number\ of\ processors\ used \leq Available\ RAM\ on\ computer \qquad (12)$$

If the simulation does not run to completion, it may be because there are an odd number of processors being used. It may also be caused by using too many threads per process. This problem can be solved by changing to an even number of processors and reducing the number of threads per process.

19.) Run Analysis

a.) Expand the acoustic response analysis case, right click on the acoustic response solution set and select update

20.) Convert Results to Function

a.)Insert → Other Analysis Cases → Vector to Function Conversion Case
b.)Select load vector to function for the conversion type
c.) Select "reference a defined vector set" and then select the acoustic response solution set in the analysis tree for the vector set
d.) Select all field points for the input and output points
e.) Select ok
f.) Expand the vector to function conversion case, right click on load vector to function solution set, and select update

21.) Average and Plot Results

a.) Insert → Functions Creator → Edited Load Function Set
b.) In the analysis tree double click on the edited load function set and select add edited function
c.) In the values tab select import a feature, then select the load vector to function solution set
d.) Do this for four values in the same field point, add them together, and then divide them by four to obtain the average acoustic pressure in the field point
e.) Add an edited function for each field point mesh
f.) In the analysis tree right click on one of the edited load functions and select new function display. Select finish in the dialogue box that opens.
g.) Repeat step f for each edited load function to plot all of the results

note:
In the edited load function editor there is a calculator. Once all four field mesh values are imported, in order to average the results, add the results using the "+" button three times. Then create a constant using the "const" button, and enter the desired value (4 in this case). Switch the locations of the values and the constant using the exchange L1 and L2 button, and divide using the divide button.

22.) Calculate TL

a.) Right click on the acoustic response solution set and select "New Function Display"
b.) Select "2D Display" and then "Finish"
c.) The "Select Data" window will show up and the user can select "Acoustic Power" for the transmitted power, "Input Power" for the incident power, and "Transmission Loss" for the transmission loss
d.) Once the desired data has been selected, click on display to have it plotted
e.)Double clicking on the different axes and selecting the format tab allows the user to select the different attributes of the chosen data and the scale it is plotted on
f.) Under the format tab choose dB(RMS) and then apply
g.)Right clicking the plot and then selecting "Export All Data" will allow the user to export the plotted data to an Excel file
h.) The file will be saved under the folder and file name indicated in the "File Name" box. This can be changed by clicking on the Browse button and choosing the folder and file name to save under

23.) Export Results

a.) In the analysis tree double click on the new function display
b.) Right click on the graph and select export all data
c.) Select browse to choose the name of the file and the folder in which it is saved

APPENDIX D

PARAMETRIC STUDY RESULTS

D.1 MODEL A

D.1.1 Length of chamber one

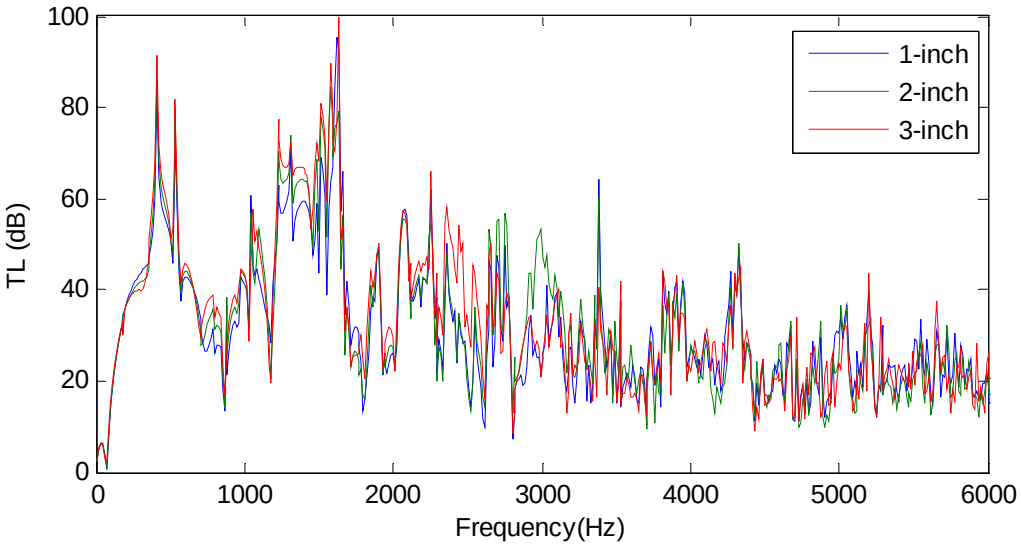

Figure D.1: Model A variation of the length of chamber one; Three of ten total models

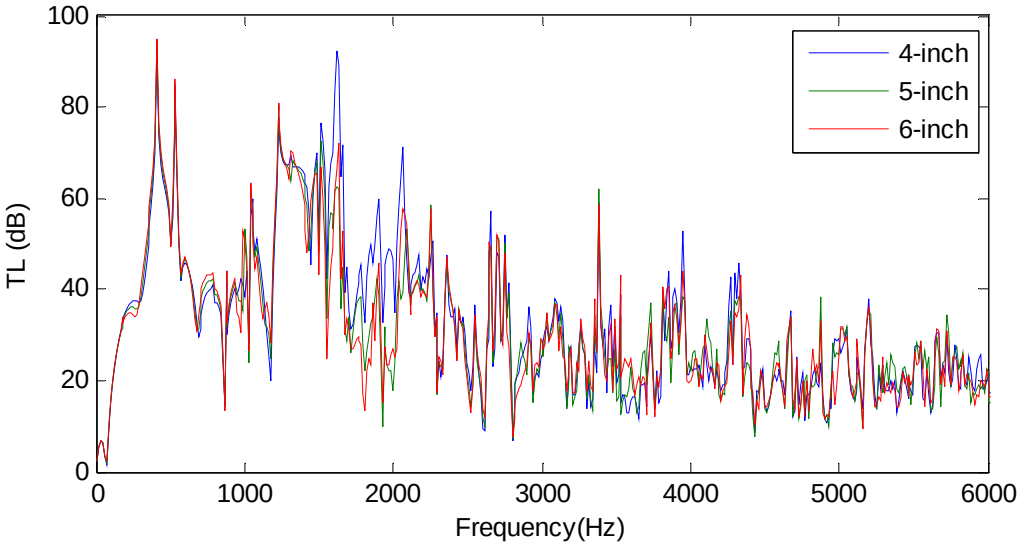

Figure D.2: Model A variation of the length of chamber one; Three of ten total models

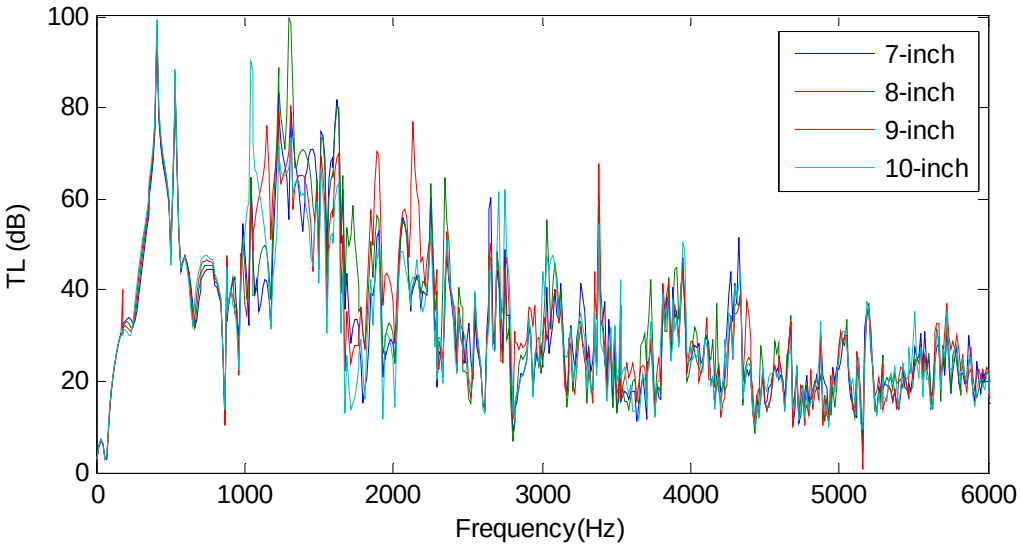

Figure D.3: Model A variation of the length of chamber one; Four of ten total models

D.1.2 Length of chamber two

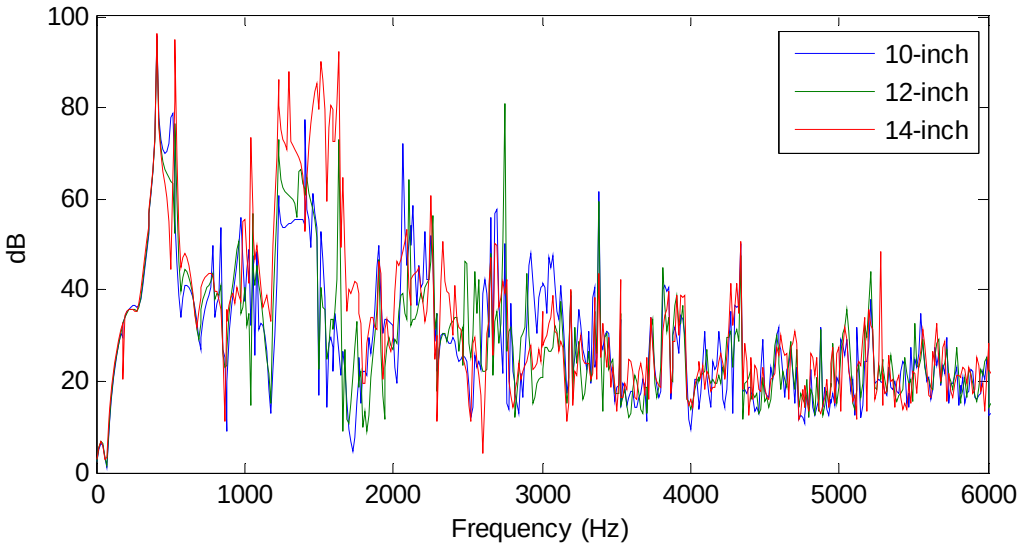

Figure D.4: Model A variation of the length of chamber two; Three of seven total models

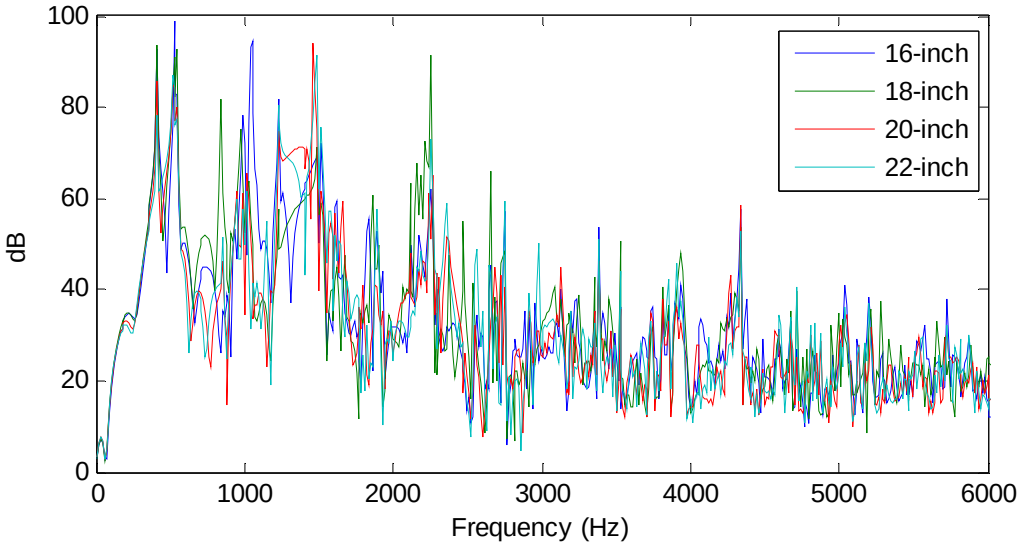

Figure D.5: Model A variation of the length of chamber two; Four of seven total models

D.1.3 Length of baffle tubes in chamber two

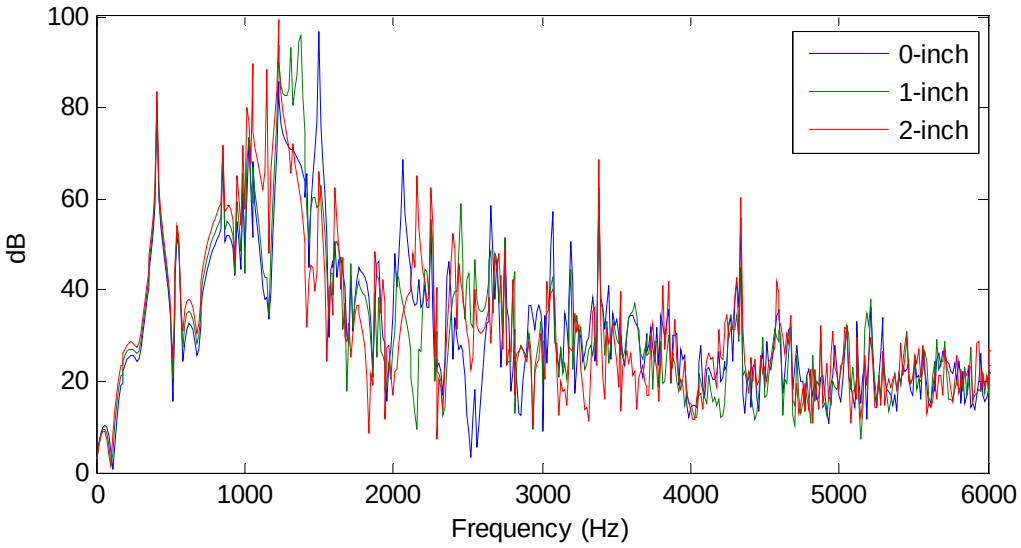

Figure D.6: Model A variation of the length of the baffle tubes in chamber two; Three of eleven total models

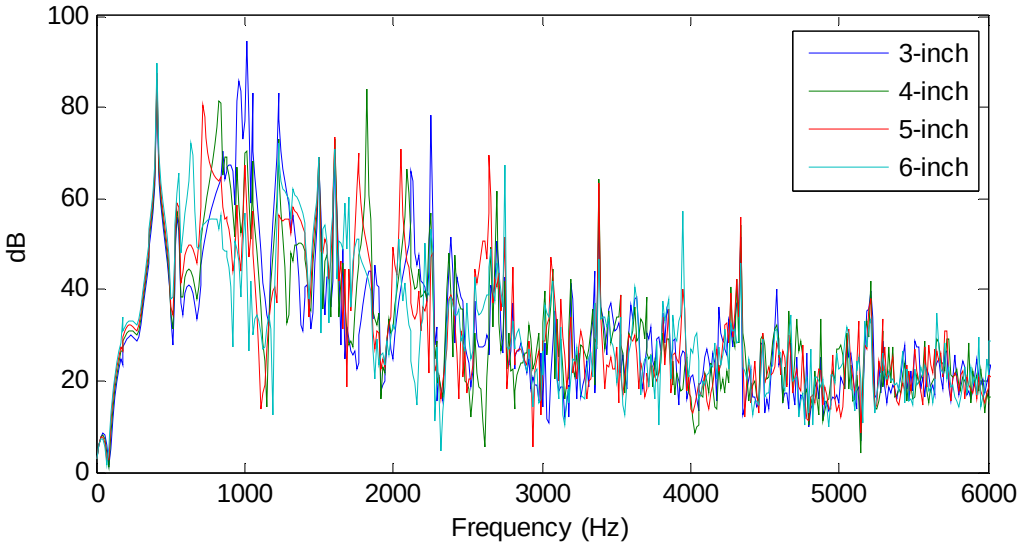

Figure D.7: Model A variation of the length of the baffle tubes in chamber two; Four of eleven total models

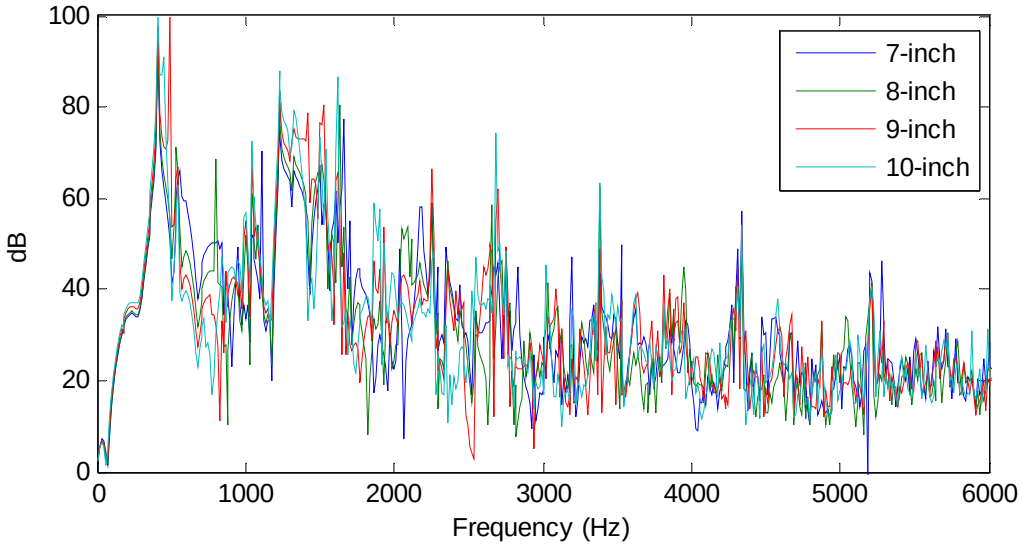

Figure D.8: Model A variation of the length of the baffle tubes in chamber two; Four of eleven total models

D.1.4 Length chamber three

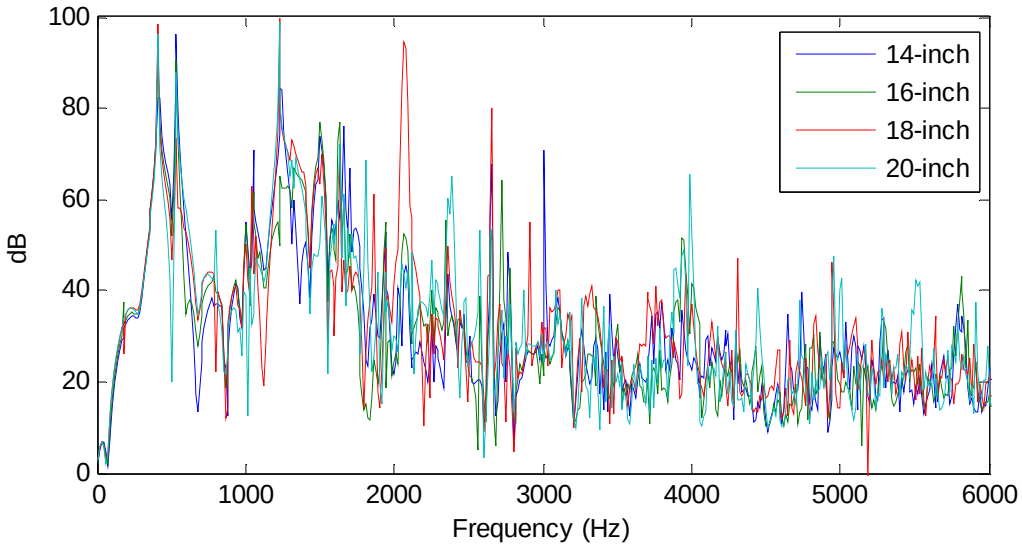

Figure D.9: Model A variation of the length of chamber three; Four of twelve total models

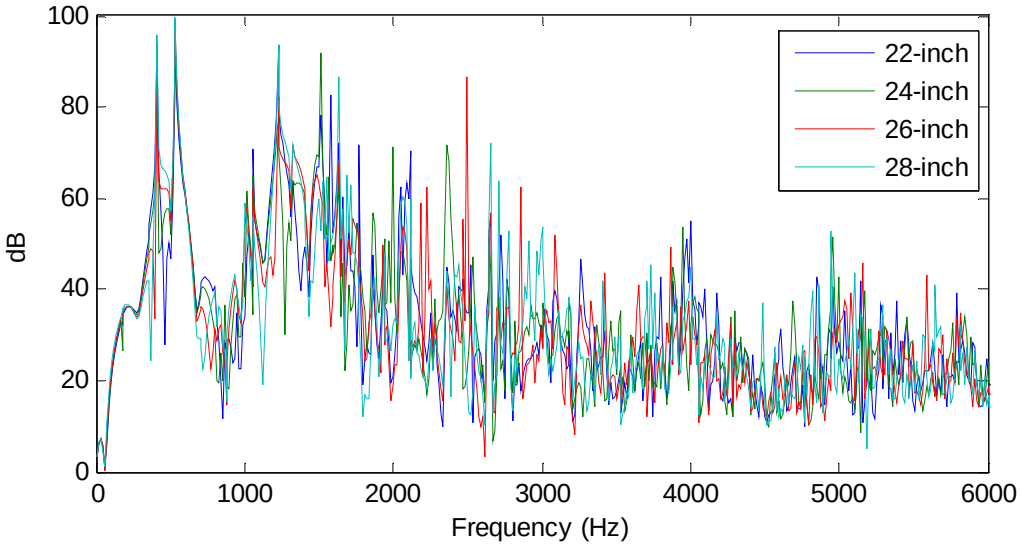

Figure D.10: Model A variation of the length of chamber three; Four of twelve total models

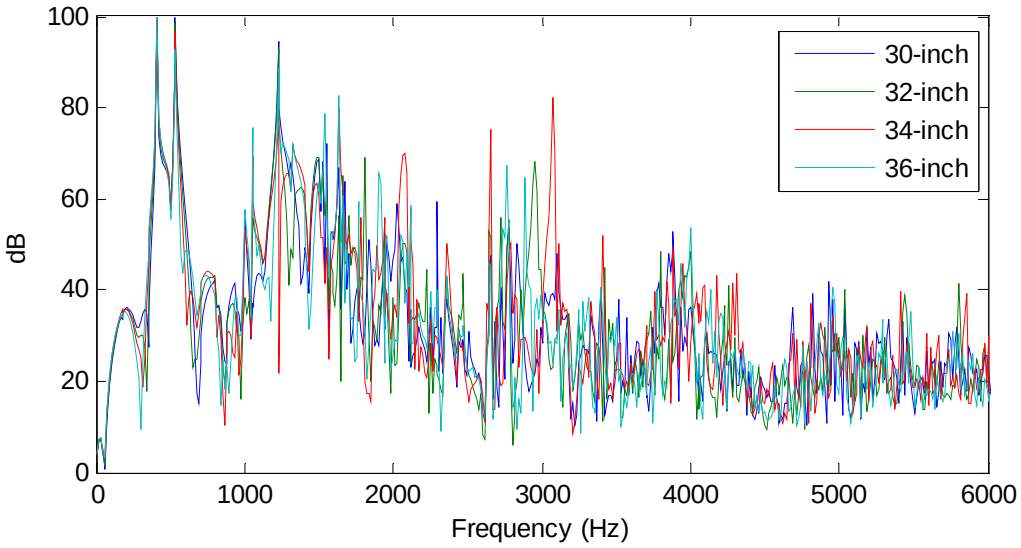

Figure D.11: Model A variation of the length of chamber three; Four of twelve total models

D.1.5 Length of the outlet baffle tube

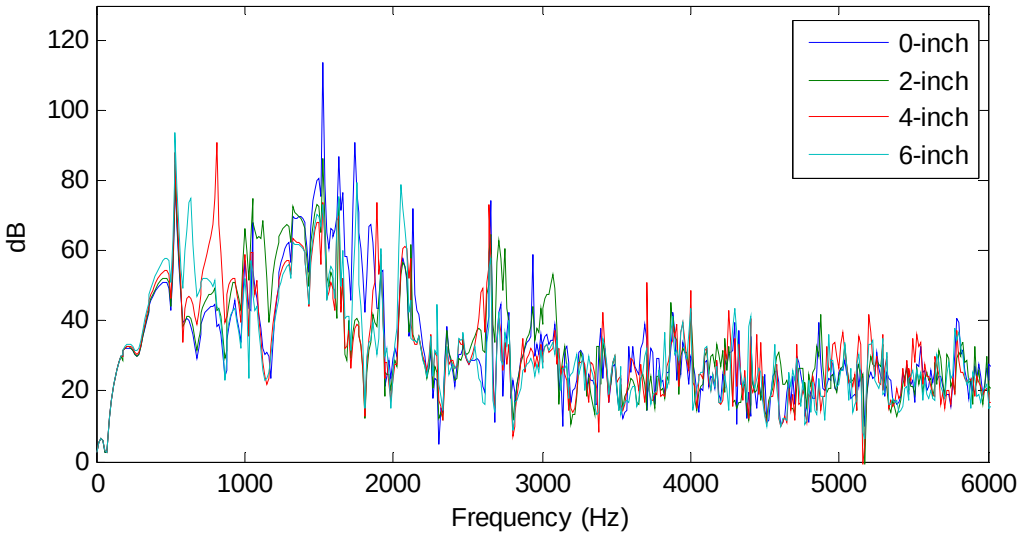

Figure D.12: Model A variation of the length of outlet baffle tube; Four of eight total models

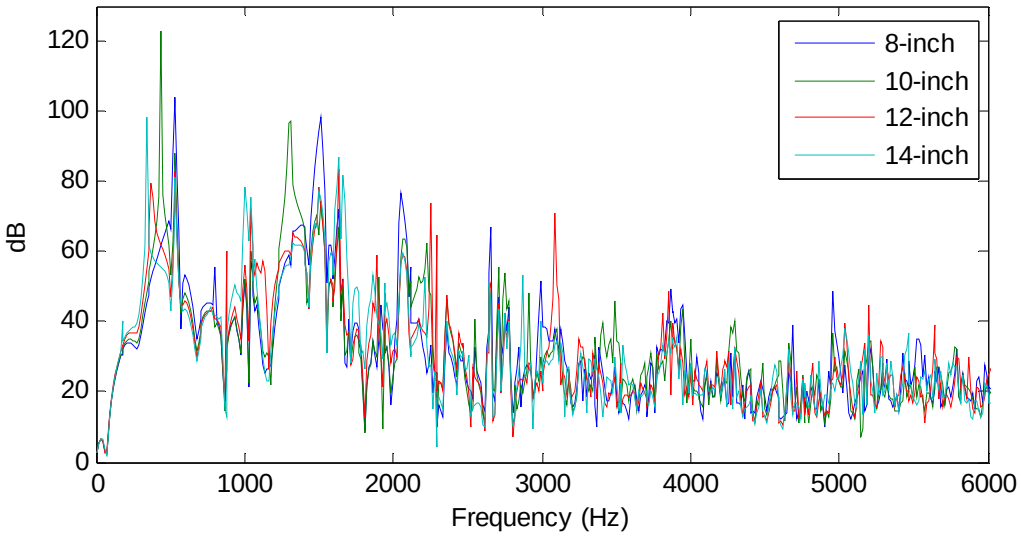

Figure D.13: Model A variation of the length of outlet baffle tube; Four of eight total models

D.1.6 Baffle tube radial position

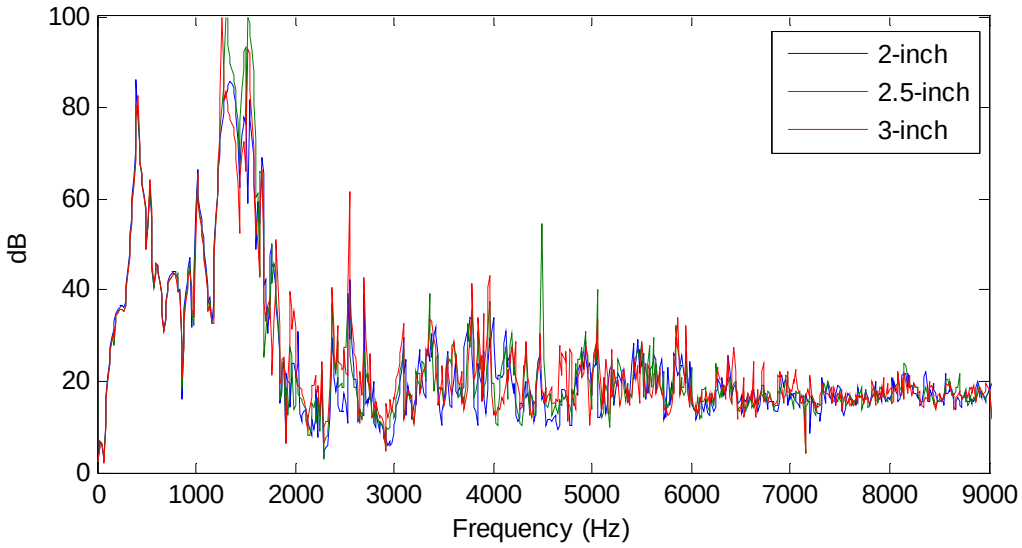

Figure D.14: Model A variation of baffle tube radial position; Three of seven total models

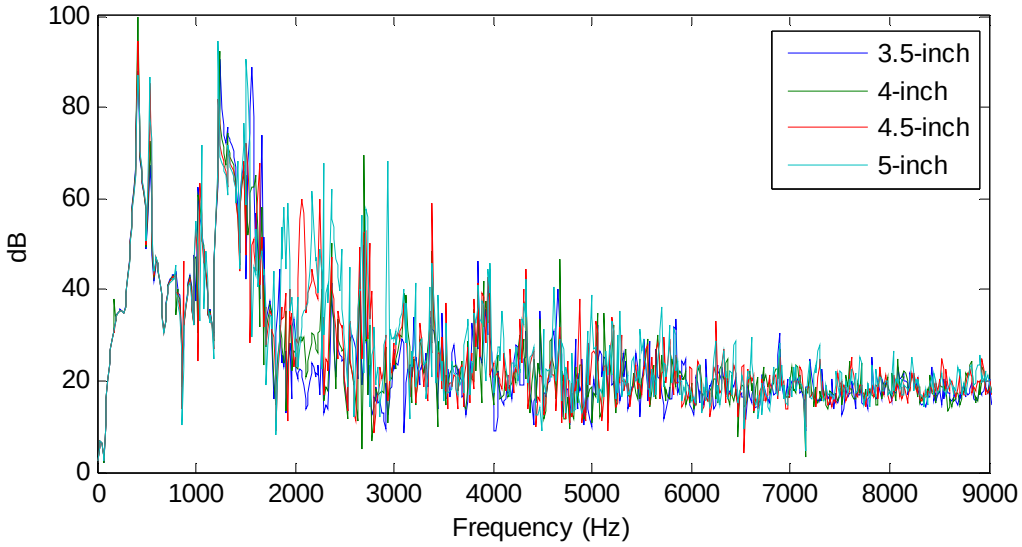

Figure D.15: Model A variation of baffle tube radial position; Four of seven total models

D.1.7 Major diameter

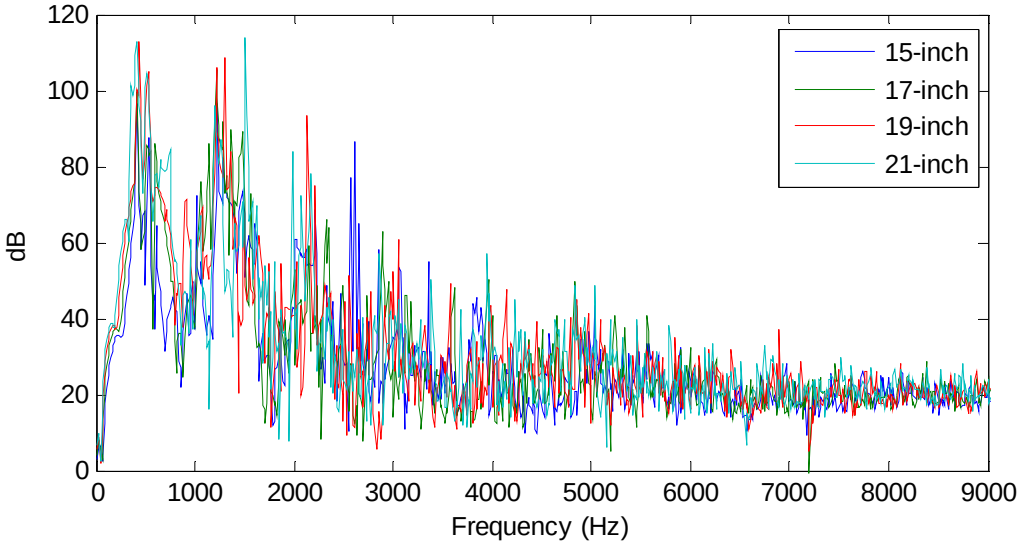

Figure D.16: Model A variation of major diameter

D.1.8 Model A special features

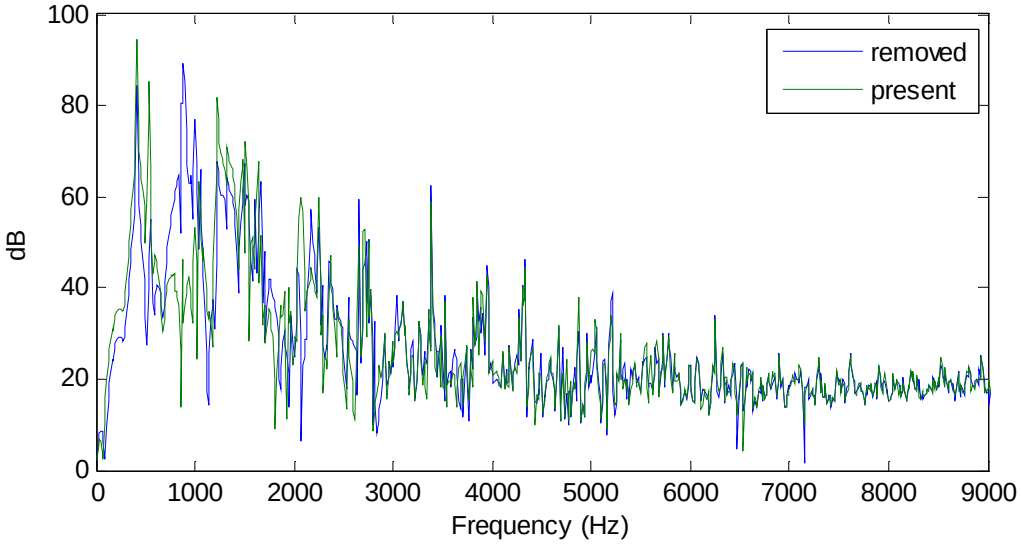

Figure D.17: Model A tube perforations

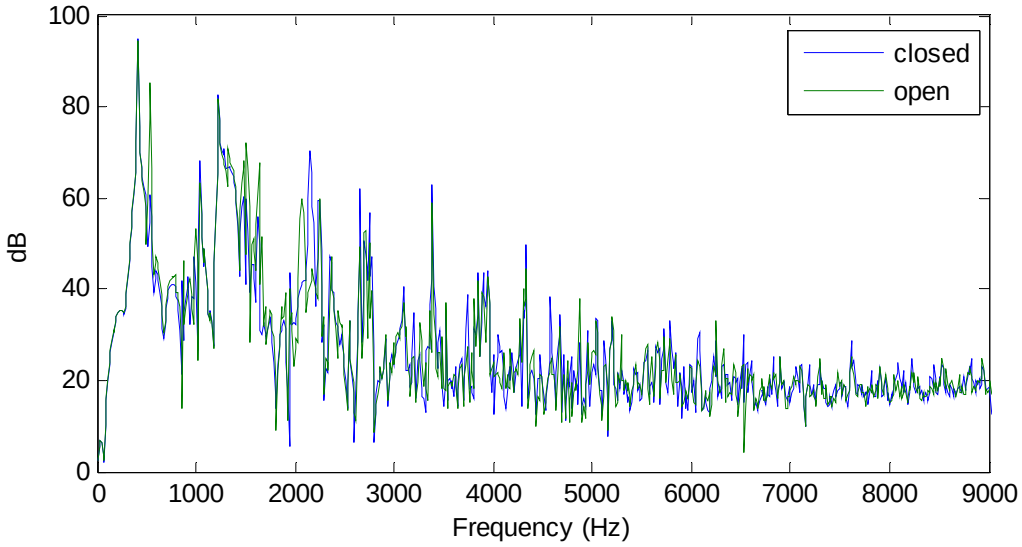

Figure D.18: Model A volume beneath catalyst

D.2 MODEL B

D.2.1 Length of chamber one

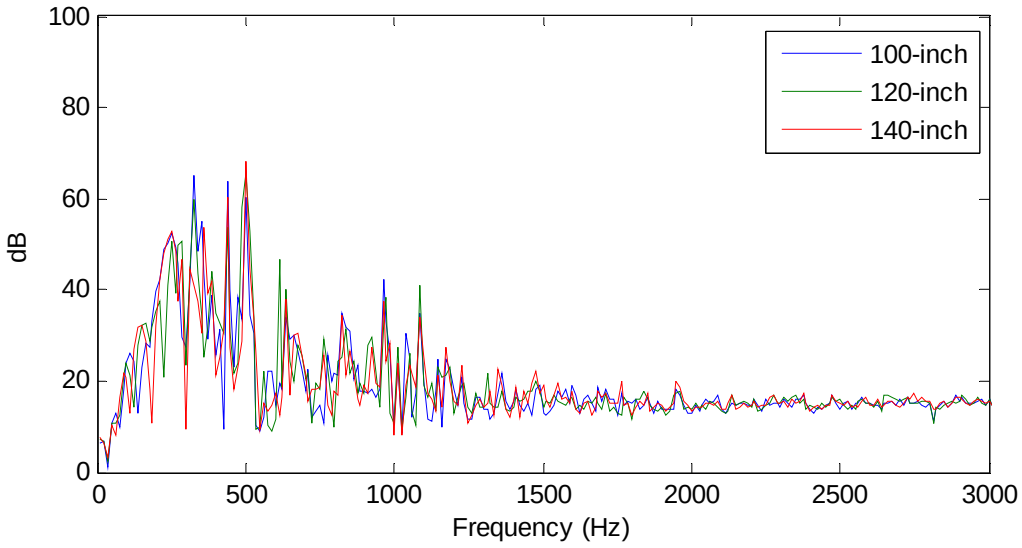

Figure D.19: Model B variation of length of chamber one

D.2.2 Length of baffle tubes in chamber two

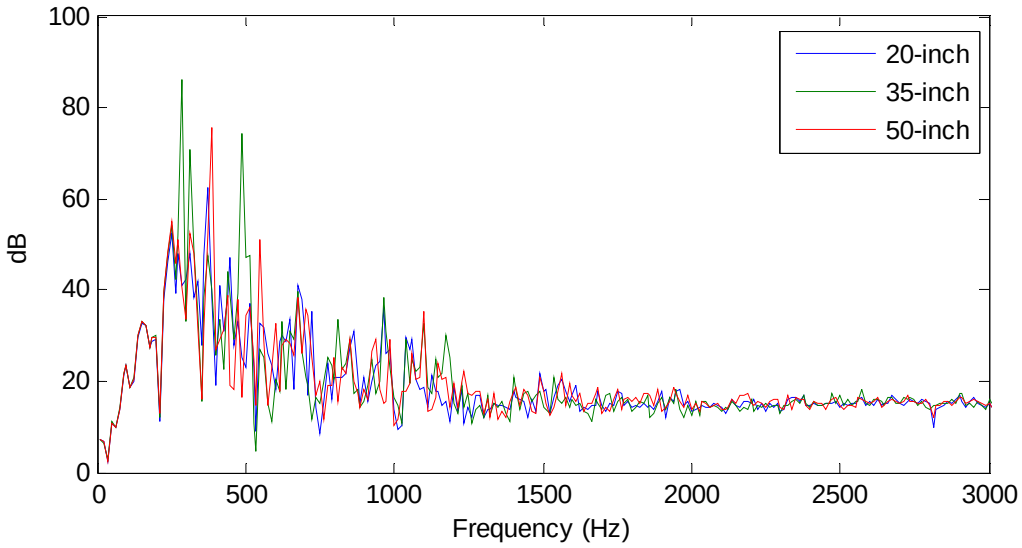

Figure D.20: Model B variation of length of baffle tubes in chamber one

D.2.3 Length of chamber two

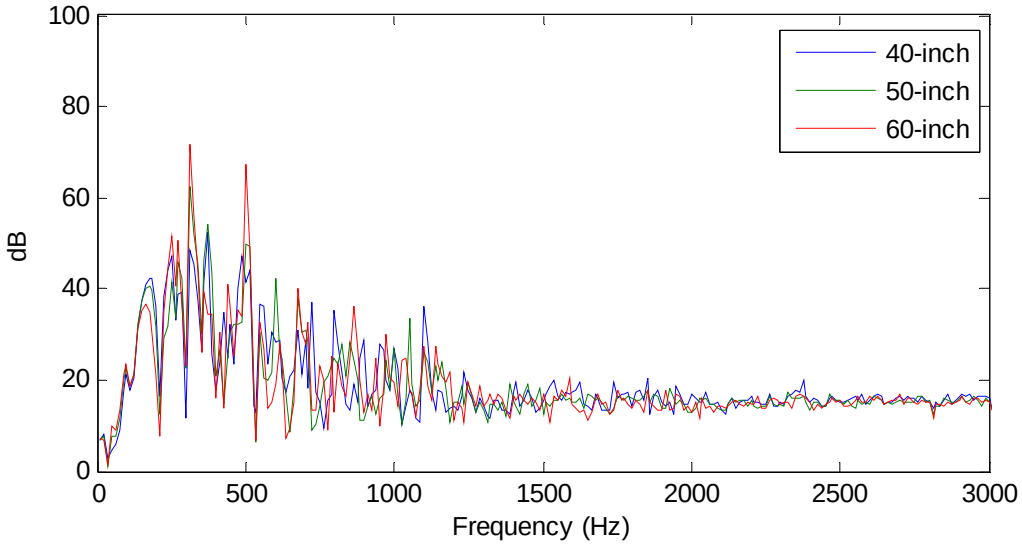

Figure D.21: Model B variation of the length of chamber two

D.2.4 Distance between catalysts

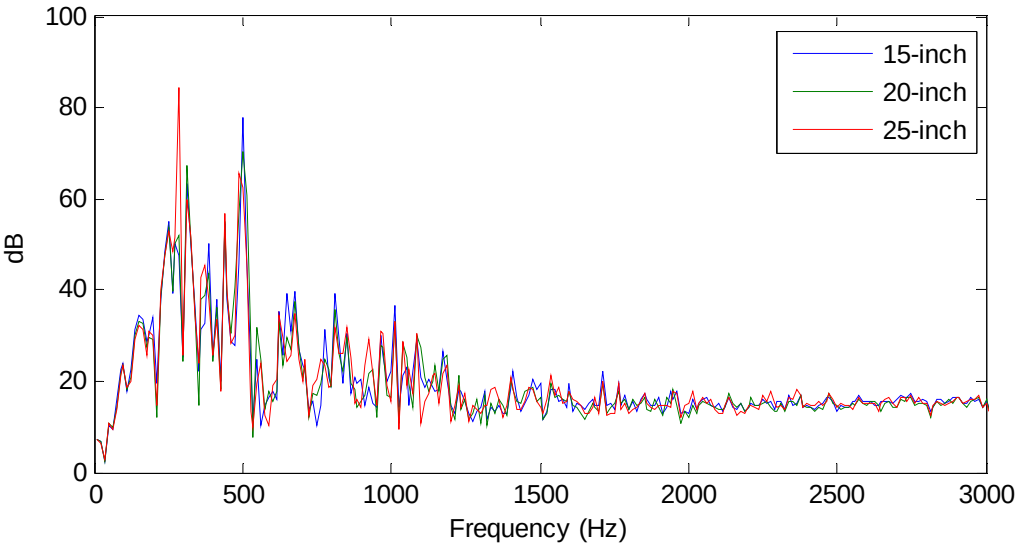

Figure D.22: Model B variation of the distance between the catalysts

D.2.5 Number of baffle tubes

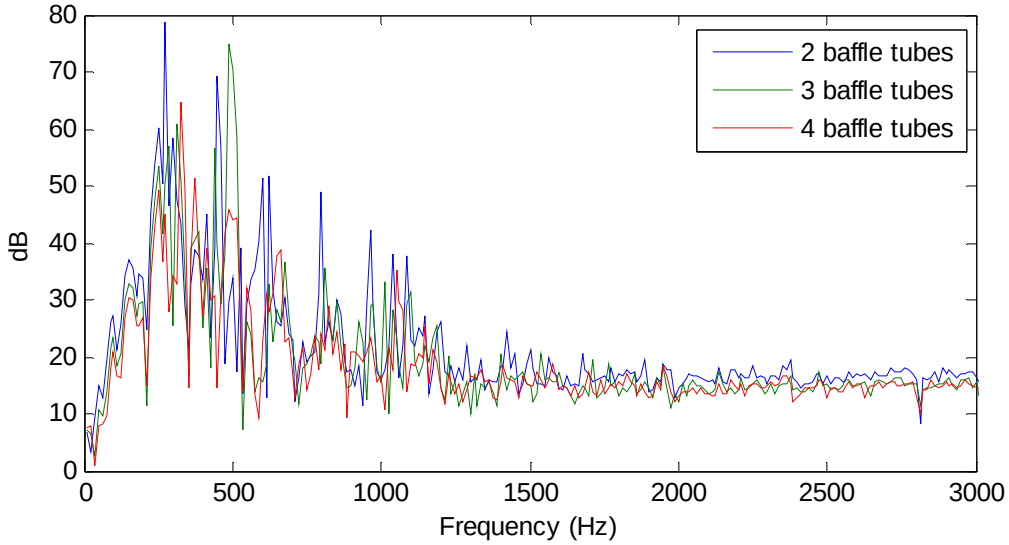

Figure D.23: Model B variation of the number of baffle tubes

D.3 MODEL C

D.3.1 Length of chamber one

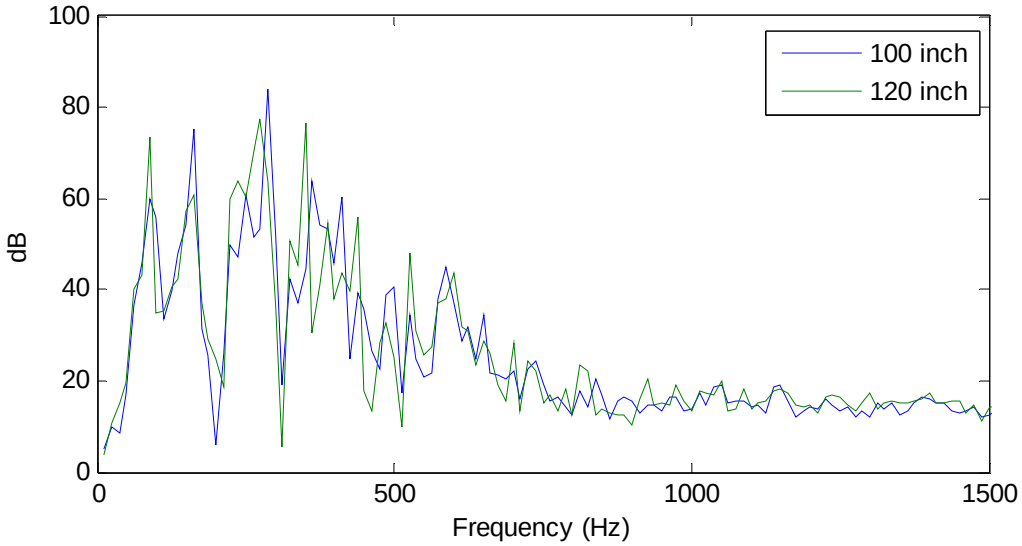

Figure D.24: Model C variation of the length of chamber one

D.3.2 Length of chamber two

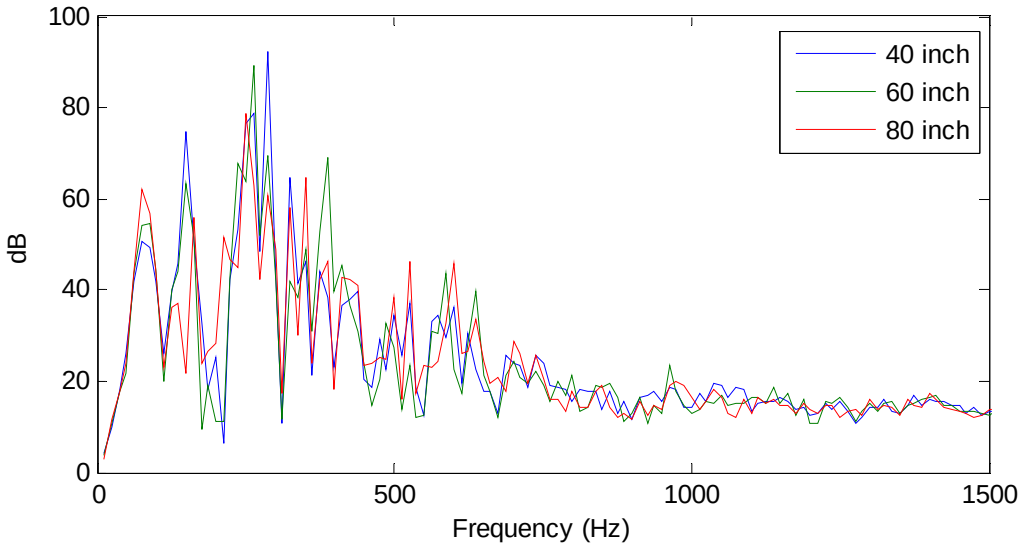

Figure D.25: Model C variation of the length of chamber two

D.3.3 Length of chamber three

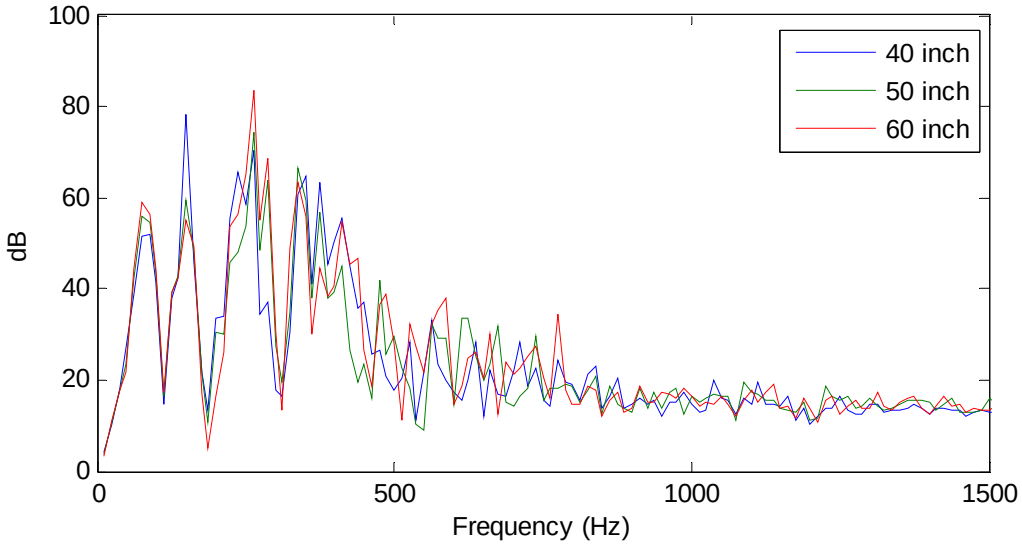

Figure D.26: Model C variation of the length of chamber three

D.3.4 Length of baffle tubes in chamber three

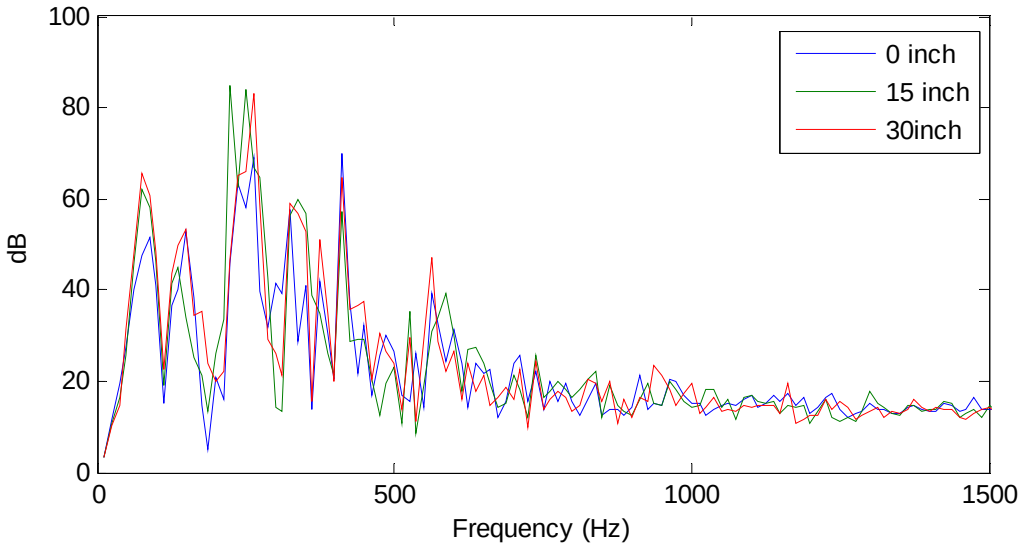

Figure D.27: Model C variation of the length of the baffle tubes in chamber three

D.3.5 Number of baffle tubes

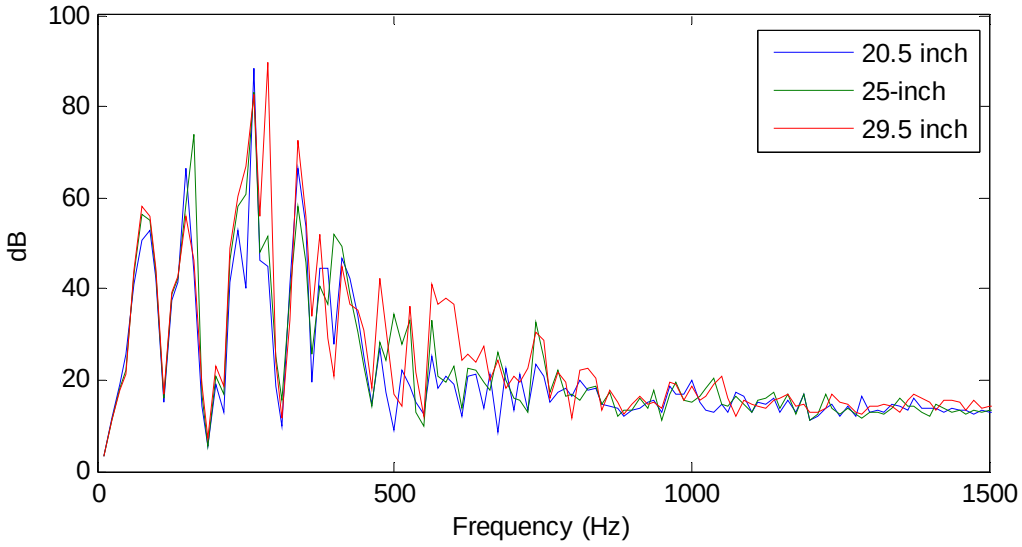

Figure D.28: Model C variation of the number of baffle tubes

D.3.6 Baffle tube radial position

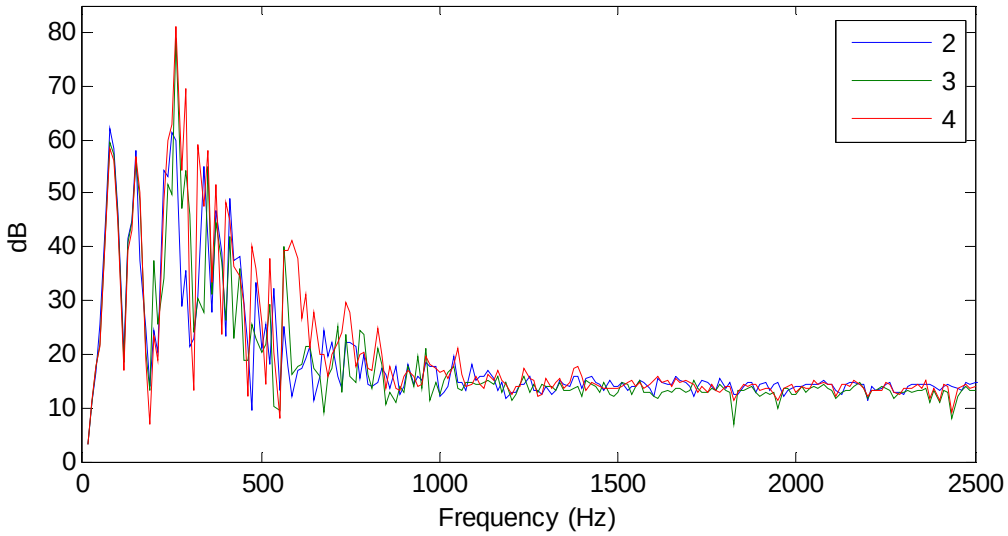

Figure D.29: Model C variation of the baffle tube radial position

APPENDIX E

OCTAVE BAND PLOTS

The modal density within a muffler increases as excitation frequency increases. As this modal density increases, it becomes more appropriate to take a statistical approach to the loss in a muffler. When many modes are present it is hard to separate them out and calculate their effects individually so instead the effects are averaged over a wider frequency band. This when octave band analysis is employed, as opposed to the narrow band analyses that are shown throughout this thesis. Octave bands represent wider bands over which the attenuation levels are averaged. As the frequency increases, so does the range of the octave bands near that frequency. Typical octave band and third octave band frequency ranges are listed in table E.1 and E.2 respectively.

Table E.1: octave band frequency ranges

Lower Band Limit (Hz)	Center Frequency (Hz)	Upper Band Limit (Hz)
11	16	22
22	31.5	44
44	63	88
88	125	177
177	250	355
355	500	710
710	1000	1420
1420	2000	2840
2840	4000	5680
5680	8000	11360

Table E.2: Third octave band frequency ranges

Lower Band Limit (Hz)	Center Frequency (Hz)	Upper Band Limit (Hz)
11	16	22
22	31.5	44
44	63	88
88	125	177
177	250	355
355	500	710
710	1000	1420
1420	2000	2840
2840	4000	5680
5680	8000	11360
141	160	178
178	200	224
224	250	282
282	315	355
355	400	447
447	500	562
562	630	708
708	800	891
891	1000	1122
1122	1250	1413
1413	1600	1778
1778	2000	2239
2239	2500	2818
2818	3150	3548
3548	4000	4467
4467	5000	5623
5623	6300	7079
7079	8000	8913
8913	10000	11220

The octave bands levels are then derived from the narrow band levels by integrating the narrow band sound level over the desired octave band frequency range and then dividing by that same octave band frequency range. The formula for this process is:

$$L_{p,band} = \frac{\sum_{i=1}^{n} \frac{[\omega(i+1)-\omega(i)]|L(i+1)+L(i)|}{2}}{f_u - f_l} \quad \text{(E-1)}$$

where $L_{p,band}$ is the octave band sound level, n is the number of narrow bands in the octave band, ω is narrow band frequency, L is narrow band sound level, f_u is the upper frequency of the octave band, and f_l is the lower frequency of the octave band. Section E.1 shows both the narrow bands and the octave bands plotted on the same figure for all of the performance metrics studied in this research. Section E.2 shows all of the performance metrics for a muffler model plotted on the same plot for narrow bands, full octave bands and third octave bands. All of the data shown below is from the ideal simulation curves that have no noise floor applied to them. While this ideal data is unrealistically high, the main purpose of this appendix is for comparison of the narrow bands to octave bands, and for the comparison of the different performance metrics with one another.

E.1 OCTAVE BAND/NARROW BAND COMPARISONS FOR MUFFLER PERFORMANCE METRICS

E.1.1 Model A full and third octave bands

Figures E.1 through E.6 show the comparison between the narrow band and octave band results for the ideal IL, NR, and TL of muffler model A. Figures E.1, E.3, and E.5 show the narrow band and full octave band comparisons. Figures E.2, E.4, and E.4 show the narrow band and third octave band comparisons.

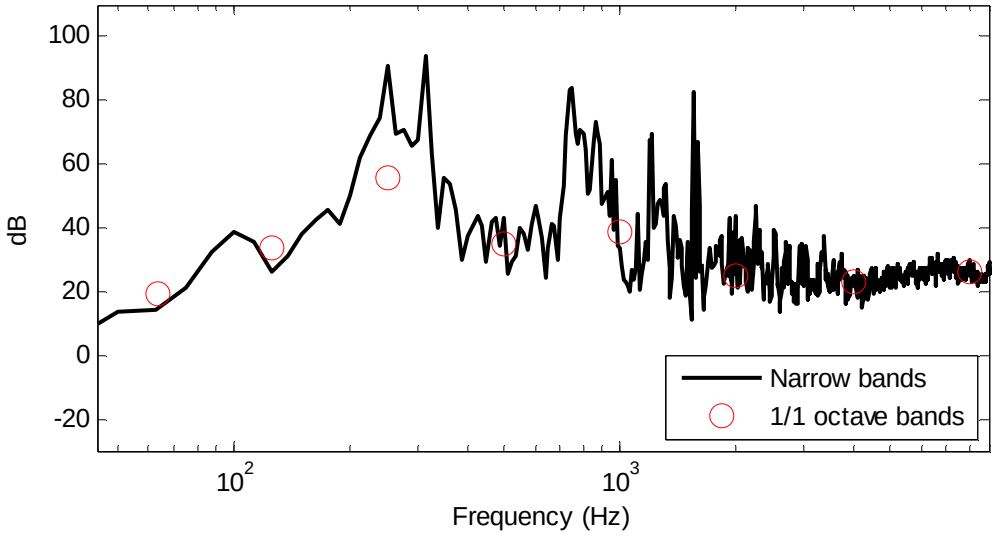

Figure E.1: Comparison of Model A ideal IL narrow bands and full octave bands

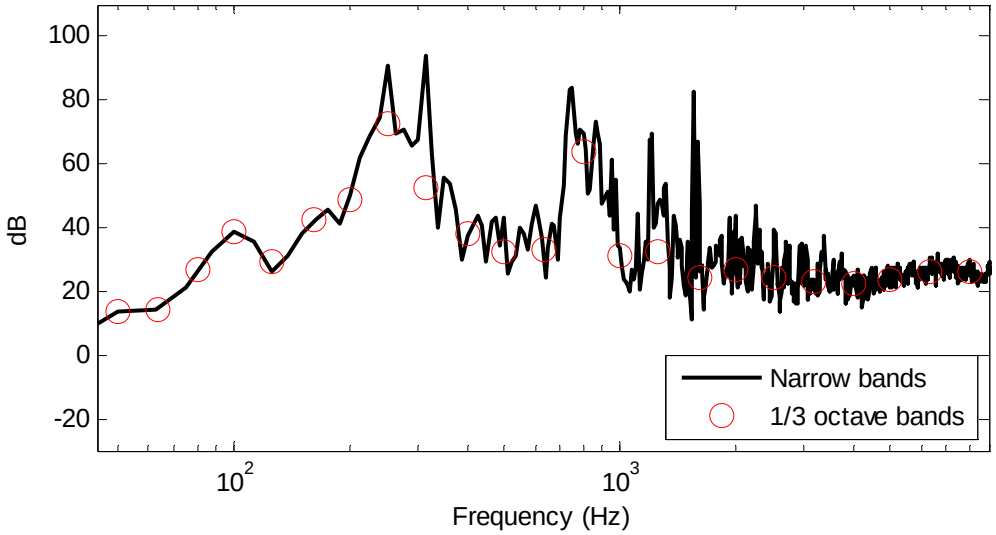

Figure E.2: Comparison of Model A ideal IL narrow bands and third octave bands

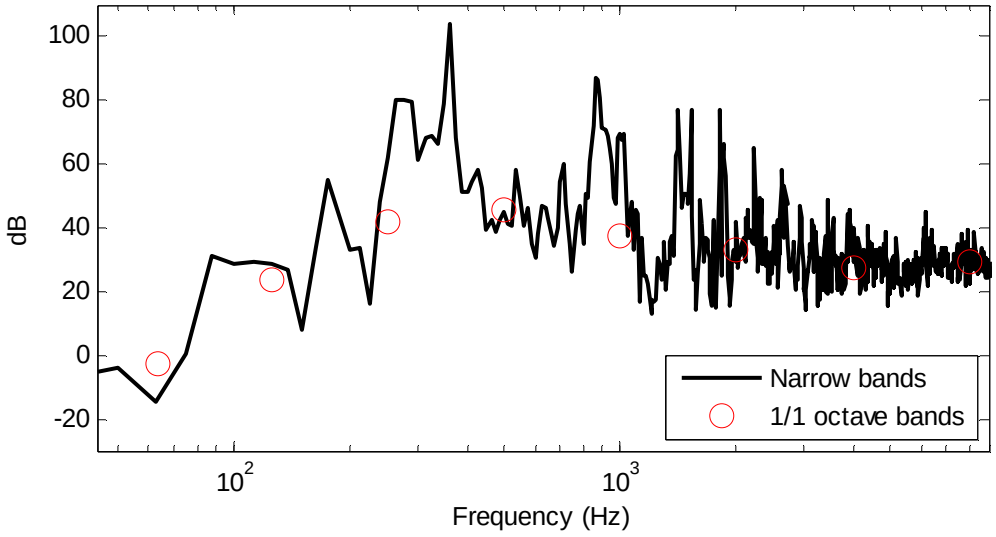

Figure E.3: Comparison of Model A ideal NR narrow bands and full octave bands

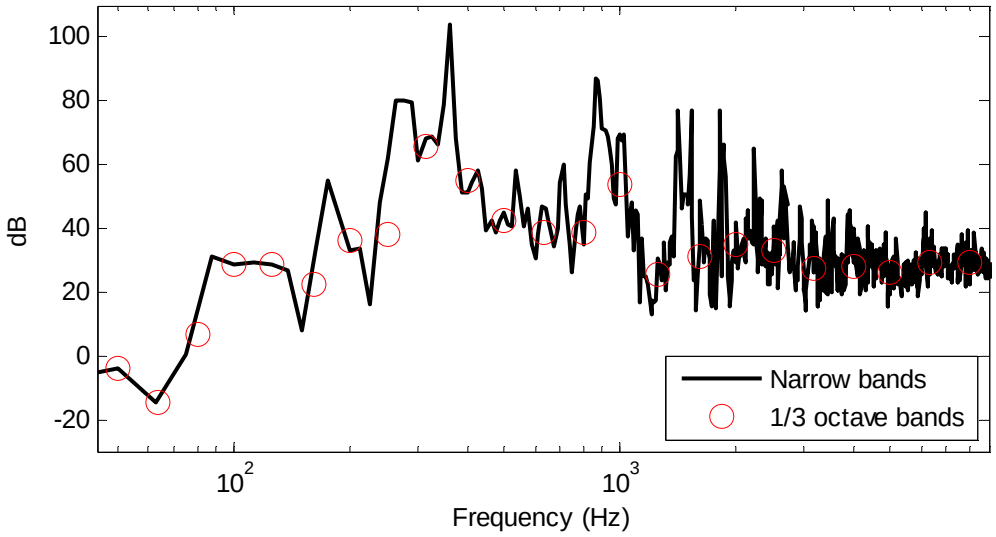

Figure E.4: Comparison of Model A ideal NR narrow bands and third octave bands

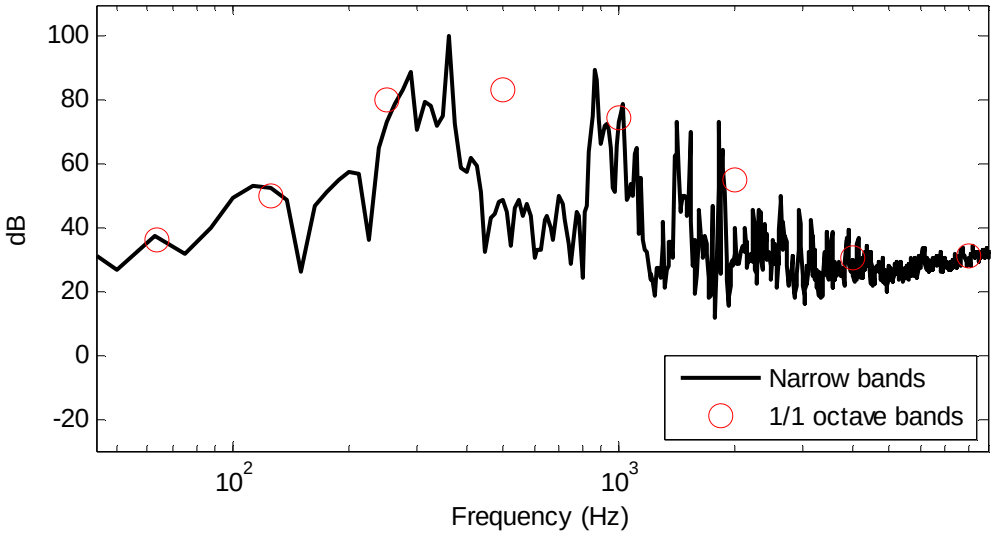

Figure E.5: Comparison of Model A ideal TL narrow bands and full octave bands

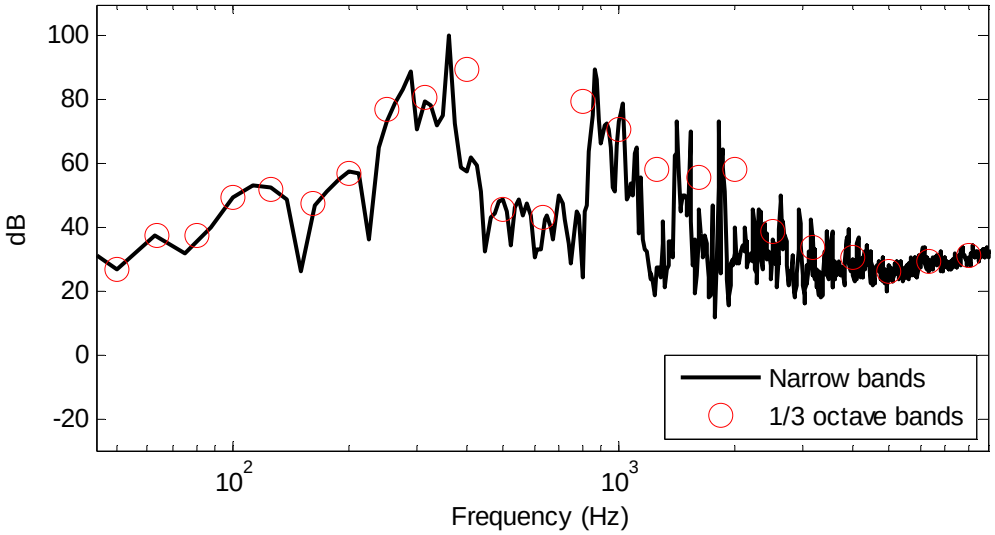

Figure E.6: Comparison of Model A ideal TL narrow bands and third octave bands

E.1.2 Model B full and third octave bands

Figures E.7 through E.10 show the comparison between the narrow band and octave band results for the ideal IL and NR of muffler model B. Figures E.7 and E.9 show the narrow band and full octave band comparisons. Figures E.8 and E.10 show the narrow band and third octave band comparisons.

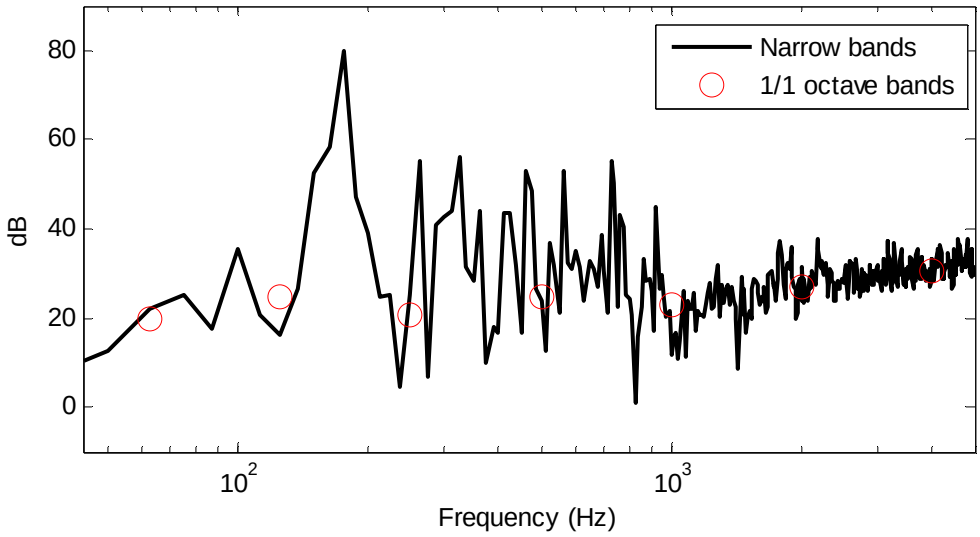

Figure E.7: Comparison of Model B ideal IL narrow bands and full octave bands

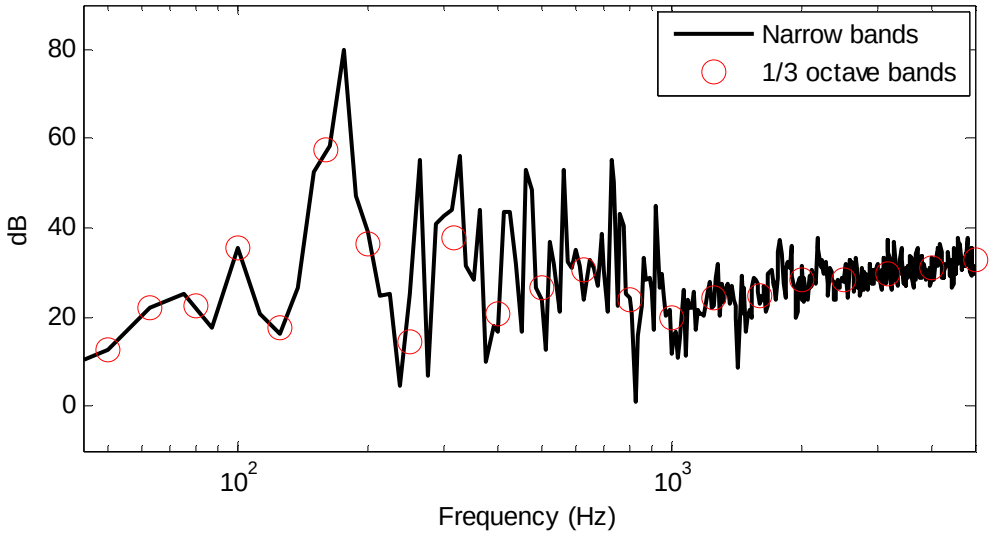

Figure E.8: Comparison of Model B ideal IL narrow bands and third octave bands

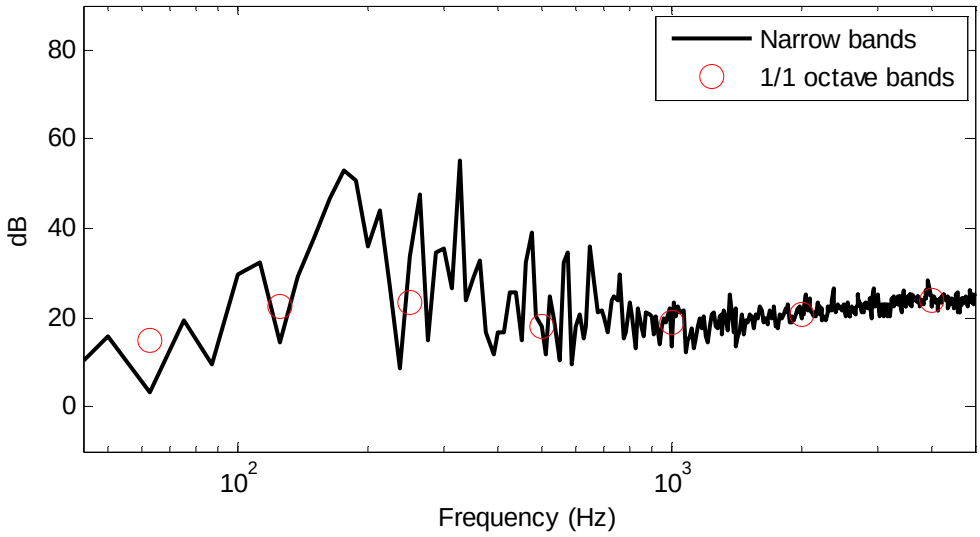

Figure E.9: Comparison of Model B ideal NR narrow bands and full octave bands

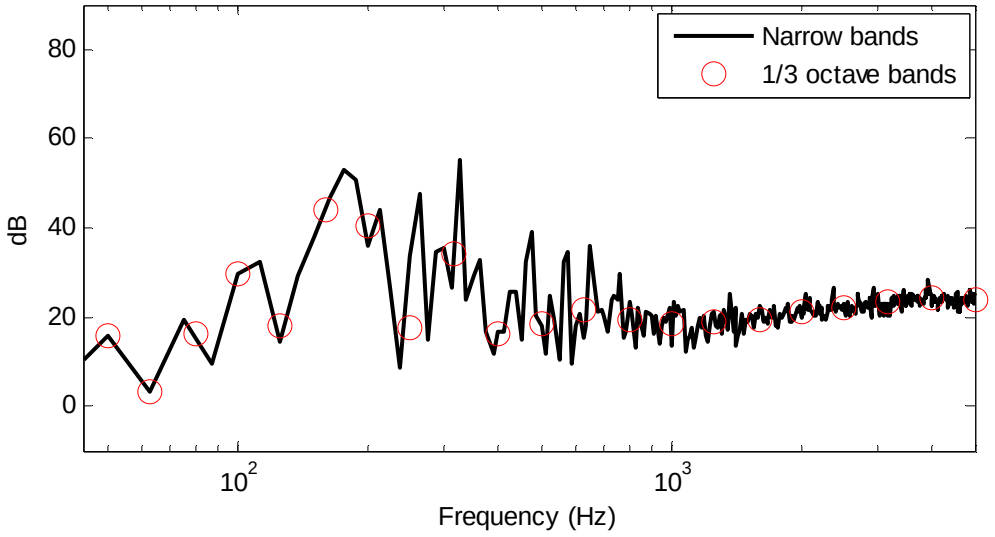

Figure E.10: Comparison of Model B ideal NR narrow bands and third octave bands

E.1.3 Model C full and third octave bands

Figures E.11 through E.14 show the comparison between the narrow band and octave band results for the ideal IL and NR of muffler model C. Figures E.11 and E.13 show the narrow band and full octave band comparisons. Figures E.12 and E.14 show the narrow band and third octave band comparisons.

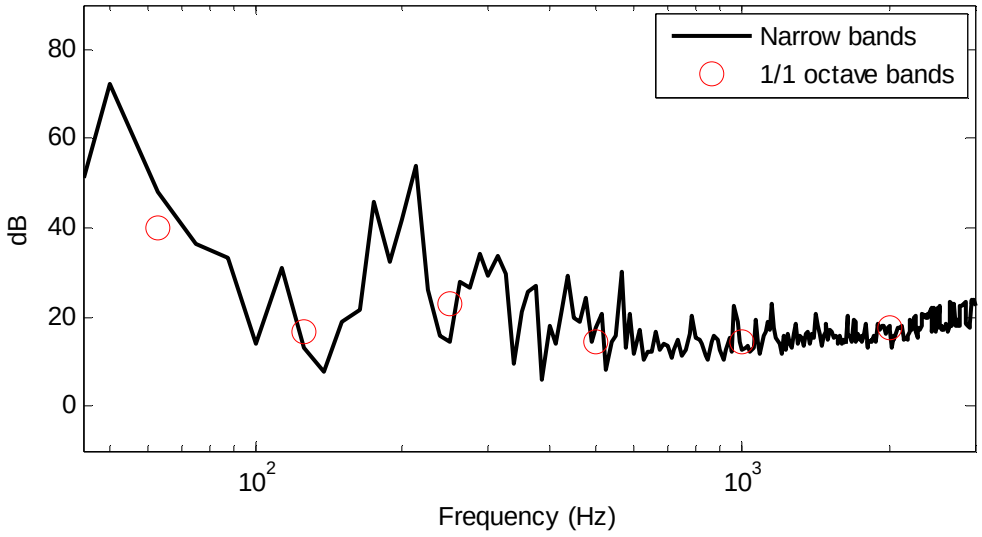

Figure E.11: Comparison of Model C ideal IL narrow bands and full octave bands

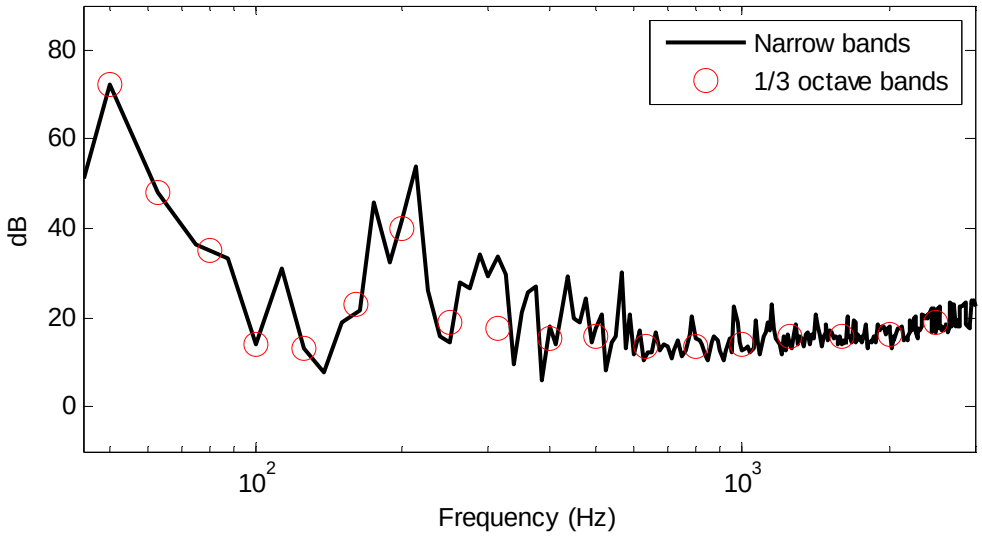

Figure E.12: Comparison of Model C ideal IL narrow bands and third octave bands

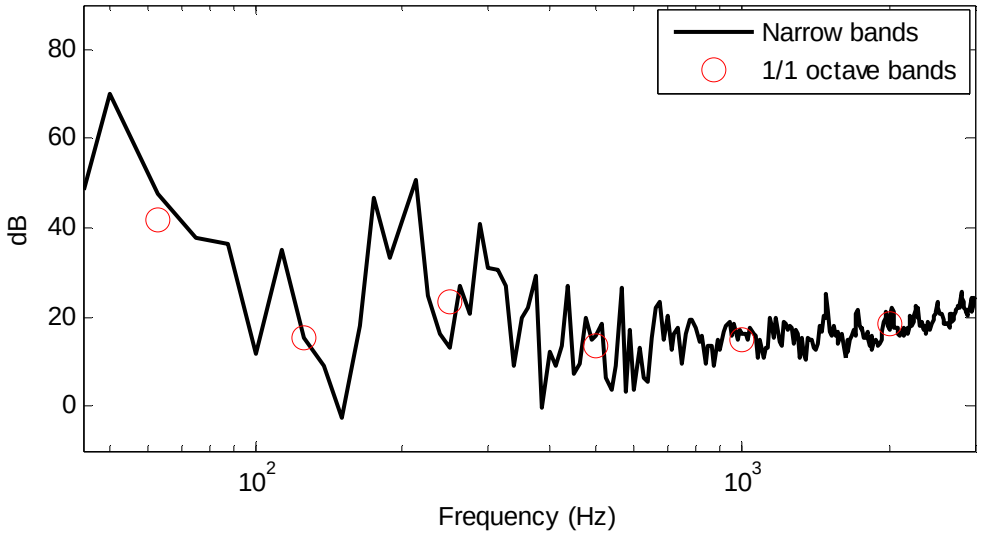

Figure E.13: Comparison of Model C ideal NR narrow bands and full octave bands

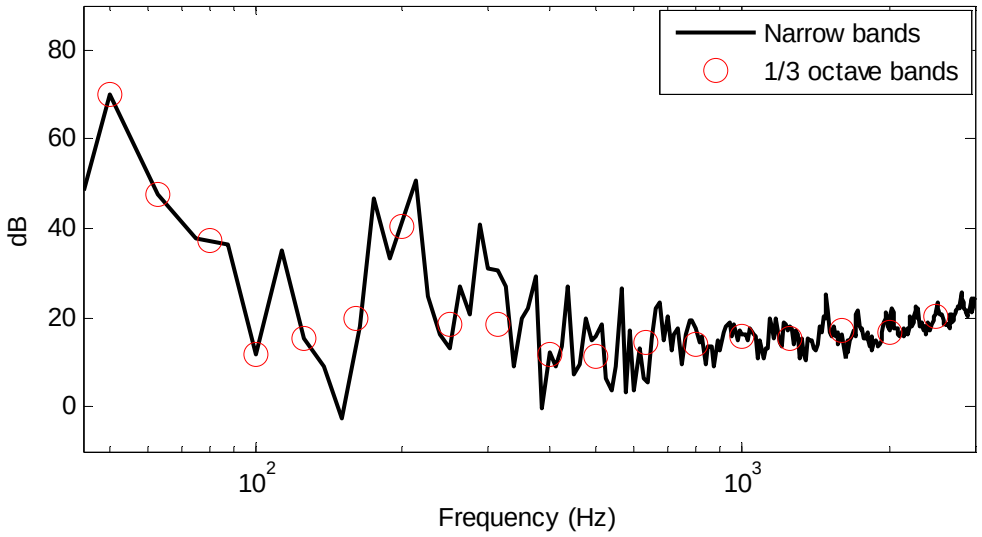

Figure E.14: Comparison of Model C ideal NR narrow bands and third octave bands

E.2 COMPARISON OF PERFORMANCE METRICS FOR EACH MODEL

E.2.1 Comparison of IL, NR, and TL for model A

Figures E.15, E.16, and E.17 show the comparison of the three performance metrics modeled for muffler model A in narrow bands, full octave bands and third octave bands respectively.

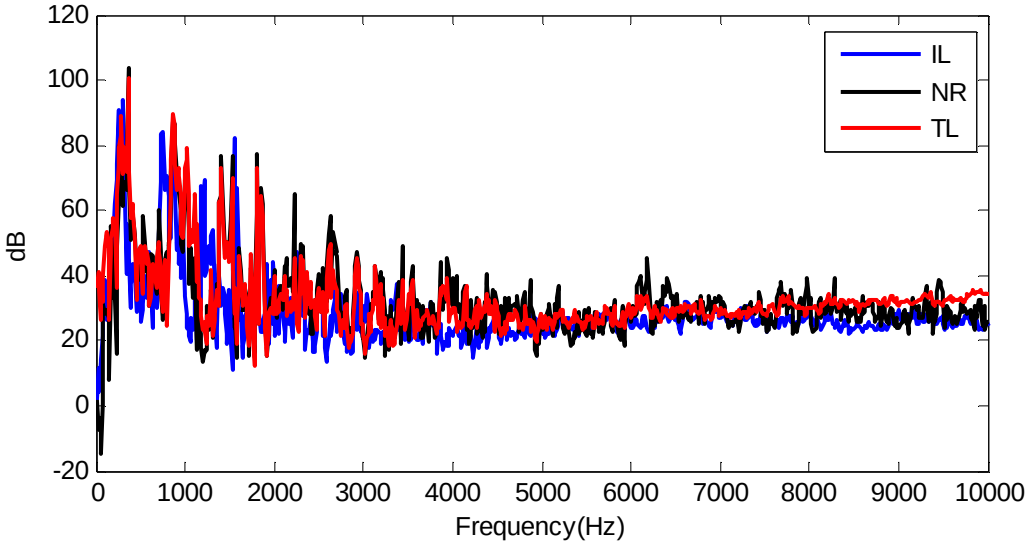

Figure E.15: Comparison of IL, NR, and TL narrow band results for model A

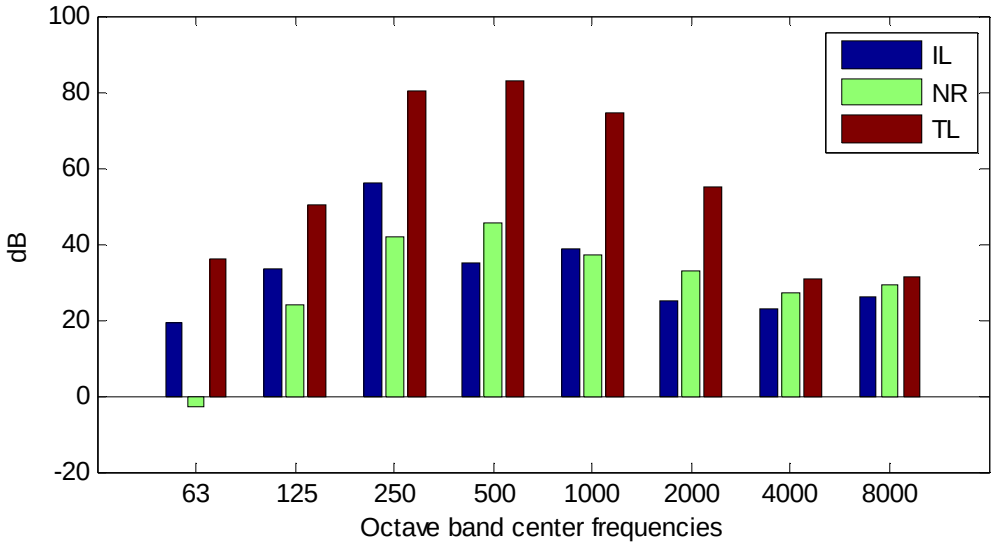

Figure E.16: Comparison of IL, NR, and TL full octave band results for model A

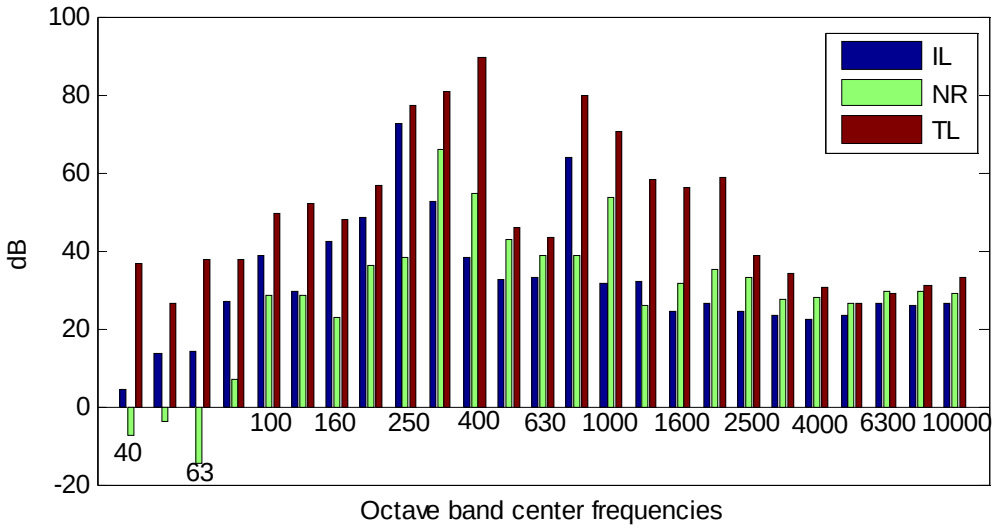

Figure E.17: Comparison of IL, NR, and TL third octave band results for model A\

E.2.2 Comparison of IL, NR for model B

Figures E.18, E.19, and E.20 show the comparison of the two performance metrics modeled for muffler model B in narrow bands, full octave bands and third octave bands respectively.

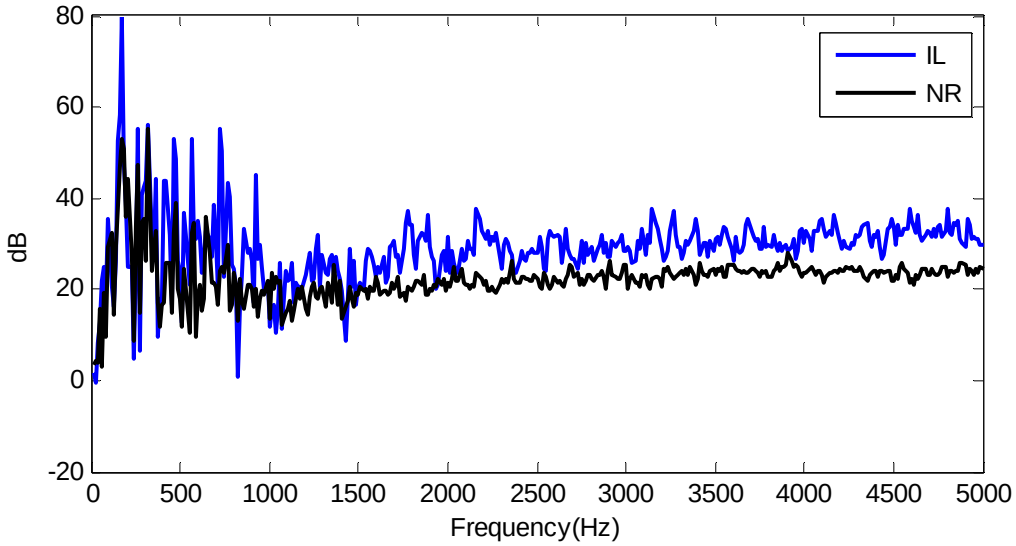

Figure E.18: Comparison of IL, NR narrow band results for model B

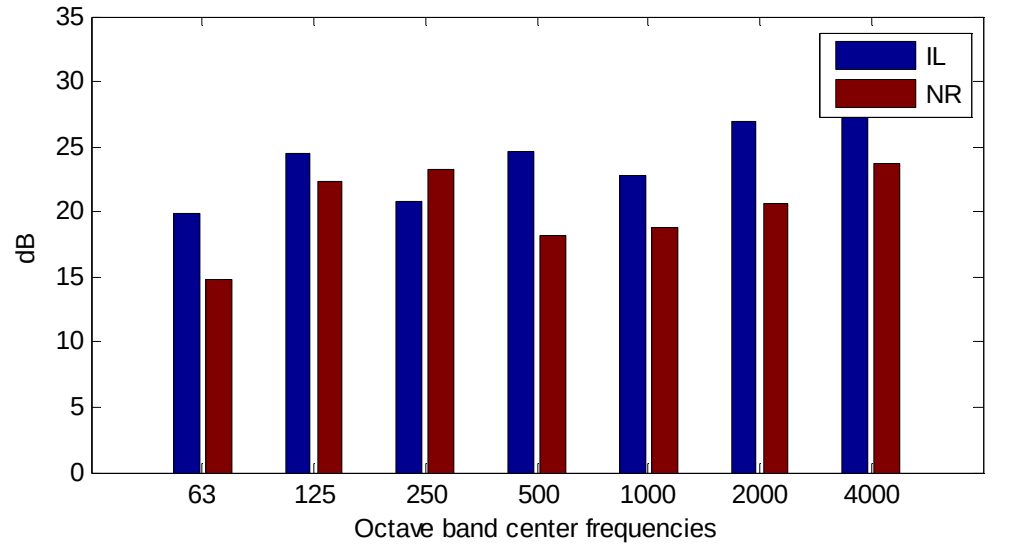

Figure E.19: Comparison of IL, NR full octave band results for model B

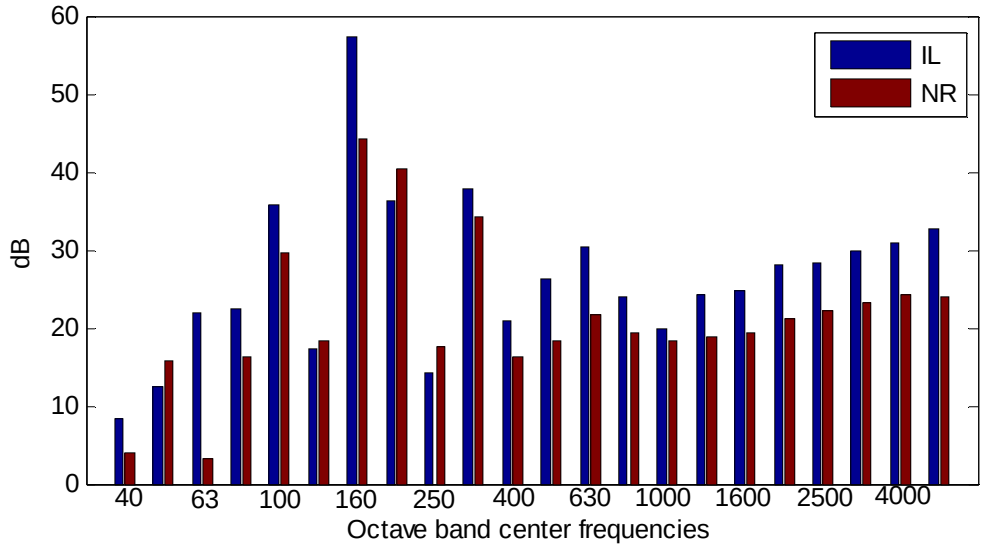

Figure E.20: Comparison of IL, NR third octave band results for model B

E.2.3 Comparison of IL, NR for model C

Figures E.21, E.22, and E.23 show the comparison of the two performance metrics modeled for muffler model C in narrow bands, full octave bands and third octave bands respectively.

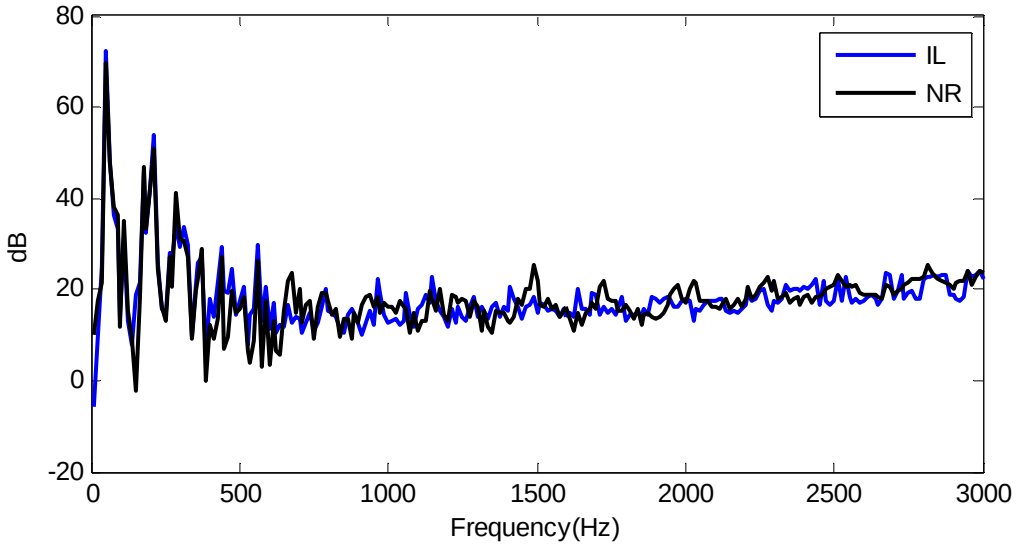

Figure E.21: Comparison of IL, NR narrow band results for model C

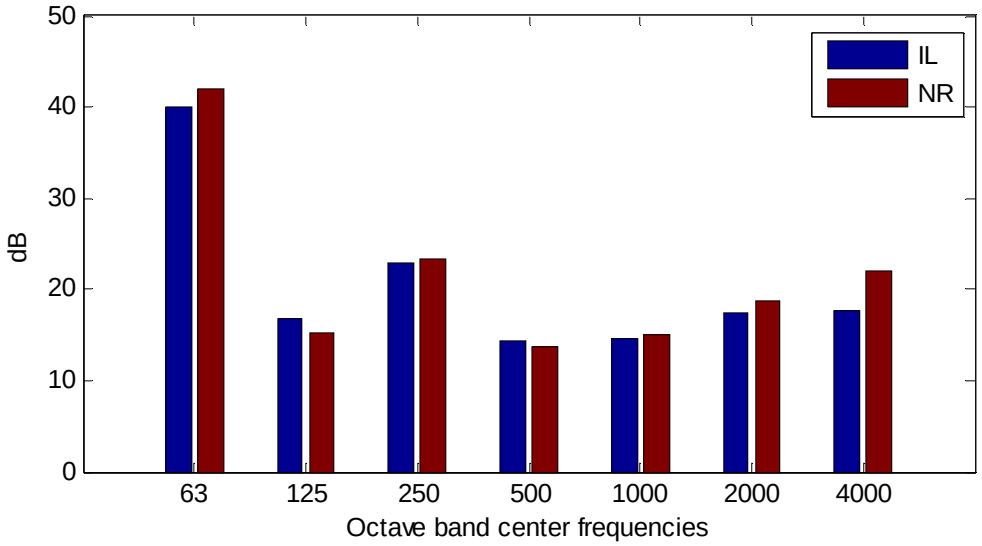

Figure E.22: Comparison of IL, NR full octave band results for model C

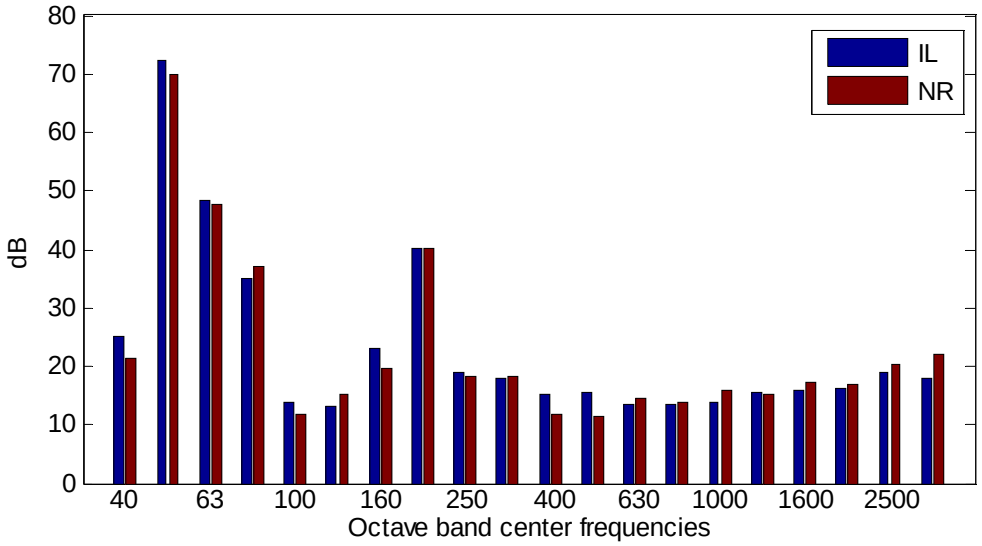

Figure E.23: Comparison of IL, NR third octave band results for model C

BIBLIOGRAPHY

1. International Organization for Standardization, "Standard 14163: Acoustics- Guidelines for Noise Control by Silencers," 1998.

2. M.L. Munjal, *Acoustics of Ducts and Mufflers,* Wiley-Interscience Inc., New York, (1987).

3. L.J. Eriksson, "Higher Order Mode Effects in Circular Ducts and Expansion Chambers," J. Acoust. Soc. Am., 68, 2, pp. 545-550 (1980).

4. L.E. Kinsler, A.R. Frey, A.B. Coppens, J.V. Sanders, *Fundamentals of Acoustics 4thed.,* John Wiley & Sons, Inc. New York, (2000).

5. O.C. Zienkiewicz, R.L. Taylor, J.Z. Zhu, *The Finite Element Method and its Basis,* Elsevier, New York,(2005).

6. O. De Weck, I. Y. Kim, Lecture on the Finite Element Method, MIT, 1/12/2004

7. D.L. Logan, *A First Course in the Finite Element Method,* Cengage Learning, Stamford, (2012).

8. W. F. Riley, L. D. Sturges, D. H. Morris, *Statics and Mechanics of Materials: An Integrated Approach*, John Wiley & Sons Inc., New York, (2002).

9. A. Craggs, "The Use of Simple Three-Dimensional Acoustic Finite Elements for Determining the Natural Modes and Frequencies of Complex Shaped Enclosures," J. Sound and Vib., 23, 3, pp. 331-339 (1972).

10. C. Young, M. Crocker. "Prediction of Transmission Loss in Mufflers by the Finite−element Method," J. Acoust. Soc. Am., 57, 1, pp.144 (1975).

11. L.L. Thompson, P.M. Pinsky, "A Galerkin Least-Squares Finite Element Method for the Two-Dimensional Helmholtz Equation," Int. J. Num. Meth. Eng. 38, pp. 371-397 (1995).

12. S. C. Chapra, R. P. Canale, *Numerical Methods for Engineers,* McGraw Hill, New York, (2006).

13. H. Boden, R. Glav, "Exhaust and Intake Noise and Acoustical Design of Mufflers and Silencers," in *Handbook of Noise and Vibration Control* (ed M. J. Crocker), John Wiley & Sons, Inc., Hoboken, (2008).

14. M.G. Prasad, M.J. Crocker, "Insertion Loss Studies on Models of Automotive Exhaust systems," J. Acoust. Soc. Am., 70, 5, pp.1339-1344 (1981).

15. V.H. Gupta, M.L. Munjal, “On the Numerical Prediction of the Acoustic Source Characteristics of an Engine Exhaust System,” J. Acoust. Soc. Am., 92, 5, pp.2716-2725 (1992).

16. Society of Automotive Engineers, “Standard J1207: Measurement Procedure for Determination of Silencer Effectiveness in Reducing Engine Intake or Exhaust Sound Level,” 2000.

17. J.H. Fang, Y.Q. Zhou, X.D. Hu, L. Wang “Measurement and Analysis of Exhaust Noise from Muffler on an Excavator,” Int. J. Precis. Eng. Manuf., 10, 5, pp. 59-66 (2009).

18. International Organization for Standardization, “Standard 11820: Acoustics- Measurements on Silencers in situ,” 1996.

19. Z. Tao, A. F. Seybert, "A Review of Current Techniques for Measuring Mufflers Transmission Loss," SAE Technical Paper 2003-01-1653.

20. A. F. Seybert, ”Two-sensor Methods for the Measurement of Sound Intensity and Acoustic Properties in Ducts,” J. Acoust. Soc. Am, 83,6, pp. 2233- 2239 (1988).

21. A. F. Seybert, D. F. Ross, “Experimental Determination of Acoustic Properties Using a Two Microphone Random Excitation Technique,” J. Acoust. Soc. Am., 61, 5, pp. 1362-1370 (1977).

22. J.Y. Chung, D.A. Blaser, “Transfer Function Method of Measuring In-duct Acoustic Properties. I. Theory,” J. Acoust. Soc. Am., 68, 3, pp. 907-913 (1980).

23. M. Abom, H. Boden, “Error Analysis of Two-Microphone Measurements in Ducts with Flow,” J. Acoust. Soc. Am., 83, 6, pp. 2429-2438 (1988).

24. A.D. Shasrabudhe, M.L. Munjal, S. Anantha Ramu, “Design of Expansion Chamber Mufflers Incorporating 3-D Effects,” Noise Control Eng. J,, 38, 1, pp. 27-38 (1992).

25. C.Q. Howard, B.S. Cazzolato, C.H. Hansen, “Exhaust Stack Silencer Design Using Finite Element Analysis,” Noise Control Eng. J., 48, 4, pp. 113-120 (2009).

26. J.G. Ih, B.H. Lee, “Analysis of Higher-Order Mode Effects in the Circular Expansion Chamber with Mean Flow,” J. Acoust. Soc. Am., 77, 4, pp.1377-1388 (1985).

27. L.J. Eriksson, “Effect of Inlet/Outlet Locations on Higher Order Modes in Silencers,” J. Acoust. Soc. Am., 72, 4, pp. 1208-1211 (1982).

28. L.L. Beranek, I.L. Ver, *Noise and Vibration Control Engineering*, John Wiley and Sons, Inc. New York, (1992).

29. M.E. Delany, E.N. Bazley, “Acoustical Properties of Fibrous Absorbent Materials,” Appl. Acoust., 3, 2, pp. 105-116 (1970).

30. A. Selamet, V. Easwaran, J.M. Novak, R.A. Kach, “Wave Attenuation in Catalytic Converters: Reactive Versus Dissipative Effects,” J. Acoust. Soc. Am., 102, 2, pp. 935-943 (1998).

31. F.D. Denia, A. G. Antebas, R. Kirby and F. J. Fuenmayor, “Multidimensional Acoustic Modelling of Catalytic Converters,” *Proceedings of the 16th International Congress on Sound and Vibration*, Kraków, (2009).

32. Allard, J. F. *Propagation of Sound in Porous Media: Modelling Sound Absorbing Materials*, Elsevier Applied Science, London, (1993).

33. S.M. Price and D.R. Smith, “Sources and Remedies of High Frequency Piping Vibration and Noise,” *Proc. of the 28th Turbomachinery Symposium* , pp. 189-212 (1999).

34. F. Fahy, P. Gardonio, *Structural Vibration: Radiation, Transmission, and Response 2nd Ed.,* Elsevier, New York, (2007).

35. A. London, “Transmission of Reverberant Sound Through Double Walls,” J. Acoust. Soc. Am., 22, pp.270-279 (1950).

36. S.C. Haung, D.J. Inman, E.M. Austin, “Some Design Considerations for Active and Passive Constrained Layer Damping Treatments,” Smart Mater. Struct., 5, 3, pp. 301-313 (1996).

37. R.D. Corsaro, L.H. Sperling, *Sound and Vibration Damping with Polymers,* American Chemical Soc., Washington D.C.,(1990)

38. British Standards Institute, “BS 0848-02: Fans for General Purposes,” 1985.

39. A.D. Pierce, "Mathematical Theory of Wave Propagation," in *Handbook of Acoustics*, Wiley-Interscience, New York, (1998).

40. W. Desmet, D. Vandepitte, “Finite Element Modeling for Acoustics,” in *Numerical Acoustics,* LMS International: internal publication.

41. M. McIver, C. M. Linton. "Waveguides," in *Lecture Notes on the Mathematics of Acoustics*, Imperial College, London (2005).

42. L.L. Thompson, "A Review of Finite-element Methods for Time-harmonic Acoustics," The J. Acoust. Soc. Am., 119, 3, pp.1315 (2006)

43. M.P. Norton, and D.G. Karczub, *Fundamentals of Noise and Vibration Analysis for Engineers*, Cambridge university press, Cambridge, (2003).

44. A.V. Oppenheim, R.W. Schafer. *Discrete-time Signal Processing*, Prentice Hall, Englewood Cliffs (1989).

45. P. Jones, N. Kessissoglou, “An Evaluation of Current Commercial Acoustic FEA Software for Modeling Small Complex Muffler Geometries: Prediction Vs. Experiment,” *Proc. of ACOUSTICS 2009*, Adelaide, 2009.